IOWA STATE UNIVERSITY
Digital Repository

Graduate Theses and Dissertations

Iowa State University Capstones, Theses and Dissertations

2009

Ions, solutes and solvents, oh my!

Daniel David Kemp
Iowa State University

Follow this and additional works at: https://lib.dr.iastate.edu/etd

Part of the Chemistry Commons

Recommended Citation

Kemp, Daniel David, "Ions, solutes and solvents, oh my!" (2009). *Graduate Theses and Dissertations*. 10735.
https://lib.dr.iastate.edu/etd/10735

This Dissertation is brought to you for free and open access by the Iowa State University Capstones, Theses and Dissertations at Iowa State University Digital Repository. It has been accepted for inclusion in Graduate Theses and Dissertations by an authorized administrator of Iowa State University Digital Repository. For more information, please contact digirep@iastate.edu.

المنارة للاستشارات

www.manaraa.com

Ions, solutes and solvents, oh my!

By

Daniel David Kemp

A dissertation submitted to the graduate faculty

in partial fulfillment of the requirements for the degree of

DOCTOR OF PHILOSOPHY

Major: Physical Chemistry

Program of Study Committee:
Mark S. Gordon, Major Professor
Brett Bode
Thomas Holme
Monica Lamm
Hans Stauffer

Iowa State University

Ames, Iowa

2009

Copyright © Daniel David Kemp, 2009. All rights reserved.

www.manaraa.com

TABLE OF CONTENTS

المنارة للاستشارات
www.manaraa.com

www.manaraa.com

CHAPTER 1. GENERAL INTRODUCTION

Overview

Modern methods in *ab initio* quantum mechanics have become efficient and accurate enough to study many gas-phase systems. However, chemists often work in the solution phase. The presence of solvent molecules has been shown to affect reaction mechanisms[1], lower reaction energy barriers[2], participate in energy transfer with the solute[3] and change the physical properties of the solute[4]. These effects would be overlooked in simple gas phase calculations. Careful study of specific solvents and solutes must be done in order to fully understand the chemistry of the solution phase.

Water is a key solvent in chemical and biological applications. The properties of an individual water molecule (a monomer) and the behavior of thousands of molecules (bulk solution) are well known for many solvents. Much is also understood about aqueous microsolvation (small clusters containing ten water molecules or fewer) and the solvation characteristics when bulk water is chosen to solvate a solute. However, much less is known about how these properties behave as the cluster size transitions from the microsolvated cluster size to the bulk. This thesis will focus on species solvated with water clusters that are large enough to exhibit the properties of the bulk but small enough to consist of fewer than one hundred solvent molecules. New methods to study such systems will also be presented.

Dissertation Organization

This introduction describes *ab initio* and solvation methods utilized in the following chapters of this thesis. The next four chapters describe studies of various solutes solvated by water molecules, while the last three chapters involve new solvation method development.

المنارة للاستشارات

www.manaraa.com

Chapter 2 details the aqueous solvation of fluorine and chlorine anions with water clusters of various size (n=1-17 for F-, n=1-20 for Cl-). The goal of this study was to visually examine the lowest energy structure for each cluster size and determine if the solute was fully solvated with a complete first solvation shell. Chapter 3 is a systematic study of the dipole moment of a single water molecule when in the presence of other water molecules. Solvent molecules were added until the dipole moment of the solute water molecule was the same as that of a single water molecule in the presence of the bulk. The aqueous solvation of two different bihalide anions is presented in Chapter 4. The global minimum structure for each cluster size (n=1-6 water molecules) is visually inspected and compared to other low energy species. The aqueous solvation of the nitrate anion is presented in Chapter 5. The goal of this project was to determine whether or not the solute was completely solvated with only 15-32 water molecules. This study is the first to explore fully optimized structures at the MP2 level of theory for clusters of this size.

The remaining chapters describe the details of the development of new solvation methods. Chapter 6 presents the open-shell effective fragment potential (EFP) method. The open-shell EFP method is based upon spin restricted open-shell Hartree Fock and describes intermolecular interactions with electrostatics, polarization and exchange repulsion. Chapter 7 introduces the derivation for open-shell dispersion for the EFP method. Chapter 8 focuses on the implementation of the exchange repulsion energy between EFPs and *ab initio* molecules. A corresponding Fock operator is also discussed, as well as what is needed to implement the gradient.

المنارة للاستشارات

www.manaraa.com

Theoretical Background

Ab initio methods

Ab initio methods are derived from the first principles of quantum mechanics. If one desires to study the behavior of quantum systems, a function must be available to describe the state of the system at any time. To attain this goal, the time dependent Schrödinger equation would have to be solved. For the general case, the time dependent Schrödinger equation is

$$\frac{\partial \phi(r,t)}{\partial t} = -\frac{i}{\hbar} H\phi(r,t) \qquad (1)$$

The state function, ϕ, describes the position of the particles (r) which changes as a function of time (t), $\hbar$ is the division of Plank's constant by 2π, i is the square root of -1 and H is the Hamiltonian operator. The number of dimensions represented by r can vary from system to system.

One simplification of *ab initio* methods comes by applying the time independent Schrödinger equation to systems that do not depend upon time. The time independent Schrödinger equation uses the Hamiltonian operator (H) to operate on the time independent wavefunction of the system (ϕ) in order to obtain the energy of the system (E) with that particular wavefunction:

$$H\phi = E\phi \qquad (2)$$

The complete Hamiltonian operator is:

$$H = \mathrm{T_n} + \mathrm{T_e} + \mathrm{V_{ne}} + \mathrm{V_{ee}} + \mathrm{V_{nn}} \qquad (3)$$

Equation 3 includes the nuclear and electronic kinetic energy, the nuclear-electronic attraction, the repulsive electron-electron potential and the repulsive nuclear-nuclear potential

www.manaraa.com

energy operators, respectively. Each term in the Hamiltonian operator can be expressed explicitly as follows

$$H = -\frac{1}{2}\sum_{A=1}^{n}\frac{\nabla^2}{m_A} - \frac{1}{2}\sum_{i=1}^{e}\nabla_i^{\,2} - \sum_{i=1}^{e}\sum_{A=1}^{n}\frac{Z_A}{r_{1A}} + \sum_{i=1}^{e}\sum_{j<i}\frac{1}{r_{ij}} + \sum_{A=1}^{n}\sum_{B<A}\frac{Z_A Z_B}{r_{AB}} \tag{4}$$

In Eq. (4), ∇ is the Laplacian operator, m_A is the mass ratio between a nucleus and an electron, Z is the nuclear charge, r is a distance between two particles, and the system contains n nuclei and e electrons. Though Eq. (4) represents the true Hamiltonian, simplifications must be made in order to make Eq. (2) easily solvable.

Use of the Born-Oppenheimer approximation[5], which assumes the nuclei to be stationary while allowing the electrons to move freely, eliminates the kinetic energy of the nuclei from Eq. (4). If the nuclei are assumed to be stationary, the nuclear-nuclear potential energy can be calculated once and held as a constant. These two simplifications allow us to write Eq. (4) as

$$H = -\frac{1}{2}\sum_{i=1}^{e}\nabla_i^{\,2} - \sum_{i=1}^{e}\sum_{A=1}^{n}\frac{Z_A}{r_{1A}} + \sum_{i=1}^{e}\sum_{j<i}\frac{1}{r_{ij}} \tag{5}$$

One can now use Eq. (5) to solve the electronic Schrödinger equation shown in Eq. (6) and obtain the electronic energy in the field of stationary nuclei:

$$H_{elec}\phi_{elec} = E_{elec}\phi_{elec} \tag{6}$$

Once the electronic Schrödinger equation has been solved, the nuclear problem can be solved separately. The nuclei are allowed to change position within a field produced by the system's electrons. The total energy then becomes the sum of the electronic energy obtained by solving Eq. (6) and the nuclear-nuclear potential energy.

www.manaraa.com

Several more approximations must be made for systems that contain more than one electron. If the system contains more than one electron, the problem cannot be solved because it becomes inseparable. Therefore, the multi-particle nature of the problem must be simplified if this challenge is to be overcome. The simplest *ab initio* method is the Hartree-Fock (HF) method, which seeks to solve the time independent Schrödinger equation in a self-consistent manner. The Hartree-Fock approximation is designed to simplify the Hamiltonian operator in Eq. (5) for multi-electron systems. The Hartree-Fock approximation simplifies the electron-electron potential energy by replacing explicit electron-electron interactions with an averaged interaction. The ith electron experiences an average interaction with all other electrons through the field potential, v^{HF}, resulting from the presence of the other electrons. The one electron Fock operator can be written as

$$F = -\frac{1}{2}\sum_{i=1}^{e}\nabla_i^2 - \sum_{i=1}^{e}\sum_{A=1}^{n}\frac{Z_A}{r_{iA}} + \sum_{i=1}^{e} v^{HF}(i) \qquad (7)$$

The electron-electron potential energy is replaced with an averaged interaction $v^{HF}(i)$ thereby eliminating the inseparability problem of the Hamiltonian operator.

A many-electron system can be described by the one-electron orbitals of a Hartree product. An anti-symmetric wavefunction is obtained by a normalized linear combination of Hartree products and a Slater determinant can be used to cast the anti-symmetric wavefunction into the form of a determinant. Each one-electron orbital is generally taken to be a linear combination of basis functions, often called atomic orbitals (LCAO). The ith molecular orbital may be represented by summing over all atomic basis functions μ

$$\psi_i = \sum_{\mu} C_{\mu i}\varphi_{\mu} \qquad (8)$$

www.manaraa.com

where $C_{\mu i}$ are the LCAO coefficients.

If a complete basis set were chosen, the expansion in Eq. (8) would be exact. However, in Hilbert space, a complete basis set is infinite, so such a calculation is not practical. To make the calculations tractable, quantum chemists truncate the basis set to a finite number of basis functions. Typically, the basis set is chosen to be as large as computationally possible, because a larger basis set gives more flexibility to the molecular orbitals.

At the beginning of a Hartree-Fock calculation, the wavefunction and the energy are unknown. In order to begin the self-consistent iterations of the HF method, a guess of the electronic orbitals is typically made from which the density can be obtained. The Fock matrix, which includes the one electron Hamiltonian and the quantum mechanical two-electron integrals, is then formed and diagonalized. The energy eigenvalues for the orthogonal molecular orbitals are obtained. Using the molecular orbitals obtained during the calculation, one can make a new guess at the density and repeat the process until convergence is reached.

Hartree-Fock is a relatively simple level of *ab initio* theory. It is advantageous because many chemical systems of interest can be calculated at the HF level of theory on modern computers. Another advantage to Hartree-Fock is that it is variational. The variation principle states that the energy of a trial set of molecular orbitals is guaranteed to be an upper bound to the true energy:

$$E \le \langle \psi_{trial} | H | \psi_{trial} \rangle = E_{trial} \qquad (9)$$

المنارة للاستشارات

www.manaraa.com

As the set of molecular orbitals changes and improves during the SCF iterations, the energy will approach the true energy.

The electronic wavefunction can be treated three different ways within the Hartree-Fock approach. Spin restricted Hartree-Fock (RHF) occupies each spatial orbital with two electrons- one alpha and one beta spin electron. RHF is used exclusively for closed shell systems where no electrons are left unpaired. Spin restricted open-shell Hartree-Fock (ROHF)[6] uses restricted spin orbitals and restricted determinants. Unlike RHF, one or two electrons can occupy the ROHF spatial orbitals. An electron of alpha or beta spin may occupy singly occupied spatial orbitals while doubly occupied spatial orbitals are occupied just as RHF spatial orbitals are.

An alternative open shell Hartree-Fock method is spin unrestricted Hartree-Fock (UHF)[7]. The UHF wavefunction partitions electrons of different spin into different spatial orbitals. Therefore, each orbital is singly occupied. The energy of UHF wavefunctions may be lower than that of ROHF wavefunctions because of the greater number of spatial orbitals in the UHF method. However, the UHF wavefunction suffers from spin contamination, because the wavefunction is not an eigenfunction of the spin operator $\hat{S}^2$.

The disadvantage to Hartree-Fock is that it includes no provision to describe the correlated motion of electrons (often referred to as dynamic correlation). The ability to include dynamic correlation is lost by averaging the electron-electron potential in Eq. (8). The exclusion of electron correlation leads to inaccurate energy predictions. Although the absolute magnitude of the dynamic correlation energy is small compared to the total electronic energy, the variation in the dynamic correlation correction across a potential

www.manaraa.com

energy surface is sufficiently large that its omission causes large errors in relative energies for chemical processes.

In order to recover the dynamic electron correlation energy, higher levels of theory must be used. These levels of theory are typically initiated with a Hartree-Fock calculation to obtain a reference wavefunction. One such method is the Møller-Plesset[8] perturbation theory and is most commonly used with a second order perturbation (MP2). This method adds a small perturbation, υ, to the Hamiltonian from the HF calculation (H_0):

$$H = H_0 + \upsilon \qquad (10)$$

The Hartree-Fock energy (E_0) includes the zeroth-order and first order (E_1) energy corrections. Therefore, the first correction to the Hartree Fock energy comes via second-order perturbation theory (MP2). The second-order energy is obtained by summing equation 12 over all states but the ground state:

$$E_0^{(2)} = \sum_n \frac{\left|\langle 0 \mid v \mid n \rangle\right|^2}{E_0^{(0)} - E_n^{(0)}} \qquad (12)$$

Though more computationally expensive than HF, an MP2 calculation is feasible for many systems of interest and can be adapted to work well on modern, parallel computer systems. Because the exact Hamiltonian is not used, perturbation theory is not variational. Perturbation theory can be extended to higher orders of energy corrections but, in general, convergence may become a problem for MPn as n grows larger.

A more robust level of theory than perturbation theory is coupled cluster theory[9,10], which is also based on many body expansions. A cluster operator in coupled cluster theory operates on a Hartree-Fock reference wavefunction. The complete cluster operator would

المنارة للاستشارات

www.manaraa.com

operate on all possible electron excitations, starting with one operator for singles, another for doubles and up to the number of electrons (n) in the system of iinterest. The operator involved in coupled cluster theory, when defined by a Taylor series expansion is

$$e^{\hat{T}} = 1 + \hat{T} + \frac{\hat{T}^{2}}{2!} + \frac{\hat{T}^{3}}{3!} + \ldots \qquad (13)$$

and the cluster operator $\hat{T}$ is equal to

$$\hat{T} = \hat{T}_1 + \hat{T}_2 + \ldots + \hat{T}_n \qquad (14)$$

where $\hat{T}_1$ is the single electron excitation operator, $\hat{T}_2$ is the double electron excitation operator and so on.

In order to keep the computational cost feasible and still obtain much of the electron correlation, it is common to use coupled cluster with singles and doubles (CCSD), or singles, doubles and triples (CCSD(T)), where the triples are obtained using perturbation theory instead of in an iterative manner.

All of the electron correlation energy could be recovered if one could use an infinite basis set within a full configuration-interaction (CI) calculation[11,12]. The CI wavefunction is defined below:

$$\Phi = \Psi_0 + \sum_{i}^{occ}\sum_{a}^{virt} c_i^a \Psi_i^a + \sum_{i<j}^{occ}\sum_{a<b}^{virt} c_{ij}^{ab} \Psi_{ij}^{ab} + \sum_{i<j<k}^{occ}\sum_{a<b<c}^{virt} c_{ijk}^{abc} \Psi_{ijk}^{abc} + \ldots \qquad (15)$$

Eq. (15) can be truncated after any term but full CI excites all n electrons of the system into the virtual orbitals. However, full CI is computationally expensive, since it scales exponentially with the size of the system, and an infinite basis set cannot be used in any application.

المنارة للاستشارات
www.manaraa.com

Density Functional Theory

Density Functional Theory (DFT) has become a popular alternative to *ab initio* methods for studying molecular structures and energies. DFT does not attempt to solve the Schrödinger equation like Hartree-Fock does. DFT starts with the premise that the energy is a functional of the density, ρ (x,y,z), and the density is a function of the Cartesian coordinates of the nuclei [**E**(ρ(x,y,z))]. While this premise is true, the function that relates the energy to the density is unknown.

Kohn and Sham proposed a method to obtain the energy from the density of a system of non-interacting electrons[13] analogous to the independent particle approach in Hartree-Fock. The determination of the density is most commonly done with the Kohn-Sham formalism which states that it is possible to calculate the molecular energy from the density without the ground-state wave function. The one-electron Hamiltonian for the reference system of non-interacting electrons is as follows

$$\hat{H} = \sum_{i=1}^{n}\left[-\frac{1}{2}\nabla_i^2 + v_s\left(r_i\right)\right] \qquad (16)$$

where $v_s\left(r_i\right)$ defines an external potential. This is an exactly solvable problem that provides a set of Kohn-Sham orbitals that provides the starting point for an iterative process that is similar to the iterative HF process. A correction term, provided by exchange and correlation functionals is added to the kinetic energy, Coulomb and electron-nuclear attraction functionals to yield the DFT energy.

The most challenging part of obtaining the total DFT energy is determining appropriate exchange and correlation functionals. Many different functionals contain fitted

المنارة للاستشارات www.manaraa.com

parameters, each having parameters fit to describe a specific type of chemical systems in order to obtain the exchange-correlation energy.

The computational cost of most commonly used DFT functionals is similar to that of Hartree-Fock. DFT does have the ability to include some electron correlation via the correlation functional. The accuracy of DFT can approach that of MP2 if the proper fitted functional is chosen, but it can be worse than Hartree-Fock if an improper functional is chosen or if a good functional does not exist for a given chemical system of interest.

Solvation Methods

Solvation methods are typically divided into two major classes: continuum models and explicit models. Continuum models do not account for individual solvent molecules and therefore do not account for individual solvent-solute interactions. Instead, a pre-defined electric field of the continuum model interacts with the solute. The advantage of continuum models is that they are computationally inexpensive and attempt to describe the characteristics of the bulk solution without the need to explicitly define tens of thousands of individual solvent molecules in a calculation.

Explicit solvent models describe specific solvent molecules and their intermolecular interactions with the solute and solvent molecules. An example of an explicit solvent model is the effective fragment potential (EFP) model. The first implementation of the EFP model was designed exclusively for the water molecule (EFP1)[14]. The original implementation of the EFP1 method was based upon Hartree-Fock and the goal of the method was to reproduce

المنارة للاستشارات

www.manaraa.com

Hartree-Fock results without the computational cost associated with Hartree-Fock. An EFP1 potential based upon DFT has also been implemented with success[15].

The EFP1 water potentials include the following intermolecular interactions: electrostatics (Coulomb effects), polarization (induction) and a term including both exchange-repulsion and charge transfer. The only difference between the two EFP1 methods is the level of theory from which the intermolecular interactions are based. The combined exchange-repulsion/charge transfer energy term was fitted based upon numerous calculations on the water dimer.

EFP1 proved to be both efficient and effective at studying a variety of solvated systems[16-19]. The biggest limitation, though, was that it was available only for the water molecule. In order to extend the EFP method to the general case, an analytic expression had to be derived for all terms, including the exchange-repulsion. The general form of the EFP method is called EFP2[20]. EFP2 also has the ability to describe charge transfer[21] and dispersion effects[22].

The EFP method is computationally cheaper than describing each solvent molecule with an *ab initio* level of theory, yet it is able to accurately reproduce *ab initio* results. In some cases, the EFP method can be used to study solvated properties of an *ab initio* solute, while to do such a calculation with a fully *ab initio* method would require careful thought and development of new methods. An example of such a study is given in Chapter 3 of this thesis.

All of the *ab initio* methods, density functional theory and the solvation methods described here are available in the General Atomic and Molecular Electronic Structure System (GAMESS)[23,24].

www.manaraa.com

References

1. Chu, J.-W.; Trout, B. L. *J. of Amer. Chem. Soc.,* **2004**, *126*, 900.

2. Kudo, T.; Gordon, M. S. *J. of Phys. Chem. A*, **2002**, *106*, 11347.

3. Shigeto, S.; Dlott, D. D. *Chem. Phys. Lett.*, **2007**, *447*, 134.

4. Gayathri, B. R.; Mannekutla, J. R.; Inamdar, S. R. *J. Mol. Structure*, **2008**, *889*, 383.

5. Born, M.; Oppenheimer, R. Zur Quantentheorie der Molekeln. *Ann. Phys. (Leipzig)* **1927**, *84*, 457.

6. Binkley, J. S.; Pople, J. A.; Dobosh, P. A. *Mol. Phys.*, **1974**, *6*, 1423.

7. Pople, J. A,; Nesbet, R. K. *J. Chem. Phys.*, **1954**, *22*, 571.

8. Møller, C.; Plesset, M. S. *Phys. Rev*. **1934**, *46*, 618.

9. Raghavachari, K.; Trucks, G. W.; Pople, J. A.; Head-Gordon, M. *Chem. Phys. Lett.* **1989**, *157*, 479.

10. Piecuch, P.; Kucharski, S. A.; Kowalski, K.; Musial, M. *Comput. Phys. Commun.* **2000**, *149*, 71.

11. Shavitt, I. The Method of Configuration Interaction. *Methods of Electronic Structure Theory*; Schaefer, H. F., Ed.; Plenum Press: New York, **1977**, p. 189-275.

12. Sherrill, C.D.; Shaefer III, H. F. *Adv. Quant. Chem.*, **1999**, *34*, 143.

13. Kohn, W.; Sham, L.J. *Phys. Rev.*, **1965**, *140*, A1133.

14. Day, P. N.; Jensen, J. H.; Gordon, M. S.; Webb, S. P.; Stevens, W. J.; Krauss, M.; Garmer, D.; Basch, H.; Cohen, D. *J. Chem. Phys.* **1996,** *105*, 1968.

15. Adamovic, I.; Freitag, M. A.; Gordon, M. S. *J. Chem. Phys.*, **2003**, *118*, 6725.

16. Merrill, G.N.; Webb, S. P.; Bivin, D. B. *J. Phys. Chem. A* **2003**, *107*, 386.

17. Webb, S. P.; Gordon, M. S. *J. Phys. Chem. A* **1999**, *103,* 1265.

www.manaraa.com

18. Adamovic, I.; Gordon, M. S. *J. Phys. Chem. A.* **2005**, *109,* 1629.

19. Day, P. N.; Pachter, R.; Gordon, M. S.; Merrill, G. N. *J. Chem. Phys.* **2000**, *112,* 2063.

20. Gordon, M. S.; Freitag, M. A.; Bandyopadhyay, P.; Jensen, J. H.; Kairys, V.; Stevens, W. J. *J. Phys. Chem. A* 2001, *105*, 293.

21. Li, H.; Gordon, M. S.; Jensen, J.H. *J. Chem. Phys.*, **2006**, *124*, 214108.

22. Adamovic, I.; Gordon, M. S. *Mol. Phys.*, **2005**, *103*, 379.

23. Schmidt, M. W.; Baldridge, K. K.; Boatz, J. A.; Jensen, J. H.; Koseki, S.; Matsunaga, N.; Gordon, M. S.; Ngugen, K. A.; Su, S.; Windus, T. L.; Elbert, S. T.; Montgomery, J.; Dupuis, M. *J. Comput. Chem.* 1993, *14*, 1347.

24. Gordon, M.S.; Schmidt, M.W. Advances in Electronic Structure Theory: GAMESS a Decade Later, *Theory and Applications of Computational Chemistry,* Dykstra, C. E., Frenking, G., Kim, K.S., Scuseria, G.E., Eds.; Elsevier: Boston, **2005;** Ch. 41.

المنارة للاستشارات

www.manaraa.com

CHAPTER 2. SOLVATION OF FLUORINE AND CHLORINE ANIONS

A paper published in The Journal of Physical Chemistry A

Daniel D. Kemp and Mark S. Gordon

Abstract

The solvation of fluoride and chloride anions (F- and Cl-, respectively) by water has been studied using effective fragment potentials (EFP) for the water molecules and ab initio quantum mechanics for the anions. In particular, the number of water molecules required to fully surround each anion has been investigated. Monte Carlo calculations have been employed in an attempt to find the solvated system $X^-(H_2O)_n$ (X= F, Cl) with the lowest energy for each value of n. It is predicted that 18 water molecules are required to form a complete solvation shell around a Cl- anion, where "complete solvation" is interpreted as an ion that is completely surrounded by solvent molecules. Although fewer water molecules may fully solvate the Cl^- anion, such structures are higher in energy than partially solvated ones until $n \geq 18$. Calculations on the F^- anion suggest that 15 water molecules are required for a complete solvation shell. The EFP predictions are in good agreement with relative energies predicted by ab initio energy calculations at the EFP geometries.

I. Introduction

Solvation effects play an important role in many different areas of chemistry. Spectroscopy, reaction mechanisms and kinetics are examples of phenomena that are affected by the presence or absence of a solvent. In this study, the effective fragment potential (EFP) method[1,2] is employed to investigate the solvation of fluoride and chloride anions (F- and Cl-, respectively). Water solvated Cl- and F- anions have been the subject of many other theoretical studies[3-48] and several relevant experimental studies[49,50] have been performed on

www.manaraa.com

the chloride ion. Smaller water clusters, usually involving < 10 water molecules, are most common because of computational limitations. When applied to a halide anion X^-, the focus of many microsolvation studies is to determine how many water molecules are required to see a transition from a surface to an interior state. A surface state is defined as X^- resting "on top" of a cluster of water molecules, while an interior state is defined as a structure in which X^- is "inside" a water cluster cage.

The primary focus of this study is to analyze the transition from surface to completely solvated anions in $X^-(H_2O)_n$ (X= F, Cl) as n increases. Also of interest is the value of n at which interior structures begin to appear even if they are not global minima. The structures involving small numbers of water molecules provide insight into the microsolvation of the anions while the fully solvated structures provide increasingly useful information about the bulk solution. Details of the computational approach are provided in Section II.

An additional motivation is to test the EFP method against the corresponding predictions of Hartree-Fock (HF) and Møller-Plesset second order perturbation theory (MP2)[51-54]. The EFP method was developed for the water molecule and was designed to reproduce HF results for aqueous solvation while requiring considerably less computational cost.[1,2]

The EFP approach has been successfully applied to a variety of problems, including the solvation of small cations[55], the solvation of the Menshutkin reaction[56], the solvation of an S_N2 reaction[57], and the energetics and structures of small water clusters[58].

Recently, Webb and Merrill studied the solvation of small anions ($X^-(H_2O)_n$) using the EFP method.[43] In their study, F- and Cl- anions were solvated by n=1-6 effective fragment potentials. The EFP predictions were compared with results obtained with HF optimizations

www.manaraa.com

and MP2 single point calculations. Their results suggest that interior anions do not exist for $X^-(H_2O)_n$, for n=1-6. The energy differences between structures within a given cluster of size n were found to be small. Comparisons between the present work and the results of Webb and Merrill will be given in Section III.

II. Computational Methods

Global minimum energy structure searches were performed using the Hartree-Fock level of theory and the 6-31++G (d,p)[59-62] basis set for X^- anions. All water molecules were treated as EFPs. The general atomic and molecular electronic structure system (GAMESS) was used for all calculations.[63]

Searches for the minimum energy structures, including the global minimum, on the $X^-(H_2O)_n$ potential energy surfaces employed a Monte Carlo[64]/simulated annealing code[65]. Simulated annealing was used to initiate structure searches at 600 K and slowly cool the system to 300 K. Geometry optimizations (at 0 K) were performed after every 10 steps in the simulation. The number of EFP water molecules n was systematically increased from 1 to 15 (20) for F^- (Cl^-) to determine the smallest water cluster that fully solvates the anion as the lowest-energy species.

To characterize each stationary point that was found by the Monte Carlo searches, the Hessian (matrix of energy second derivatives) was calculated and diagonalized at each stationary point. Local minima are characterized by a positive definite Hessian. Double differencing was used to calculate the Hessians.

Single point fully ab initio energy calculations were performed on at least the five lowest-energy structures for each value of n to compare relative EFP/HF, HF and MP2 energies for surface and interior structures. The same 6-31++G (d,p) basis set was used for

www.manaraa.com

the fully HF and MP2 calculations. Reported energies at all levels of theory include zero point energy (ZPE) corrections that were obtained from the Hessians in which the anion was treated with HF and the EFP model described the water molecules.

In addition, MP2/6-311++(2df,p)[66,67] geometry optimizations were initiated at the equilibrium geometries found from the Monte Carlo calculations for $F^-(H_2O)_n$, (for n=1-4). The criterion for convergence was 10^{-5} Hartree/bohr. Hessians were calculated at these equilibrium geometries using double differencing. Single point CCSD(T)[68,69] calculations were then performed on these optimized structures using the same basis set.

Although a few $F^-(H2O)_n$ and $Cl^-(H2O)_n$ structures were found that have one imaginary frequency, the magnitude of these frequencies is small (usually < 50 cm^{-1}) and they are floppy modes involving the solvent molecules. Because the Hessians are calculated using finite differences of analytic gradients, these small imaginary frequencies may be numerical noise. In any case, none of the structures with an imaginary frequency were predicted to be the lowest-energy structure by any level of theory. Therefore, the structures that have imaginary frequencies have no effect on the trend of moving from a surface anion to a completely solvated anion for either fluoride or chloride.

III. Results and Discussion

A. $F^-(H_2O)_n$ n=1-15

Global minimum structures with < 11 water molecules are always surface anions. The first interior anion is seen when n=6 but interior anions exist as high-energy species until n=12. The Monte Carlo simulations predict that 15 water molecules are required to fully solvate the fluoride anion. Calculations were also performed on the fluoride anion with 17 water molecules in order to ensure that the solvation trend observed from 12 to 15 waters

www.manaraa.com

continues as n increases further. If so, the surrounded anions should also exist with larger water clusters. This is found to be the case.

Starting with the first structure in Figure 2.1, all structures in this paper are labeled with a unique name underneath the structure. The names for each structure follow the format XnI where X represents the anion in the structure, n is the number of water molecules present and I is an alphabetical letter. The structures marked by a pound symbol (#) are interior anions. The structures marked with an asterisk (*) are the EFP global minimum structures. When the global minimum structure for a given n is an interior anion, the lowest energy surface anion is marked by an ampersand (&).

Following each XnI designation is a nomenclature used to describe the solvation shells of the solvent environment. First solvation shell solvent molecules participate in hydrogen bonding with the solute anion, while second solvation shell molecules form hydrogen bonds with the first solvation shell molecules. Likewise, third shell molecules hydrogen bond with second shell molecules. A number in parenthesis (x) denotes the number of water molecules in the first shell. If separate groups of first solvation shell molecules are present they are distinguished as (x,y) where x and y are the number of first solvation shell water molecules in the two distinct groups. Groups are considered separate if they are not within hydrogen bonding distance (2.5 Å) of each other. Similarly, the second [x,y] and third {x,y} solvation shell water molecules are indicated, if present. The total number of water molecules can be obtained by adding the number of first, second and third shell molecules. Except for the first row in Figures 2.1 and 2.4, the structures in each row of Figures 2.1-2.8 contain the same number of water molecules n. Each consecutive row adds one water molecule.

www.manaraa.com

Below this nomenclature, the EFP (HF) and [MP2] relative energies (kcal/mol) are given in Figures 2.1-2.9. The energy difference (ΔE) between the energy E* of the EFP global minimum structure and that of another structure (E) is obtained by subtracting E* from E:

$$E - E^* = \Delta E \quad \textbf{(1)}$$

Therefore, a positive *ΔE* indicates that the global minimum structure, determined using EFP waters, is more stable than the structure with energy *E*. A negative *ΔE* value indicates that the structure with energy *E* is more stable at the corresponding level of theory.

Local minima for $F^-(H_2O)_n$, n=1-5 are illustrated in Figure 2.1. Global minimum structures are given in the first column of the figure. Structures F2C, F3C and F5C are either planar or nearly planar and therefore cannot exist as interior anions. Therefore, interior anions do not exist for n=1-5. Note that for n=1-4, all water molecules reside in a given hemisphere. The second column of Figure 2.1 presents local minima that are neither global minimum nor interior structures. Generally, the relative energies predicted by EFP are in good agreement with those found using HF or MP2 at the EFP geometries, with deviations on the order of 1 kcal/mol or less.

Figure 2.2 is organized similarly to Figure 2.1; only three structures are shown for each value of n, n=6-11. Structure F6C# is the first interior structure observed; however, it is not the global minimum structure for n=6. Although in a few cases the relative energies of the structures changes as the level of theory changes, HF and MP2 agree that the EFP global minimum is lower in energy than the lowest energy interior anion for n=6-11, and the quantitative agreement among the three levels of theory is again very good, typically within 1 kcal/mol.

المنارة للاستشارات

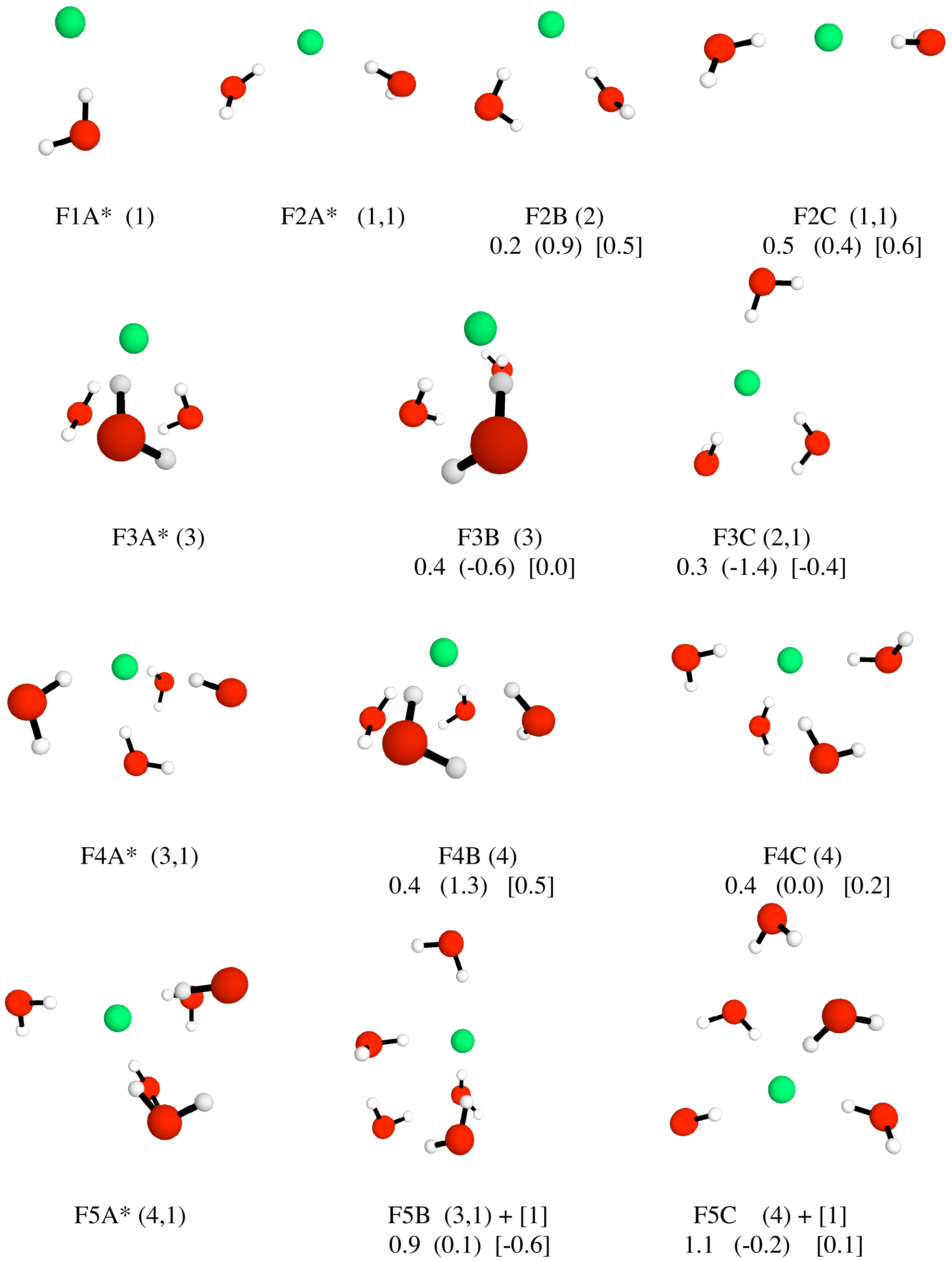

F1A* (1)

F2A* (1,1)

F2B (2)
0.2 (0.9) [0.5]

F2C (1,1)
0.5 (0.4) [0.6]

F3A* (3)

F3B (3)
0.4 (-0.6) [0.0]

F3C (2,1)
0.3 (-1.4) [-0.4]

F4A* (3,1)

F4B (4)
0.4 (1.3) [0.5]

F4C (4)
0.4 (0.0) [0.2]

F5A* (4,1)

F5B (3,1) + [1]
0.9 (0.1) [-0.6]

F5C (4) + [1]
1.1 (-0.2) [0.1]

Figure 2.1. Local minimum structures for $F^-(H_2O)_n$ n=1-5. An asterisk denotes the global minimum structure for each value of n. Each structure is given a unique name, XnI. X is the anion present, n is based on the number of water molecules and I is a unique alphabetic character. The number of hydrogen bonds present in different solvation shells is given. Relative energy differences between the higher energy local minimum structures and the EFP global minimum are given at the EFP (HF) [MP2] level of theory. All relative energies are given in kcal/mol.

www.manaraa.com

The EFP method suggests that the first global minimum structure that exists as an interior anion occurs for n=12, F12A* in Figure 2.3. Figure 2.3 also presents the lowest energy surface anion structure in the third column. All structures are local minima, including those in the second column which represents a higher-energy species than the global minimum. The lack of water molecules in the lower right quadrant (F12A*, F13A*, and F14A*) and the lower left quadrant (F12A* and F14A*) illustrates incomplete solvation. As for the smaller clusters, there is generally good agreement among the three levels of theory. An exception occurs for n=14. Here, the EFP method predicts structure F14A* to be the global minimum, whereas HF and MP2 predict structure F14B to be lower in energy. Both are interior structures, so the methods are in qualitative agreement.

The global minimum structure for n=15 (F15A* in Figure 2.3) is completely solvated. Unlike n=12-14, every quadrant in structure 15A* has roughly the same concentration of water molecules. The other structure for n=15, F15B, is the lowest energy structure for n=15 that is not completely solvated. This solvation trend continues for n=17, for which the global minimum structure is F17A*.

The structures presented here generally agree with those of Webb and Merrill.[43] However, their study optimized structures that were previously presented in the literature. These authors predict EFP, HF and MP2 structures with two distinct groups of waters in the first solvation shell to be the lowest energy species for n=2, 4, and 5 (EFP, HF and MP2).

المنارة للاستشارات

www.manaraa.com

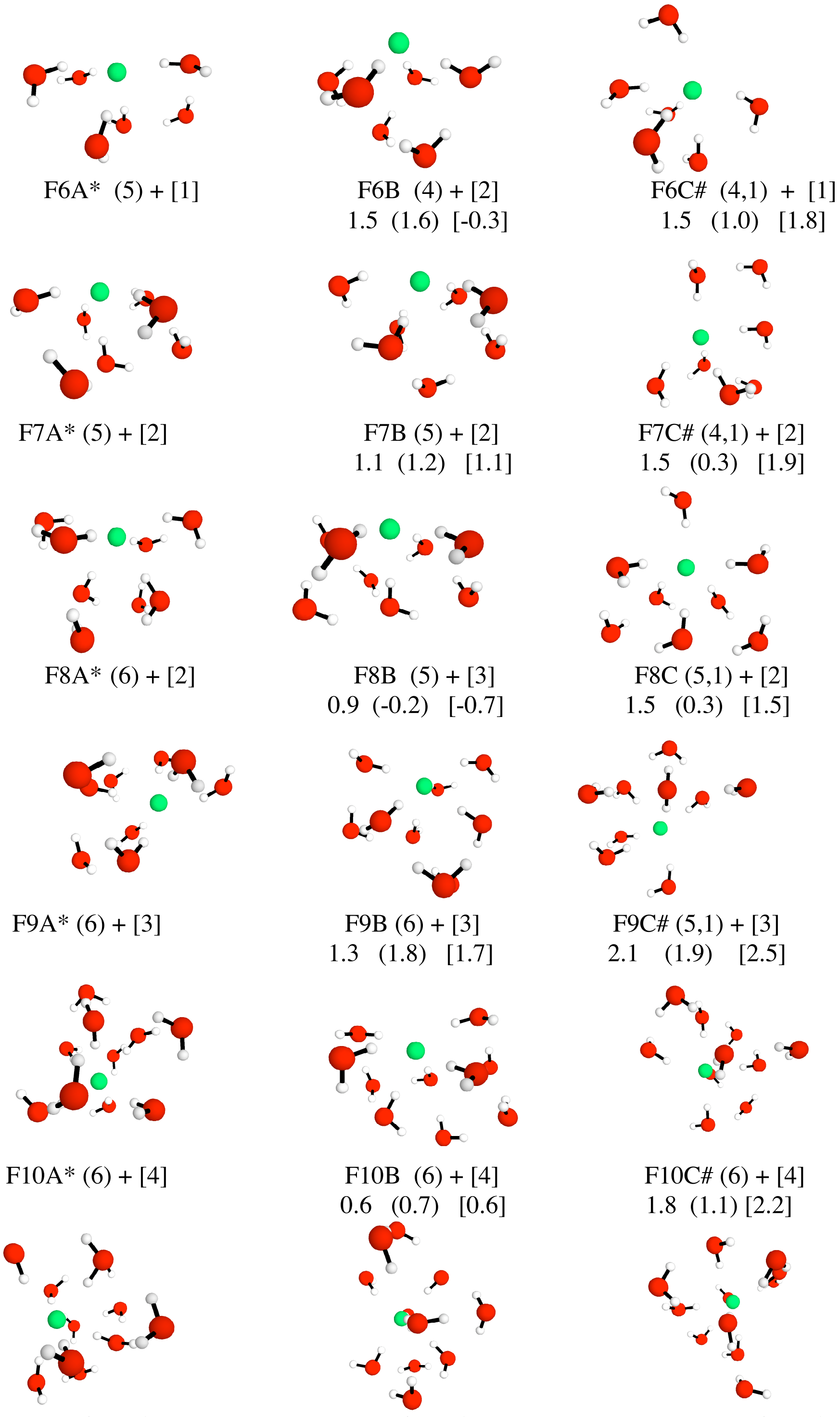

F6A* (5) + [1]

F6B (4) + [2]
1.5 (1.6) [-0.3]

F6C# (4,1) + [1]
1.5 (1.0) [1.8]

F7A* (5) + [2]

F7B (5) + [2]
1.1 (1.2) [1.1]

F7C# (4,1) + [2]
1.5 (0.3) [1.9]

F8A* (6) + [2]

F8B (5) + [3]
0.9 (-0.2) [-0.7]

F8C (5,1) + [2]
1.5 (0.3) [1.5]

F9A* (6) + [3]

F9B (6) + [3]
1.3 (1.8) [1.7]

F9C# (5,1) + [3]
2.1 (1.9) [2.5]

F10A* (6) + [4]

F10B (6) + [4]
0.6 (0.7) [0.6]

F10C# (6) + [4]
1.8 (1.1) [2.2]

F11A* (6) + [5]

F11B (6) + [5]
1.3 (0.6) [1.7]

F11C# (6) + [5]
1.9 (1.0) [2.3]

Figure 2.2. Local minimum structures are given for $F^-(H_2O)_n$ where n=6-11. The structures in the first column are marked by an asterisk and are the global minima while # denotes the lowest energy interior anion for each value of n.

المنارة للاستشارات
www.manaraa.com

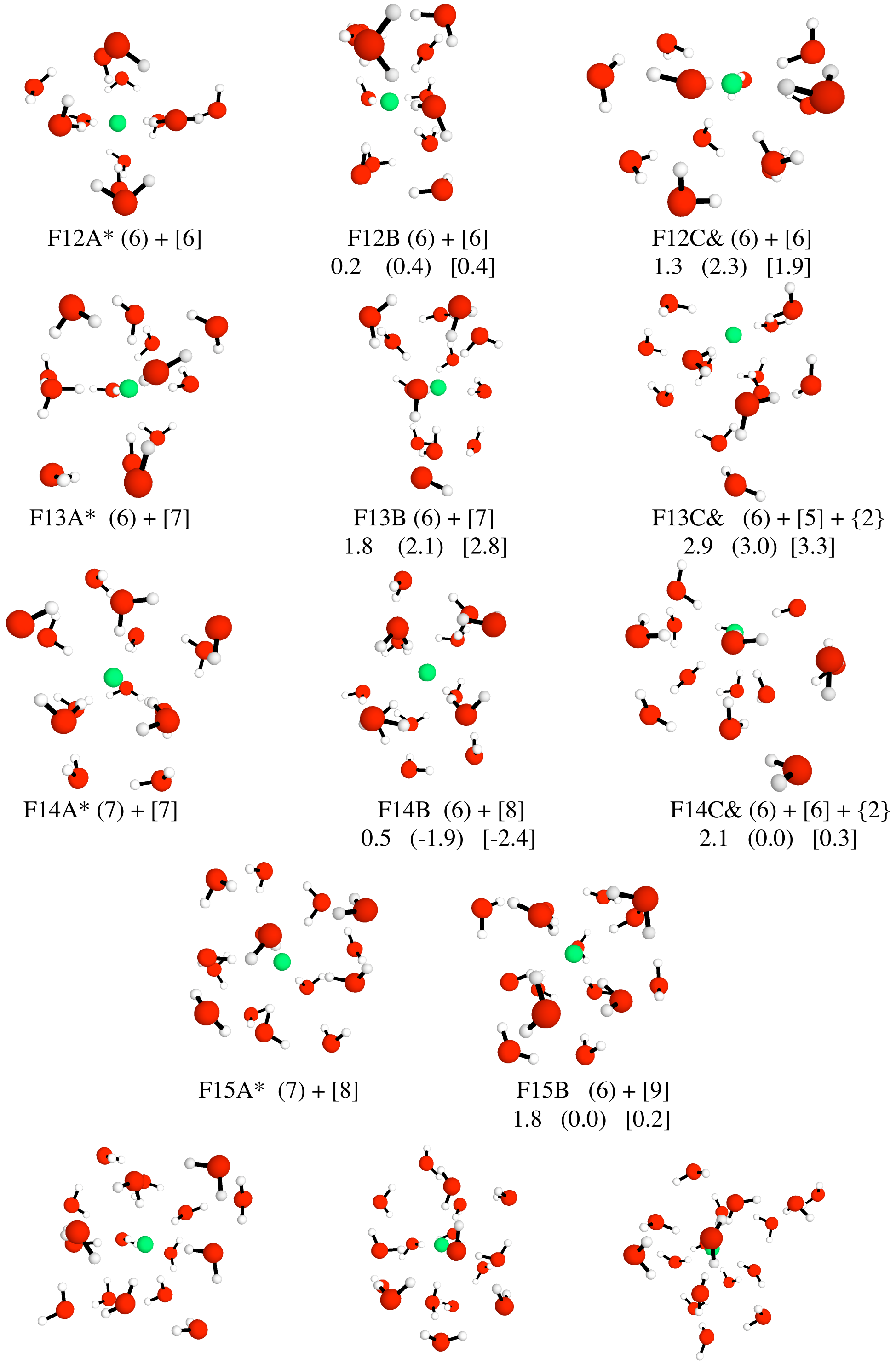

F12A* (6) + [6]

F12B (6) + [6]
0.2 (0.4) [0.4]

F12C& (6) + [6]
1.3 (2.3) [1.9]

F13A* (6) + [7]

F13B (6) + [7]
1.8 (2.1) [2.8]

F13C& (6) + [5] + {2}
2.9 (3.0) [3.3]

F14A* (7) + [7]

F14B (6) + [8]
0.5 (-1.9) [-2.4]

F14C& (6) + [6] + {2}
2.1 (0.0) [0.3]

F15A* (7) + [8]

F15B (6) + [9]
1.8 (0.0) [0.2]

F17A*

F17B
1.0 (-0.2) [0.2]

F17C&
1.1 (-1.8) [0.3]

Figure 2.3. The structures in the first column are global minima for $F^-(H_2O)_n$ n=12-15,17. The second column shows structures that are local minima but are higher in energy. The structures in the third column are marked by & and are the lowest energy structure that most closely resemble a surface anion. Both F15A* and F17A*, are completely solvated.

المنارة للاستشارات
www.manaraa.com

The global minimum structure found by the Monte Carlo calculations reported here for n=5 is composed of two groups of water molecules, one of which appears to reside in a second solvation shell. For n=6 (EFP, HF and MP2), both the results of the Monte Carlo calculations and those of Webb and Merrill predict a single group of first solvation shell molecules in the global minimum structure.

B. $Cl^-(H_2O)_n$ n=1-18

Monte Carlo calculations predict that no fewer than 18 water molecules are required to completely solvate Cl^-. Monte Carlo calculations were also performed with the Cl- anion and a water cluster with twenty water molecules to confirm the findings for n=18. Global minima for $Cl^-(H_2O)_n$ are given in Figures 2.4-2.8 in the left hand column. The same nomenclature as that for the F^- anion is used.

The second column in Figures 2.4-2.8 presents a higher-energy local minimum. The structures that most resemble an interior anion structure for n=1-5 are given in the third column of Figure 2.4. Structures CL2B and CL3C are planar, while structures CL4C and CL5C have a large space without water molecules located towards the right-hand side of each structure. While these structures are closest to being an interior anion for n=2-5, they are actually surface anions. This is similar to the results found for F^-. The global minima obtained for $Cl^-(H_2O)_n$ n=1-6 are in good agreement with the results of Webb and Merrill at all levels of theory.[43] No interior anions were found for n=1-5 by either the Monte Carlo calculations or Webb and Merrill. The relative energies predicted by the three levels of theory are in good agreement with each other.

المنارة للاستشارات

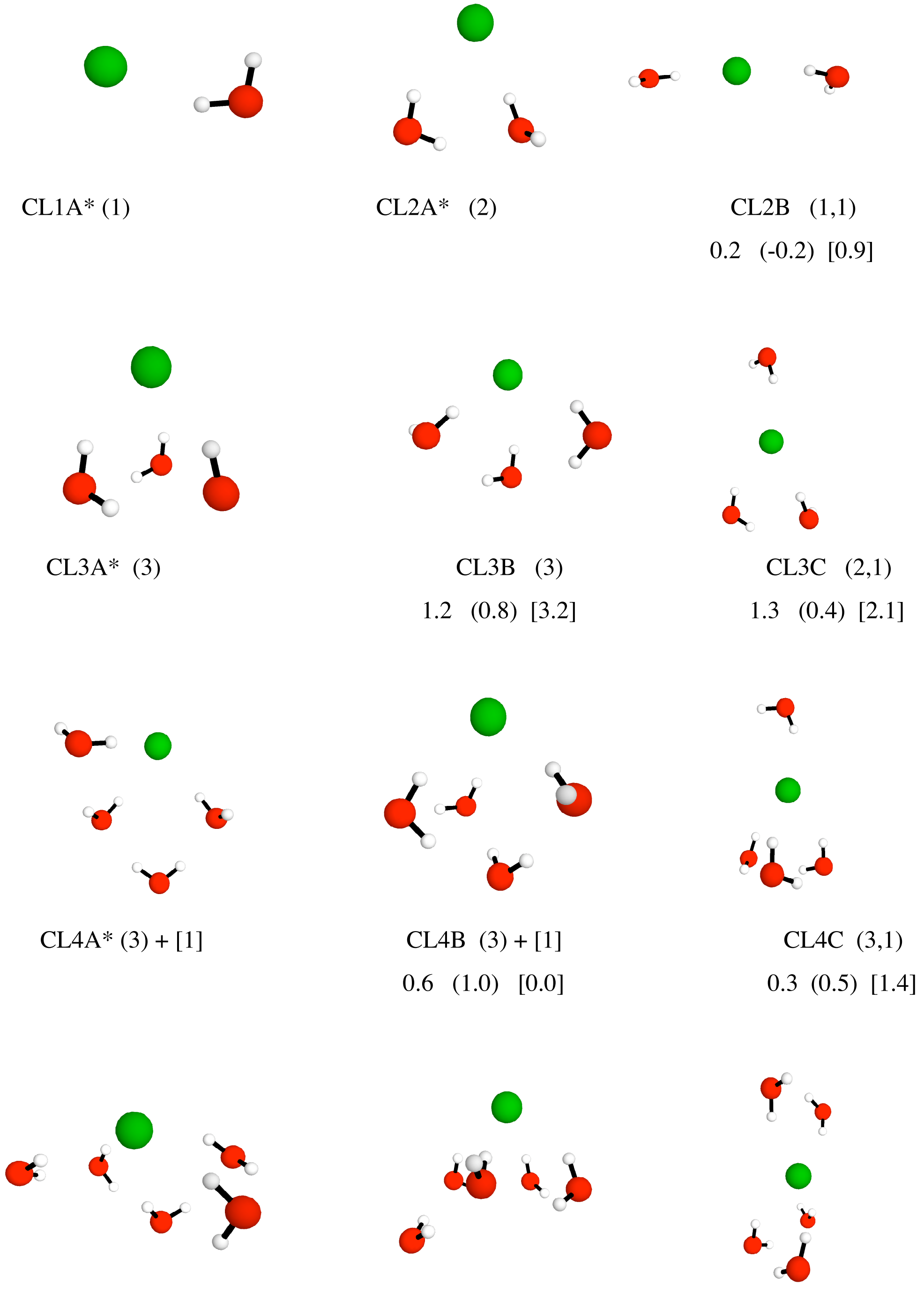

CL1A* (1)

CL2A* (2)

CL2B (1,1)
0.2 (-0.2) [0.9]

CL3A* (3)

CL3B (3)
1.2 (0.8) [3.2]

CL3C (2,1)
1.3 (0.4) [2.1]

CL4A* (3) + [1]

CL4B (3) + [1]
0.6 (1.0) [0.0]

CL4C (3,1)
0.3 (0.5) [1.4]

CL5A* (5)

CL5B (4) + [1]
0.2 (-0.6) [-0.7]

CL5C (3,2)
0.9 (0.0) [1.6]

Figure 2.4. Local minimum structures for $Cl^{-}(H_2O)_n$ n=1-5. The first column represents the global minimum structure for a given n. The second column is a local minimum structure, but a higher energy species than the global minimum. The structure in the third column is the lowest energy species that most resembles an interior anion. The nomenclature used for Figures 2.1-2.3 is used here also.

www.manaraa.com

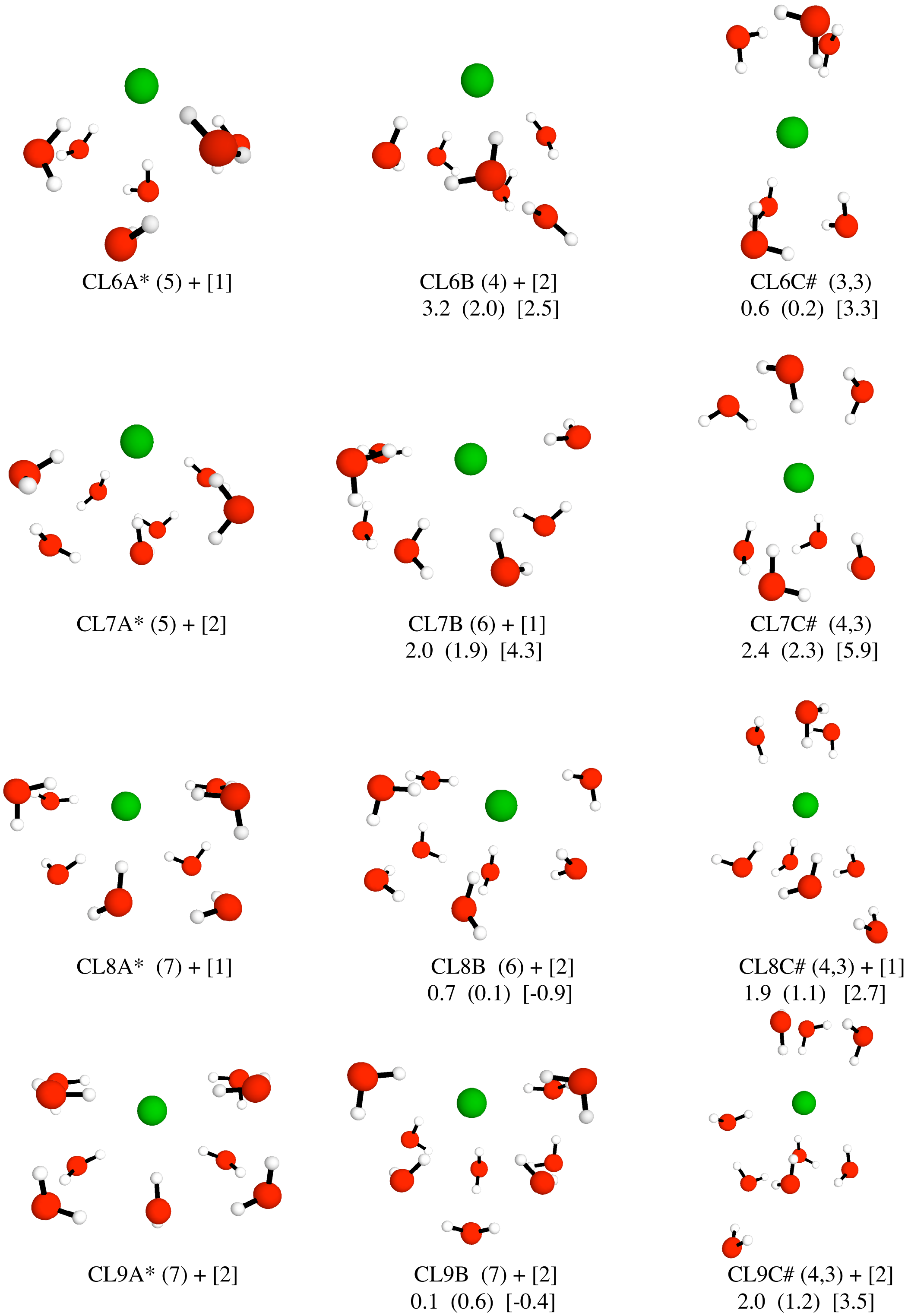

CL6A* (5) + [1]

CL6B (4) + [2]
3.2 (2.0) [2.5]

CL6C# (3,3)
0.6 (0.2) [3.3]

CL7A* (5) + [2]

CL7B (6) + [1]
2.0 (1.9) [4.3]

CL7C# (4,3)
2.4 (2.3) [5.9]

CL8A* (7) + [1]

CL8B (6) + [2]
0.7 (0.1) [-0.9]

CL8C# (4,3) + [1]
1.9 (1.1) [2.7]

CL9A* (7) + [2]

CL9B (7) + [2]
0.1 (0.6) [-0.4]

CL9C# (4,3) + [2]
2.0 (1.2) [3.5]

Figure 2.5. Local minimum structures for $Cl^-(H_2O)_n$ for n=6-9. The first column shows the global minimum structure for a given n. The second column is a local minimum structure, but a higher energy species than the structure in the first column. The third column represents the lowest energy interior anion structures.

www.manaraa.com

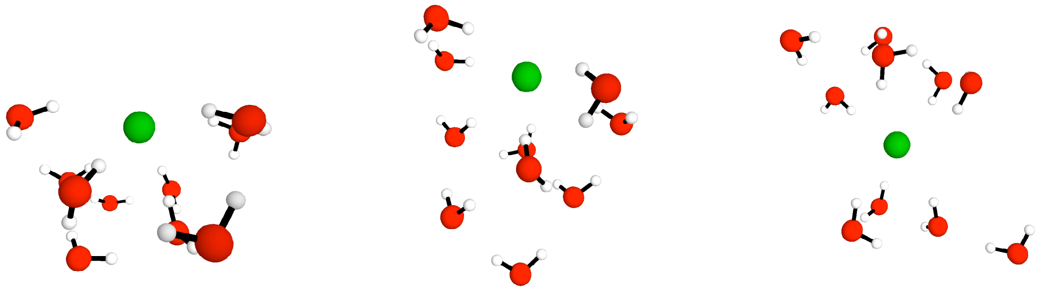

CL10A* (7) + [3]

CL10B (7) + [2] + {1}
1.2 (0.3) [1.5]

CL10C# (7) + [3]
3.3 (1.5) [5.2]

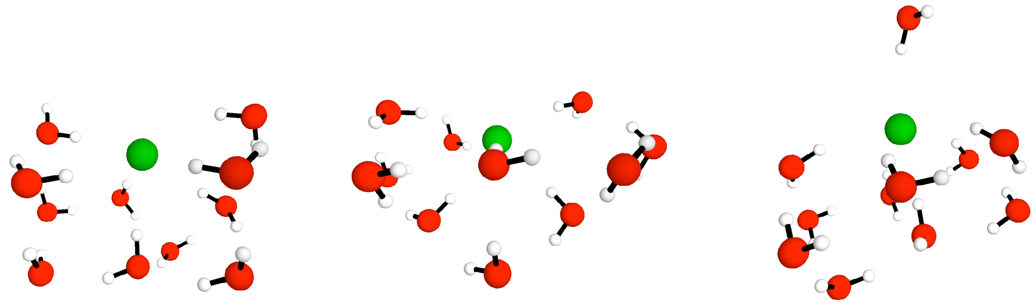

CL11A* (7) + [4]

CL11B (6) + [5]
0.9 (0.2) [1.0]

CL11C# (6,1) + [4]
3.2 (3.2) [4.2]

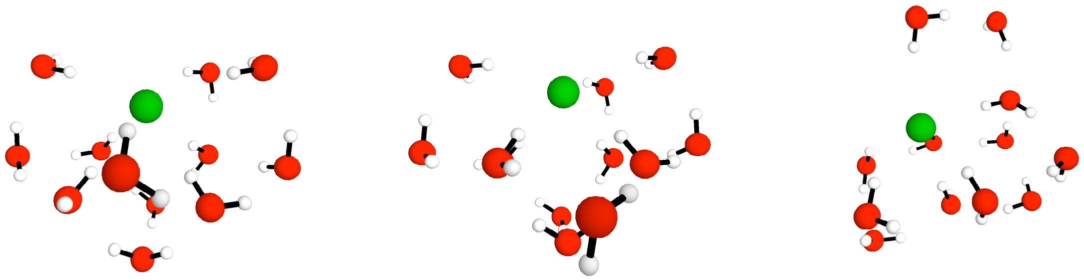

CL12A* (7) + [5]

CL12B (7) + [5]
0.0 (-0.3) [-0.2]

CL12C# (7) + [5]
3.9 (3.5) [4.1]

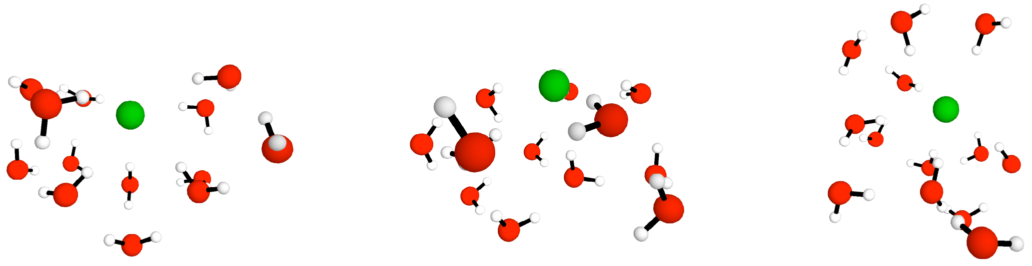

CL13A* (8) + [5]

CL13B (6) + [6] + {1}
0.7 (-0.5) [-0.9]

CL13C# (7) + [6]
2.9 (2.1) [4.5]

Figure 2.6. Local minimum structures for $Cl^-(H_2O)_n$, n=10-13. The same nomenclature and format of Figure 2.5 is used here. Although interior anions exist for each value of n, none of these are the global minimum structure.

المنارة للاستشارات

www.manaraa.com

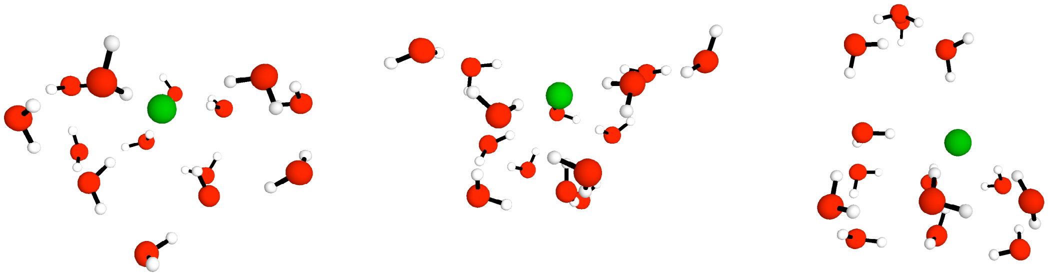

CL14A* (7) + [7]

CL14B (8) + [6]
0.5 (0.6) [0.6]

CL14C# (7) + [6] + {1}
4.5 (4.1) [7.1]

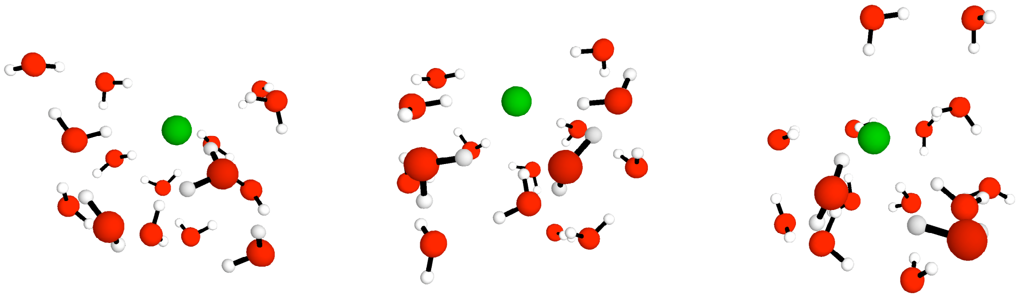

CL15A* (8) + [7]

CL15B (7) + [7] + {1}
0.2 (-1.9) [-1.5]

CL15C# (8) + [7]
4.1 (3.1) [4.3]

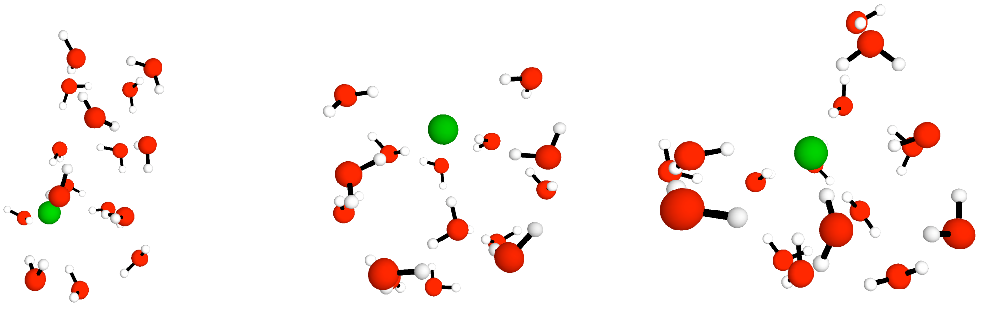

CL16A* (7) + [6] + {3}

CL16B (7) + [7] + {2}
1.0 (1.7) [0.4]

CL16C# (8) + [8]
2.0 (3.0) [2.9]

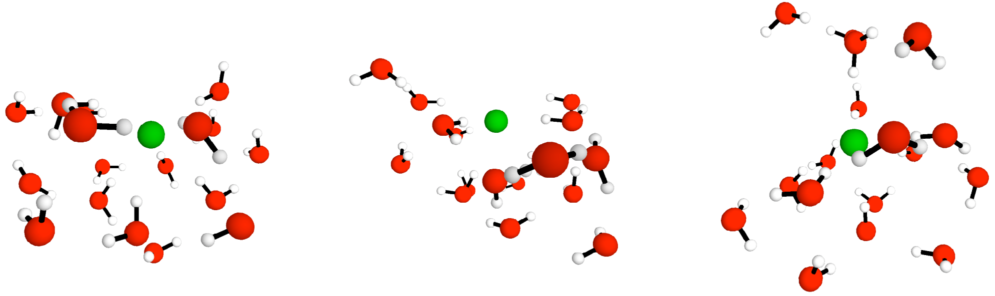

CL17A* (8) + [9]

CL17B (7) + [8] + {2}
2.1 (-0.3) [1.9]

CL17C# (8) + [9]
1.7 (-0.1) [1.6]

Figure 2.7. Three structures for $Cl^-(H_2O)_n$, n=14-17. The same nomenclature and format of Figures 2.5 and 2.6 is used here again. As with the smaller clusters, none of the interior anions are global minimum structures.

www.manaraa.com

Figures 2.5-2.7 give local minima for $Cl^-(H_2O)_n$ for n=6-17. As for F^-, the first interior anions are observed for $Cl^-(H_2O)_n$ when n=6; the lowest energy example is given in the third column of Figure 2.5. As the water cluster size grows, the anion approaches complete solvation. The interior anions do not exist as global minima until the completely solvated structure is found (n=18): Recall the global minima in Figure 2.3 for examples of interior anions. Somewhat greater disagreement among the three levels of theory is observed for Cl^- than for F^-. Disparities as large as 2-3 kcal/mol are found for CL7B and CL7C#, for example. In nearly all cases, EFP and HF are in good agreement, whereas these two methods deviate somewhat from the MP2 relative energies. Therefore, these errors arise from deficiencies in the HF method, from which this EFP method is derived, and are not inherent in the EFP approach itself. Nonetheless, the three methods do consistently predict similar trends with regard to the relative stabilities of interior versus exterior structures.

Positive relative energies for n=18 illustrate the stability of the fully solvated anion relative to the partially solvated anion. HF and MP2 single point energies at the five lowest EFP structures for $Cl^-(H_2O)_{18}$ predict that the global minimum is the completely solvated CL18A* structure (see Figure 2.8). The EFP, HF and MP2 relative energies predict a fully solvated anion to be lower in energy by 4.3, 1.8, 4.2 kcal/mol, respectively. HF and MP2 single points at the five lowest EFP structures for n=20 suggest a completely solvated anion to be more stable than a partially solvated anion by 1.3 (EFP), 2.1 (HF), 4.2 (MP2) kcal/mol.

www.manaraa.com

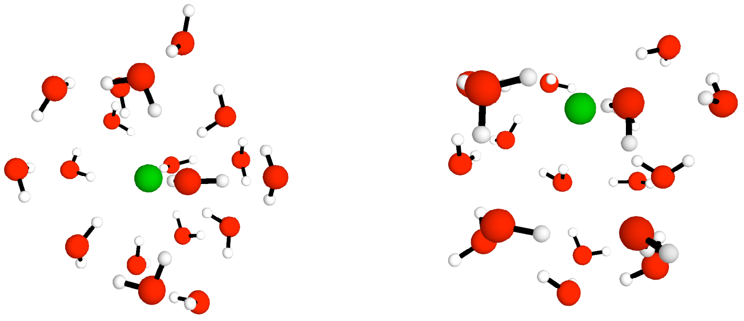

CL18A* (8) + [10]

CL18B& (7) + [8] + {3}
4.3 (1.8) [4.2]

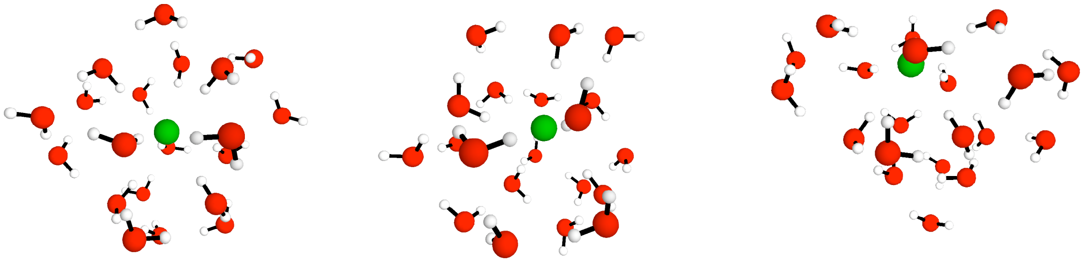

CL20A

CL20B (8) + [12]
0.6 (-1.1) [0.7]

CL20C& (8) + [10] + {2}
3.6 (3.1) [6.3]

Figure 2.8. The local minima $Cl^-(H_2O)_n$ for n=18,20. The global minima for n=18 and n=20 are interior anions and are completely solvated. The relative energies between the global minimum and the lowest energy surface anion is larger for n=20. The structures in the last column are marked by & and are the lowest energy structures that are not completely solvated.

Larger energy differences between interior and surface anions are observed for $Cl^-(H_2O)_n$ than for $F^-(H_2O)_n$. The source of these higher energy differences may be the fact that Cl- resists becoming an interior anion until complete solvation is obtained at n=18. Comparing the experimental differential binding energies for each anion in Tables 2.1 and 2.2 show that small water clusters are more tightly bound to F- than Cl-. The strong interaction between F- and water molecules is likely to encourage interactions between the water cluster and the anion resulting in interior anions that are relatively lower in energy than the analogous chloride structures.

المنارة للاستشارات

www.manaraa.com

Table 2.1

Differential binding energies for F-(H2O)n are given at the EFP, HF and MP2 levels of theory. The error columns were obtained by taking the difference between the predicted value for a given value of n and the experimental value. Percent errors were calculated by dividing the error column by the experimental column and multiplying by 100. All values are in kcal/mol.

F-

n # Water	Experiment[a,b]	EFP/HF	Error	% Error	HF	Error	% Error	MP2	Error	% Error
1	-23.3	-17.3	6.0	25.7	-20.2	3.1	13.5	-20.8	2.5	10.7
2	-19.2	-15.3	3.9	20.1	-17.2	2.0	10.3	-17.9	1.3	6.6
3	-15.3	-14.0	1.3	8.8	-14.1	1.2	7.6	-15.3	0.0	0.2
4	-13.9	-12.4	1.5	11.0	-11.4	2.5	18.0	-13.2	0.7	4.8
5	-12.3	-10.1	2.2	18.2	-10.1	2.2	17.8	-12.6	-0.3	-2.3
6	-10.9	-10.0	0.9	8.3	-8.5	2.4	21.7	-11.6	-0.7	-6.8
7	-10.4	-10.7	-0.3	-2.8	-9.2	1.2	11.9	-12.0	-1.6	-15.8
8	-11.2	-9.6	1.6	14.6	-8.5	2.7	24.1	-10.9	0.3	2.4
9	-11.1	-7.9	3.2	28.5	-7.4	3.7	33.5	-9.3	1.8	16.5
10		-9.7			-8.4			-11.7		
11		-7.3			-7.1			-9.9		
12		-8.7			-8.6			-11.0		
13		-9.1			-7.8			-11.5		
14		-8.3			-6.6			-11.0		
15		-8.6			-5.7			-8.5		

[a] Reference 70
[b] Reference 71

www.manaraa.com

Table 2.2

Differential binding energies for $Cl^-(H_2O)_n$ at the EFP, HF and MP2 levels of theory. All values are kcal/mol. Values were obtained in the same manner as in Table 1.

Cl-										
n # Water	Experiment[a]	EFP/HF	Error	% Error	HF	Error	% Error	MP2	Error	% Error
1	-14.7	-10.8	3.9	26.2	-10.4	4.3	29.0	-12.4	2.3	15.8
2	-13.0	-10.3	2.7	20.5	-9.5	3.5	27.2	-11.7	1.3	9.7
3	-11.8	-10.6	1.2	10.2	-9.0	2.8	24.1	-12.3	-0.5	-4.4
4	-10.6	-9.1	1.5	14.2	-8.8	1.8	17.1	-10.7	-0.1	-1.3
5	-9.5	-8.3	1.2	12.2	-6.6	2.9	30.7	-9.5	0.0	0.3
6	-8.8	-10.1	-1.3	-14.3	-8.2	0.6	7.3	-12.2	-3.4	-38.9
7		-8.7			-7.9			-10.6		
8		-6.5			-5.3			-7.6		
9		-8.6			-7.1			-10.0		
10		-7.4			-5.7			-8.1		
11		-9.7			-9.1			-12.3		
12		-7.8			-6.2			-9.1		
13		-6.6			-6.1			-9.6		
14		-7.3			-6.7			-9.0		
15		-6.5			-5.6			-8.5		
16		-8.0			-7.0			-9.7		
17		-8.7			-5.4			-9.9		
18		-8.6			-7.3			-12.8		

www.manaraa.com

C. Binding energies

Binding energies and differential binding energies were calculated for $F^-(H_2O)_n$ (n=1-15) and $Cl^-(H_2O)_n$ (n=1-18) at the EFP/HF, HF and MP2 levels of theory. Boltzmann averaged energies were calculated for each water cluster using the Boltzmann equation:

$$\frac{\sum_i X_i e^{-\Delta E_i / RT}}{\sum_i e^{-\Delta E_i / RT}} = \mathbf{E_n} \qquad \textbf{(2)}$$

where X_i is the calculated energy of the *ith* structure including a zero point vibrational energy correction (obtained from the EFP/HF Hessians). ΔE_i is calculated by taking the difference between the energy of the *ith* structure and the lowest energy structure of a given cluster of n water molecules; T = 298 K. The result, E_n, is the Boltzmann averaged energy for all structures composed of n water molecules.

The differential binding energy is defined as the energy difference for the following process:

$$\mathbf{\Delta D_e = X^-(H_2O)_n + H_2O \rightarrow X^-(H_2O)_{n+1}} \qquad \textbf{(3)}$$

where X= F^- (Cl^-) and n=0-14 (0-17). The differential binding energies were calculated by taking the Boltzmann averaged energy for $X^-(H_2O)_{n+1}$ and subtracting it from the sum of the Boltzmann averaged energy for $X^-(H_2O)_n$ and the energy of one water molecule. The calculated differential binding energies are compared with available experimental values in Table 2.1 and Table 2.2.

www.manaraa.com

Table 2.3

Total binding energies (kcal/mol) for $F^-(H_2O)_n$ are given at the EFP, HF and MP2 levels of theory. The error columns were obtained by taking the difference between the predicted value for a given value of n and the experimental value. Percent errors were calculated by dividing the error column by the experimental column and multiplying by 100.

F-

n # Water	Experiment[a,b]	EFP/HF	Error	% Error	HF	Error	% Error	MP2	Error	% Error
1	-23.3	-17.3	6.0	25.7	-20.2	3.1	13.5	-20.8	2.5	10.7
2	-42.5	-32.7	9.8	23.2	-37.4	5.1	12.0	-38.7	3.8	8.9
3	-57.8	-46.6	11.2	19.4	-51.5	6.3	10.9	-54.0	3.8	6.6
4	-71.7	-59.0	12.7	17.7	-62.9	8.8	12.3	-67.2	4.5	6.2
5	-84.0	-69.0	15.0	17.8	-73.0	11.0	13.1	-79.8	4.2	5.0
6	-94.9	-79.0	15.9	16.7	-81.6	13.3	14.1	-91.5	3.4	3.6
7	-105.3	-89.7	15.6	14.8	-90.7	14.6	13.8	-103.5	1.8	1.7
8	-116.5	-99.3	17.2	14.8	-99.2	17.3	14.8	-114.4	2.1	1.8
9	-127.6	-107.2	20.4	16.0	-106.6	21.0	16.5	-123.7	3.9	3.0
10		-116.9			-115.0			-135.4		
11		-124.2			-122.1			-145.3		
12		-132.9			-130.7			-156.3		
13		-142.1			-138.5			-167.7		
14		-150.3			-145.1			-178.7		
15		-159.0			-150.8			-187.2		
17		-171.4			-162.1			-203.8		

[a] Reference 70

[b] Reference 71

المنارة للاستشارات

www.manaraa.com

Table 2.4
Total binding energies (kcal/mol) for $Cl^-(H_2O)_n$ at the EFP, HF and MP2 levels of theory. Values were obtained in the same manner as in Table 3.

Cl-										
n # Water	Experiment[a]	EFP/HF	Error	% Error	HF	Error	% Error	MP2	Error	% Error
1	-14.7	-10.8	3.9	-26.2	-10.4	4.3	-29.0	-12.4	2.3	-15.8
2	-27.7	-21.2	6.5	-23.5	-19.9	7.8	-28.2	-24.1	3.6	-12.9
3	-39.5	-31.8	7.7	-19.6	-28.9	10.6	-26.9	-36.4	3.1	-7.8
4	-50.1	-40.9	9.2	-18.4	-37.6	12.5	-24.9	-47.2	2.9	-5.8
5	-59.6	-49.2	10.4	-17.4	-44.2	15.4	-25.8	-56.7	2.9	-4.9
6	-68.4	-59.3	9.1	-13.3	-52.4	16.0	-23.4	-68.9	-0.5	0.7
7		-68.0			-60.2			-79.5		
8		-74.4			-65.5			-87.1		
9		-83.0			-72.6			-97.1		
10		-90.5			-78.3			-105.2		
11		-100.1			-87.3			-117.5		
12		-107.9			-93.6			-126.6		
13		-114.5			-99.6			-136.2		
14		-121.8			-106.3			-145.2		
15		-128.3			-111.9			-153.7		
16		-136.3			-118.9			-163.4		
17		-145.0			-124.4			-173.3		
18		-153.6			-131.7			-186.0		
20		-169.2			-146.2			-206.7		

[a] Reference 70

www.manaraa.com

The total binding energy is:

$$\mathbf{D_e = X^- + nH_2O \rightarrow X^-(H_2O)_n} \qquad \mathbf{(4)}$$

The binding energies were calculated by taking the sum of the energy of the anion and n water molecules and subtracting it from the Boltzmann averaged energy for the $X^-(H_2O)_n$ system. The results of these calculations are given in Table 3 and Table 4.

Both the experimental and calculated differential binding energies generally decrease with increasing n. For Cl^-, the experimental values decrease monotonically, through n=6, while some fluctuations are observed for all of the computed ΔD_e values. For F^-, some fluctuations are found for both experiment and theory. The fluctuations are not consistent enough to be explained by obvious structural differences for the smaller clusters.

The most surprising fluctuation occurs for $Cl^-(H_2O)_{18}$, for which MP2 predicts that the 18th water molecule is more tightly bound than the first! It may be that the unexpectedly high differential binding energy for n=18 is due to the fact that the 18th water molecule enables the water cluster to form an interior anion and to completely solvate Cl^-. While there is a smaller fluctuation at the HF level from n=17 to n=18, no significant fluctuation exists for EFP. Similar fluctuations were found by Webb and Merrill, for small values of n.

With some exceptions, the error in differential binding energies decreases as n increases, so the percent error is roughly constant. The HF errors are somewhat larger than those found for the EFP method while, not surprisingly, MP2 is in the best agreement with experiment.

In general, the HF and EFP total binding energies are in good agreement with each other, with errors of approximately 15-25% relative to the experimental values. So, once

www.manaraa.com

again, errors in the EFP predictions most likely reflect inadequacies in the underlying HF method upon which the EFP parameterization is based,[1,2] rather than on any inherent failing of the EFP method itself. Both methods exhibit the correct qualitative trends when compared with experiment, but have significant quantitative errors. However, the MP2 total binding energies agree both quantitatively and qualitatively with experiment, suggesting the importance of dynamic correlation.

D. A Comparison between $F^-(H_2O)_n$ and $HF(OH^-)(H_2O)_{n-1}$

In order to further assess the reliability of the EFP method, MP2 geometry optimizations were performed on the lowest energy structures for $F^-(H_2O)_n$ n=1-4. Since the EFP method[1,2] freezes the internal coordinates of the water molecule, it is important to determine the impact of this approximation. In the fully MP2 optimizations, the internal coordinates of the water molecules were not constrained.

The MP2 optimizations explored both $F^-(H_2O)_n$ (n=1-4) and HF + OH^- + (n-1) H_2O. The latter system could be formed from the former if the fluoride anion extracts a proton from one of the water molecules. If HF + OH^- + (n-1) H_2O is the global minimum, especially if $F^-(H_2O)_n$ is not even a local minimum, the EFP method would be less meaningful for those values of n.

The MP2 potential energy surface of $F^-(H_2O)$ was calculated previously by Janoschek[37] who chose a 6-311+G(2df,p)[66,67] basis set. For consistency, the 6-311++G(2df,p) basis set was used. The optimized MP2 structure for $F^-(H_2O)$ agrees well with the global minimum found by Janoschek. $HF(OH^-)$ is not a minimum on the potential energy surface. The formation of HF is first observed when two water molecules are present to stabilize its coexistence with OH^-. The resulting equilibrium geometry, F3D in Figure 2.9, is a local

www.manaraa.com

minimum. At the CCSD(T)//MP2 level of theory, this local minimum is 5.8 kcal/mol above the $F^-(H_2O)_3$ global minimum. The HF bond distance in F3D is 1.06Å, while that of an unsolvated hydrogen fluoride molecule is 0.96Å. So, the HF bond is stretched due to the presence of the OH^-.

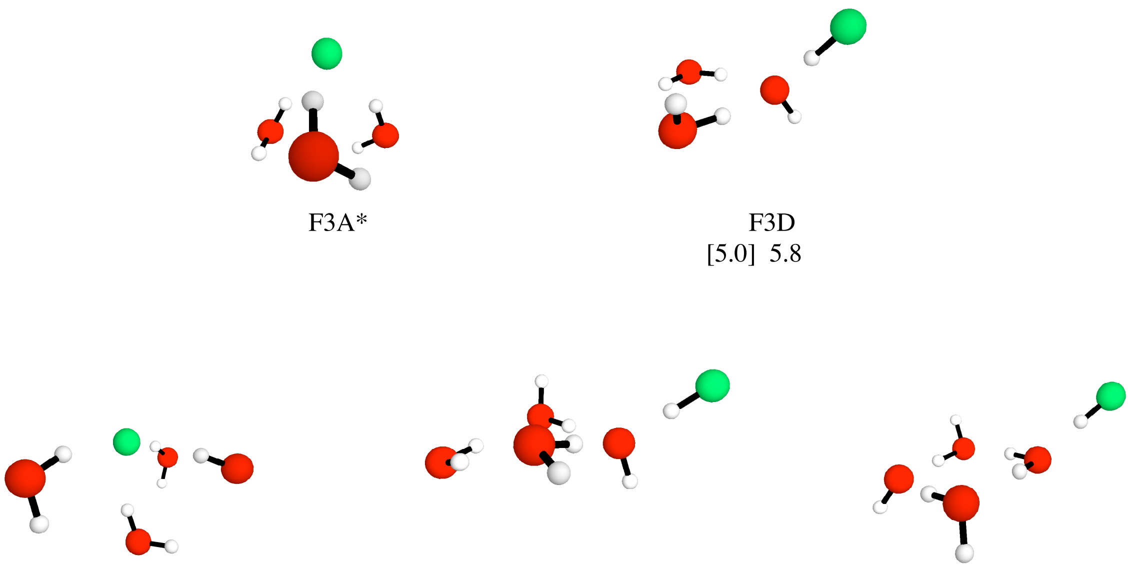

F3A*

F3D
[5.0] 5.8

F4A*

F4D
[5.7] 4.5

F4E
[12.9] 11.0

Figure 2.9. $F^-(H_2O)_n$ n=3,4 structures (left) are compared with the HF + OH^- + n H_2O n=2, 3 structures. The solvated fluoride structure is the global minimum in both cases and is marked by an asterisk. Relative energy differences in kcal/mol are given at the [MP2] and CCSD(T) levels of theory.

Two local minima for HF + OH^- + $3H_2O$ are shown in Figure 2.9. One structure involves a hydrogen bond between HF and hydroxide (structure F4D), while the other involves a hydrogen bond between HF and a water molecule (F4E). At the CCSD(T) level of theory, structure F4D (F4E) is 4.5 (11.0) kcal/mol higher than the solvated fluoride anion shown as structure F4A.

These results suggest that while HF + OH^- do coexist with solvated F^-, they are higher on the potential energy surface. Using frozen internal coordinates in the EFP method is

www.manaraa.com

therefore reasonable for studying the solvated anions because protons are not easily extracted from the water molecules.

IV. Conclusions

The EFP method coupled with Monte Carlo simulations was employed to study the solvation of fluoride and chloride anions. The method provides a reliable approach for analyzing anion solvation. The EFP, HF and MP2 calculations predict that no fewer than 15 water molecules are required to fully solvate a single fluoride anion. All three levels of theory predict that 18 water molecules are required for complete solvation of the chloride anion. The frozen internal coordinates of the EFP are appropriate for studying small water clusters in the presence of F^-, since proton transfer from a water molecule to the anion is not favored thermodynamically. It is important to keep in mind, of course, that these results are based on electronic energies at 0K. It possible that the incorporation of temperature and entropic effects could modify the number of waters needed to make interior anions most favorable.

All three levels of theory predict the correct qualitative trends for both total and differential binding energies. MP2 binding energies are quantitatively accurate for both the fluoride and the chloride anion when compared to experimental values. EFP and HF errors are similar, suggesting that these errors are inherent in the HF method, from which this version of the EFP method is derived. Chloride differential binding energies fluctuate as a function of n for all levels of theory. The largest error in nearly all cases arises from the binding of the first water molecule to the anion.

Acknowledgements

المنارة للاستشارات

www.manaraa.com

Funding for this study was provided by an NSF REU program, the Air Force Office of Scientific Research, and the Iowa State University Chemistry Department. Several helpful discussions with Drs. Simon Webb and Grant Merrill are gratefully acknowledged. The authors would also like to thank Professor Tony Haymet for suggesting this project, and Professor Benny Gerber for helpful discussions.

References

1. Day, P. N.; Jensen, J. H.; Gordon, M. S.; Webb, S. P.; Stevens, W. J.; Krauss, M.; Garmer, D.; Basch, H.; Cohen, D. *J. Chem. Phys.* **1996**, *105*, 1968.
2. Gordon, M. S.; Freitag, M. A.; Bandyopadhyay, P.; Jensen, J. H.; Kairys, V.; Stevens, W. J. *J. Phys. Chem. A* **2001**, *105*, 293.
3. Hall, R. J.; Hillier, I. H.; Vincent, M. A.; *Chem. Phys. Lett.* **2000**, *320*, 139.
4. Majumdar, D.; Kim, J.; Kim, K. S.; *J. Chem. Phys.* **2000**, *112*, 101.
5. Vaughn, S. J.; Akhmatskaya, E. V.; Vincent, M. A.; Masters, A. J.; Hillier, I. H. *J. Chem. Phys.* **1999,** *110*, 4338.
6. Baik, J.; Kim, J.; Majumdar, D.; Kim, K. S. *J. Chem. Phys.* **1999,** *110*, 9116.
7. Bryce, R. A.; Vincent, M. A.; Hillier, I. H. *J. Phys. Chem.* **1999**, *103*, 4094.
8. Xantheas, S. S.; Dunning Jr., T. H. *J. Phys. Chem.* **1994**, *98*, 13489.
9. Hobza, P.; Sauer, J.; *Theor. Chim. Acta.* **1984**, *65*, 279.
10. Kim, J.; Lee, H. M.; Suh, S. B.; Majumdar, D.; Kim, K. S. *J. Chem. Phys.* **2000**, *113*, 5259.
11. Gamba, A.; Manunza, B.; Gatti, C.; Simonetta, M. *Theor. Chim. Acta.* **1983**, *63*, 245.
12. Probst, M. M.; Rode, B. M.; *J. Mol. Structure: THEOCHEM* **1982**, *88*, 91.
13. Cabarcos, O. M.; Weinheimer, C. J.; Lisy, J. M.; Xantheas, S. S. *J. Chem. Phys.* **1999**, *110*, 5.
14. Gora, R. W.; Roszak, S.; Leszczynski, J. *Chem. Phys. Lett.* **2000**, *325*, 7.
15. Choi, J.; Kuwata, K. T.; Cao, Y.; Okumura, M. *J. Phys. Chem. A.* **1998**, *102*, 503.
16. Truong, T. N.; Stefanovich, E. V. *Chem. Phys. Lett.* **1996**, *256*, 348.
17. Xantheas, S. S. *J. Phys. Chem.* **1996**, *100*, 9703.
18. Schindler, T. Berg, C.; Niedner-Schatteburg, G.; Bondybey, V. E. *J. Phys. Chem.* **1995**, *99*, 12434.
19. Combariza, J. E.; Kestner, N. R.; Jortner, J. *J. Chem. Phys.* **1994**, *100*, 2851.
20. Asada, T.; Nishimoto, K.; Kitaura, K. *J. Phys. Chem.* **1993**, *97*, 7724.
21. Foresman, J. B.; Brooks III, C. L. *J. Chem. Phys.* **1987**, *87*, 5892.
22. Chaban, G. M.; Jung, J. O.; Gerber, R. B. *J. Phys. Chem. A* **2000**, *104*, 2772.
23. Morita, A.; Hynes, J. T.; *Chem. Phys.* **2000**, *258*, 371.
24. Topol, I. A.; Tawa, G. J.; Burt, S. K. *J. Chem. Phys.* **1999**, *111*, 10998.
25. Combariza, J. E.; Kestner, N. R. *J. Phys. Chem.* **1995**, *99*, 2717.
26. Caldwell, J. W.; Kollmar, P. A. *J. Phys. Chem.* **1992**, *96*, 8249.
27. Kistenmacher, H.; Popkie, H.; Clementi, E.; *J. Chem. Phys.* **1973**, *59*, 5842.

www.manaraa.com

28. Xantheas, S. S.; Dang, L. X. *J. Phys. Chem.* **1996**, *100*, 3989.
29. Zhao, X. G.; Gonzalez-Lafont, A.; Truhlar, D. G.; Stecker, R. *J. Chem. Phys.* **1991**, *94*, 5544.
30. Tobias, D. J.; Jungwirth, P.; Parrinello, M. *J. Chem. Phys.* **2001**, *114*, 7036.
31. Lee, H. M.; Kim, D.; Kim, K. S. *J. Chem. Phys.* **2002**, *116*, 5509.
32. Perera, L.; Berkowitz, M. L. *J. Chem. Phys.* **1994**, *100*, 3085.
33. Dang, L. X. *J. Chem. Phys.* **1992**, *96*, 6970.
34. Cabarcos, O. M.; Weinheimer, C. J.; Lisy, J. M.; Xantheas, S. S. *J. Chem. Phys.* **1999**, *110*, 5.
35. Jorgensen, W. L.; Severance, D. L.   *J. Chem. Phys.* **1993**, *99*, 4233.
36. Gao, J.; Garner, D. S.; Jorgensen, W. L. *J. Am. Chem. Soc.* **1986**, *108*, 4784.
37. Janoschek, R. *Mol. Phys.* **1996**, *89*, 1301.
38. Perera, L.; Berkowitz, M. L. *J. Chem. Phys.* **1991**, *95*, 1954.
39. Yoo, S.; Lei, Y. A.; Zeng, X. C.; *J. Chem. Phys.* **2003**, *119*, 6083.
40. Heuft, J. M.; Meijer, E. J. *J. Chem. Phys.* **2003**, *119*, 11788.
41. Ayala, R.; Martinez, J. M.; Pappalardo, R. R.; Marcos, E. S. *J. Chem. Phys.* **2003**, *119*, 9538.
42. Jungwirth, P.; Tobias, D. J.; *J. Phys. Chem. A*, **2002**, *106*, 379.
43. Merrill, G. N.; Webb, S. P. *J. Phys. Chem. A*, **2003**, *107*, 7852.
44. Heuft, J. M.; Meijer, E. J. *J. Chem. Phys.* **122,** 094501 (2005)
45. Heuft, J. M.; Meijer, E. J. *J. Chem. Phys.* **2003,** *119,* 11788.
46. Hagberg, D.; Brdarski, S.; Karlström, G. *J. Phys. Chem. B.* **2005**, *109*, 4111.
47. Ayala, R.; Martinez, J. M.; Pappalardo, R. R.; Marcos, E. S. *J. Chem. Phys.* **2004,** *121,* 7269.
48. Perera, L.; Berkowitz, M. L. *J. Chem. Phys.* **1992**, *96*, 8288.
49. Markovich, G.; Giniger, R.; Levin, M.; Cheshnovsky, O. *Zeitschrift fur Physik D*, **1991**, *20*, 69-72.
50. Markovich, G.; Pollack, S.; Giniger, R.; Cheshnovsky, O. *J. Chem. Phys.* **1994**, *101*, 9344.
51. Pople, J. A.; Binkley, J. S.; Seeger, R. *Int. J. Quantum Chem. Sym.* **1976,** *10,* 1.
52. Frisch, M. J.; Head-Gordon, M.; Pople, J. A. *Chem. Phys. Lett.* **1990,** *166,* 275.
53. Fletcher, G. D.; Schmidt, M. W.; Gordon, M. S. *Adv. Chem. Phys.* **1999,** *110,* 267.
54. Aikens, C. M.; Webb, S. P.; Bell, R. L.; Fletcher, G. D.; Schmidt, M. W.; Gordon, M. S. *Theor. Chem. Acc.,* **2003,** *110,* 233.
55. Merrill, G.N.; Webb, S. P.; Bivin, D. B. *J. Phys. Chem. A* **2003,** *107*, 386.
56. Webb, S. P.; Gordon, M. S. *J. Phys. Chem. A* **1999,** *103,* 1265.
57. Adamovic, I.; Gordon, M. S. *J. Phys. Chem. A.* **2005,** *109,* 1629.
58. Day, P. N.; Pachter, R.; Gordon, M. S.; Merrill, G. N. *J. Chem. Phys.* **2000,** *112,* 2063.
59. Hehre, W. J.; Ditchfield, R.; Pople, J. A. *J. Chem. Phys.* **1972,** *56,* 2257.
60. Francl, M. M.; Pietro, W. J.; Hehre, W. J.; Binkley, J. S.; Gordon, M. S.; DeFrees, D. J. Pople, J. A. *J. Chem. Phys.* **1982,** *77,* 3654.
61. Hariharan, P.C.; Pople, J.A. *Theor. Chim. Act.* **1973,** *28*, 213.
62. Clark, T.; Chandrasekhar, J.; Schleyer, P.V.R. *J. Comp. Chem.* **1983,** *4*, 294.

المنارة للاستشارات

63. Schmidt, M. W.; Baldridge, K. K.; Boatz, J. A.; Jensen, J. H.; Koseki, S.; Matsunaga, N.; Gordon, M. S.; Ngugen, K. A.; Su, S.; Windus, T. L.; Elbert, S. T.; Montgomery, J.; Dupuis, M., *J. Comput. Chem.* **1993**, *14*, 1347.
64. Metropolis, N.; Rosenbluth, A.; Tellor, A. *J. Chem. Phys.* **1953,** *21,* 1089.
65. Kirkpatrick, S.; Gelatt, C. D.; Vecchi, M. P. *Science* **1983,** *220*, 671.
66. Krishnan, R.; Binkley, J. S.; Pople, J.A. *J. Chem. Phys.* **1980,** *72*, 650.
67. Frisch, M. J.; Pople, J. A.; Binkley, J. S. *J. Chem. Phys.* **1984,** *80,* 3265.
68. Crawford, T. D.; Schaefer, H. F.; Lipkowitz, K. B.; Boyd, D. B. *Rev. Comput. Chem.* **2000,** *14,* 33.
69. Piecuch, P.; Kucharski, S. A.; Kowalski, K.; Musial, M. *Comput. Phys. Commun.* **2002,** *149,* 71.
70. Hiraoka, K.; Mizuse, S.; Yamabe, S. *J. Phys. Chem.* **1988**, *92*, 3943.
71. Arshadi, M.; Yamdagni, R.; Kebarle, P**.** *J. Phys. Chem.* **1970,** *74,* **1474**

المنارة للاستشارات

www.manaraa.com

CHAPTER 3. DIPOLE MOMENT OF WATER IN THE PRESENCE OF OTHER WATER MOLECULES

A paper published in the Journal of Physical Chemistry A

Daniel D. Kemp, Mark S. Gordon

Abstract

The dipole moment of the gas phase water monomer is 1.85D. When solvated in bulk water, the dipole moment of an individual water molecule is observed to be enhanced to the much larger value of 2.9 ± 0.6D. In order to understand the origin of this dipole moment enhancement, the effective fragment potential (EFP) method is used to solvate an *ab initio* water molecule to predict the dipole moments for various cluster sizes. The dipole moment as a function of cluster size, nH_2O, is investigated (for n=6-20 (even n), 26, 32, 41, and 50). Localized charge distributions are used in conjunction with localized molecular orbitals to interpret the dipole moment enhancement. These calculations suggest that the enhancement of the dipole moment originates from the decrease of the angle between the dipole vectors of the lone pairs on oxygen as the number of hydrogen bonds to that oxygen increases. Thus, the decreased angle, and the consequent increase in water dipole moment, is most likely to occur in environments with a larger number of hydrogen bonds, such as the center of a cluster of water molecules.

I. Introduction

Water is arguably the most important liquid and solvent, especially for biological and biochemical applications. Despite its broad impact and importance, many properties of water are not fully understood. One important property is the dipole moment of water, which has been the subject of many experimental[1-6] and theoretical[7-52] investigations. Though the dipole

المنارة للاستشارات

www.manaraa.com

moment of the water monomer has been experimentally[1-2, 4-6] and computationally[7-9] determined to be 1.85 D, there has been only one experimental report regarding the dipole moment of a water molecule in bulk liquid water: Badyal et al[3] employed x-ray diffraction experimental techniques to determine that the dipole moment of a solvated water molecule is 2.9 ± 0.6 D.

Many theoretical studies have predicted the dipole moments of water clusters.[9-53] These calculations have employed a variety of methods, including fully *ab initio* calculations on relatively small clusters[9] (n=1-6), molecular dynamics simulations on larger clusters using model potentials (n=216,[13,14] n=256,[12,15] n=512[10]), and a mix of quantum mechanical/molecular mechanical (QM/MM) methods[17-19]. Some studies have focused on the dipole moment of a single water molecule in an ice lattice[20-23]. Each of these studies produces a slightly different result, with most estimating that the dipole moment of a water molecule in the bulk falls in the range 2.5D-3.5D.

The methods that use model potentials[10-15,24] that include a polarization term generally predict dipole moments more accurately than those that employ model potentials without polarization. Potentials that include only point charges and electrostatics apparently do not accurately predict the dipole moment enhancement. Dang[11] has developed a polarizable potential and has predicted average dipole moments per water molecule that closely resemble the MP2 study of Gregory[9] et. al for n=1-6. The NCC model developed by Niesar et al.[10] adds many-body polarizability to a previously developed potential and obtains an average dipole moment of 2.8D per water molecule in a 512 water molecule cluster.

Tu and Laaksonen[18] predicted the dipole moment of one *ab initio* water molecule solvated by 1-4 water molecules represented by model potentials. The dipole moment of the

المنارة للاستشارات
www.manaraa.com

ab initio water increased to ~2.6D for n=4. Molecular dynamics simulations of 256 water molecules yielded an average value of 2.65 D for each water molecule within the cluster.

The present work systematically examines the dipole moment of an *ab initio* water molecule as a function of the number of additional water molecules that are represented by a sophisticated model potential. In addition, an analysis of the origin of the dipole moment enhancement is presented. The computational methods are presented in Section II. Section III presents the results and discussion of the calculations. This is followed in Section IV by a summary and conclusions.

II. Computational methods

Dipole moments have been calculated by surrounding a quantum mechanics (QM) water molecule by a cluster of n-1 effective fragment potential[54,55] (EFP) waters. An EFP is a explicit model potential that is based on quantum mechanics and implemented in the General Atomic and Molecular Electronic Structure System[56,57] (GAMESS) software suite. The EFP1 method was originally developed to model liquid water interactions. That initial implementation was based on Hartree-Fock, with a goal to reproduce *ab initio* calculations while requiring significantly less computational effort[54]. This method was later extended to model water at the DFT level of theory[58]. It was demonstrated in the latter work that a combination of EFP1/DFT waters with an MP2 substrate provides an efficient and accurate representation of a full MP2 calculation. An EFP includes three separate energy interaction energies: Coulomb, polarization and exchange repulsion + charge transfer. In each EFP, Coulomb interaction sites are placed at all atom centers and all bond midpoints. Polarizability centers are at the centroids of all LMOs. The DFT based EFP1 also includes some correlation effects at short range. Because of the success of the EFP1 model[58-61] for water, a more

المنارة للاستشارات

www.manaraa.com

general model called EFP2 has also been developed[55]. EFP2 can be used to generate a model potential for any species, but EFP2 has not yet been fully interfaced with quantum mechanics. The EFP1/DFT method is used in this paper. The QM water is represented by second order perturbation theory (MP2)[62-65].

For the water monomer, MP2 optimizations were performed using three different basis sets, to assess which basis sets(s) can accurately predict the gas phase water dipole moment: (1) the Dunning-Hay basis set with d and p polarization functions on O and H respectively (DH(d,p))[66], (2) the augmented correlation-consistent double-zeta basis set (aug-cc-pVDZ),[67,68] and (3) the corresponding triple-zeta basis set, aug-cc-pVTZ[67,68].

The general approach used here is similar to that employed by Tu and Laaksonen[18,19]. For clusters containing n water molecules, with n≥1, n-1 waters are represented by EFPs, while the remaining water is described by MP2 with one of the aforementioned basis sets. A Metropolis-based Monte Carlo[69] method was used in conjunction with simulated annealing[70] (SA) to study clusters that contain up to 50 water molecules. For 6-20 water molecules, the MP2 water molecule is described using the DH(d,p), aug-cc-pVDZ and aug-cc-pVTZ basis sets. Monte Carlo (MC) sampling on clusters containing 26, 32, 41, and 50 water molecules employed only the DH (d,p) basis. Dipole moments are predicted for the final structures using the larger basis sets.

The matrix of energy second derivatives (Hessian) was calculated for each structure to ensure that the structure is a local minimum on the potential energy surface and to provide vibrational zero point energies.

In order to analyze the calculated dipole moments for various water clusters, the localized charge distribution (LCD)[73,74] method was employed. Based on the use of the

www.manaraa.com

Hartree-Fock localized molecular orbitals (LMO)[75,76], an LCD is a charge neutral localized system that contains two electrons and two protons. One can therefore calculate origin-invariant LCD dipole moments that sum vectorially to the total molecular dipole moment. These LCD dipoles can then be used to analyze the origin of the dipole moment enhancement. For the LMO and LCD calculations, the QM water is represented by Hartree Fock with the aug-cc-pVTZ basis set, while the remaining waters are represented by EFPs. The LMOs were obtained using the Boys[75] approach first introduced by Edmiston and Ruedenberg[76]. Once the localized charge distributions are determined, individual dipole moments for each LCD can be calculated. Finally, we note that if an entire water cluster were represented by a particular level of electronic structure theory (e.g., MP2) in a supermolecule sense, it would be difficult (although not impossible[77]) to rigorously separate the electron density of each water due to delocalization. Since only one quantum water is present in this work, delocalization effects are not included here.

III. Results and Discussion

A. Water Monomer

As shown in Table 3.1, MP2/DH(d,p) overestimates the monomer dipole moment by approximately 0.3D, while MP2/aug-cc-pVDZ and MP2/aug-cc-pVTZ predict monomer dipole moments that are in excellent agreement with the experimental value.[1,2,4-9] Since the aug-cc-pVTZ basis set is significantly more computationally demanding than the other two basis sets, the strategy followed here is to perform geometry optimizations and MC/SA simulations using the two smaller basis sets, followed by single point calculations with the largest basis set.

www.manaraa.com

Table 3.1. Predicted MP2 dipole for the water monomer using three basis sets. Computational cost is given in basis functions.

Basis Set	# Basis Functions	MP2 Dipole
DH (d,p)	25	2.17 D
aug-cc-pVDZ	43	1.88 D
aug-cc-pVTZ	105	1.85 D

B. Small clusters containing 6-20 water molecules

Day et al[78] have previously performed EFP1/HF Monte Carlo simulations on water clusters $(H_2O)_n$, for even n, ranging in size from 6-20 water molecules. In the present work the minima from this previous effort were used to initiate MC/SA simulations.

In order to sample all possible locations for the ab initio water molecule, the MP2/DH(d,p) water molecule was placed at each unique position within the cluster; then a Monte Carlo simulation was performed. In each case, the lowest energy structure was retained. Once the lowest energy configuration was found for each n, the structure was re-optimized using the DH (d,p) and aug-cc-pVDZ basis sets. Single point energy calculations using the aug-cc-pVTZ basis set were performed at the MP2/aug-cc-pVDZ geometries to predict the dipole moment more accurately.

Example structures and their associated dipole moments for each value of n are given in Figures 3.1-3.3. All figures were produced using MacMolPlt[79]. Energies relative to the global minimum are given in kcal/mol. The MP2/DH(d,p) dipole moment is given followed by the aug-cc-pVDZ dipole moment in parentheses and the aug-cc-pVTZ dipole moment in square brackets.

www.manaraa.com

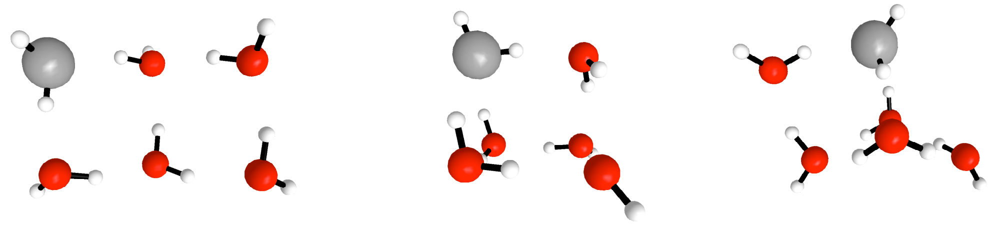

6 H_2O 2.85D (2.68 D) [2.60 D] 2.78 D (2.51 D) [2.46 D] 2.9 D (2.72 D) [2.65 D]

0.0 2.0 2.2 kcal/mol

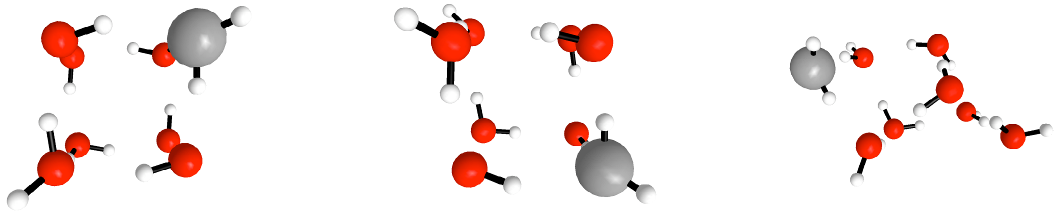

8 H_2O 2.91 D (2.72D) 2.99 D (2.87 D) [2.72 D] 2.91 D (2.79 D) [2.48 D]

0.0 2.8 4.9 kcal/mol

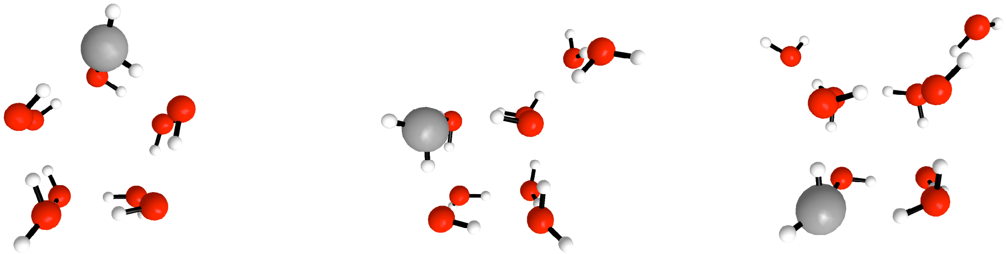

10 H_2O 3.0 D (2.88D) [2.73 D] 2.91 D (2.73 D) [2.65] 2.93 D (2.76 D) [2.63]

0.0 1.2 7.0 kcal/mol

Figure 3.1. A sample of minima from each cluster size containing 6, 8 and 10 water molecules. The DH (d,p) (aug-cc-pVDZ) [aug-cc-pVTZ] dipole (in Debye) of the ab initio water molecule within the cluster is given. The global minimum structure found using the aug-cc-pVDZ is given on the left, with two higher energy structures given for each value of n. Relative energy differences (kcal/mol) from the global minimum are given underneath each structure.

For each value of n, the Boltzmann averaged dipole moment, shown in Table 3.2, was determined for T = 298 K. As noted above for the water monomer, MP2 with the smaller DH (d,p) basis set consistently predicts dipole moments that are 0.1 – 0.2D larger than those predicted by MP2/aug-cc-pVDZ and approximately 0.2-0.3D larger than MP2/aug-cc-pVTZ. The dipole moment enhancement is apparent even at six waters, for which the predicted MP2/aug-cc-pVTZ dipole moment is already 2.54D, about 0.7D larger than that predicted for

www.manaraa.com

the water monomer at the same level of theory, and only ~0.4D less than the experimental value for a water molecule in the bulk environment.

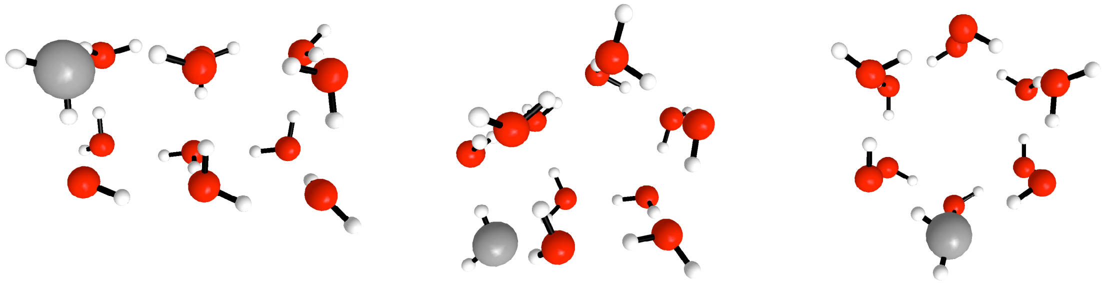

12 H_2O 2.91 D (2.73 D) [2.64] 2.91 D (2.72 D) [2.64] 2.99 D (2.82 D) [2.73]
0.0 0.7 1.6 kcal/mol

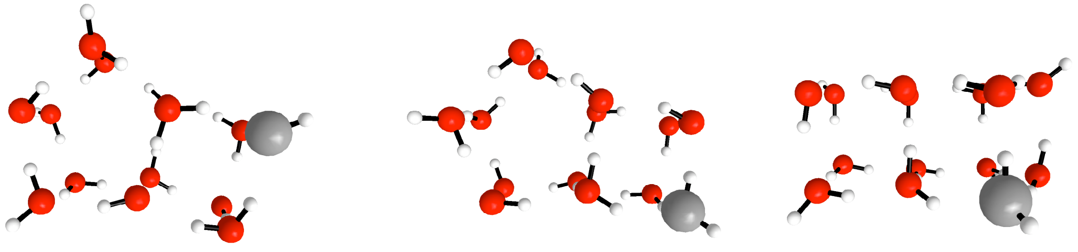

14 H_2O 2.95 D (2.8 D) [2.70 D] 2.92 D (2.74 D) [2.65 D] 2.98 D (2.87 D) [2.73 D]
0.0 0.3 0.7 kcal/mol

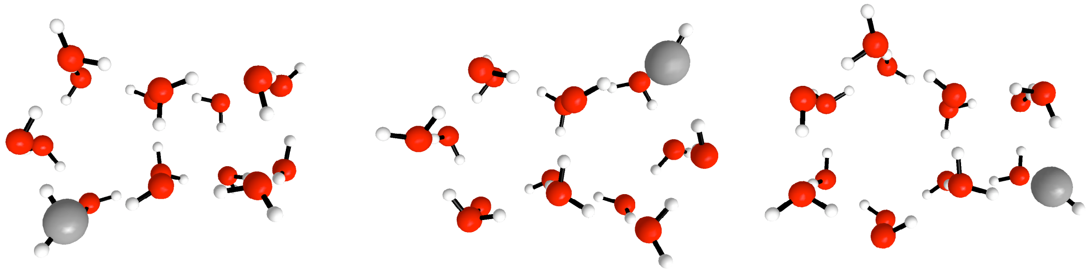

16 H_2O 3.0 D (2.87 D) [2.76] 2.96 D (2.83 D) [2.69 D] 2.93 D (2.76 D) [2.67 D]
0.0 0.4 0.9 kcal/mol

Figure 3.2. Minimum energy structures for n=12, 14 and 16 H_2O. The same format used for the previous figure is used here.

المنارة للاستشارات
www.manaraa.com

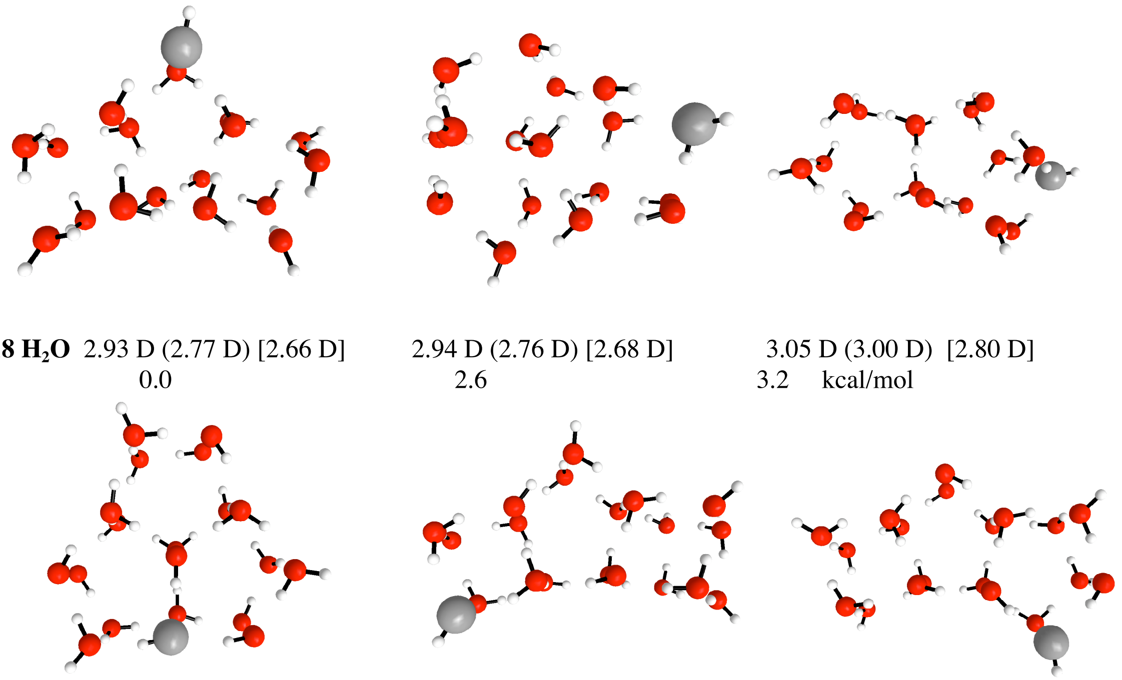

18 H_2O 2.93 D (2.77 D) [2.66 D] 2.94 D (2.76 D) [2.68 D] 3.05 D (3.00 D) [2.80 D]
0.0 2.6 3.2 kcal/mol

20 H_2O 3.16 D (2.97 D) [2.90 D] 2.94 D (2.77 D) [2.69 D] 2.97 D (2.83 D) [2.71 D]
0.0 0.2 2.4 kcal/mol

Figure 3.3. Minima for n= 18, 20. The same format used for the previous two figures is used here.

This is in good agreement with a previous *ab initio* study by Gregory et al[9] in which the MP2 dipole moment of a single water molecule in water hexamer was predicted to be 2.7D. Although the dipole moment fluctuates a bit as the cluster size grows from 6-20, MP2/aug-cc-pVTZ predicts a Boltzmann averaged dipole moment of 2.90 D for 20 water molecules, close to the experimental value for a water molecule in the bulk.

Table 3.2. Boltzmann averaged $(H_2O)_n$ MP2 dipole moments for n=6-20.

n H2O	DH (d,p) Avg. Dipole	aug-cc-pVDZ Avg. Dipole	aug-cc-pVTZ Avg. Dipole
6	2.85	2.67	2.54
8	2.91	2.72	2.64
10	3.00	2.87	2.74
12	2.92	2.76	2.70
14	2.93	2.77	2.67
16	2.98	2.82	2.74
18	2.96	2.77	2.67
20	3.11	2.91	2.90

المنارة للاستشارات

www.manaraa.com

C. Structures containing 26, 32, 41 and 50 water molecules

Monte Carlo simulations were next performed on larger clusters, in order to examine convergence of the predicted dipole moment. As the cluster size increases, the extent of required sampling increases, since the number of possible configurations increases. As before, one water molecule was treated with MP2, while all the other waters are represented by EFP1/DFT.

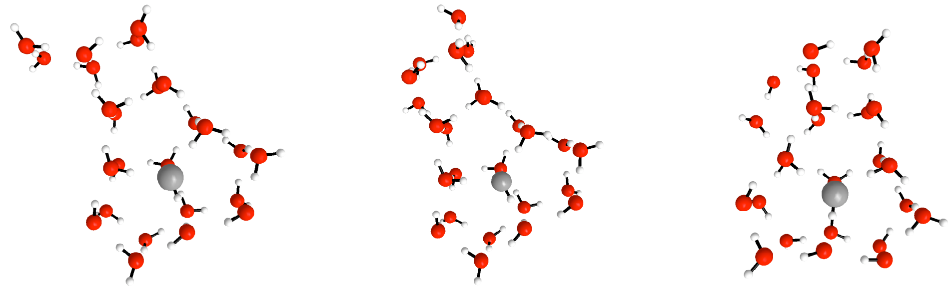

26 H_2O 3.31 D [3.07 D] 3.31 D [3.08D] 3.27 D [3.02 D]
0.0 0.1 3.5 kcal/mol

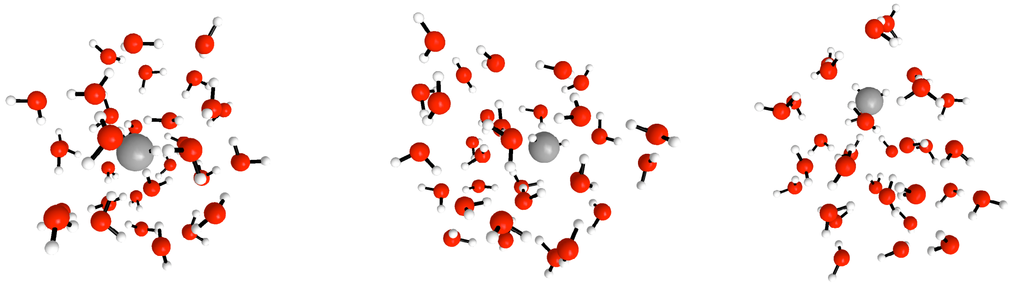

32 H_2O 3.44 D [3.24 D] 3.03 D [2.65 D] 3.29 D [3.03 D]
0.0 0.2 0.6 kcal/mol

Figure 3.4. A sample of minima for 26 and 32 water molecules. The left-most structure is the global minimum structure while the two structures to the right of it are higher-energy structures. The oxygen atom of the ab initio water molecule is shaded and larger in size to illustrate where the ab initio water molecule is located within the cluster. Relative energies (in kcal/mol) and DH (d,p) (aug-cc-pVDZ) [aug-cc-pVTZ] dipoles (in Debye) are given underneath each structure.

Initially, the MP2/DH(d,p) water molecule was placed as close as possible to the center of the water cluster. Of course, no constraints were placed on the Monte Carlo simulations, but experience suggests that dramatic changes in the structure do not occur.

المنارة للاستشارات
www.manaraa.com

Once a sample of structures was found for each cluster size, the results were Boltzmann averaged. Relative energies and sample structures are shown Figures 3.4 and 3.5. The affect of moving the MP2 water molecule to other regions of the cluster is discussed in the next subsection.

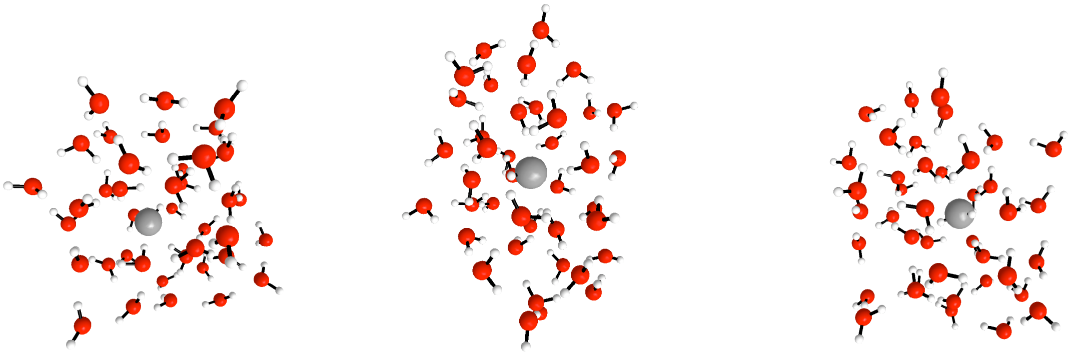

41 H_2O 3.53 D [2.91 D] 3.54 D [3.32 D] 3.44 D [2.99 D]
0.0 4.1 4.2 kcal/mol

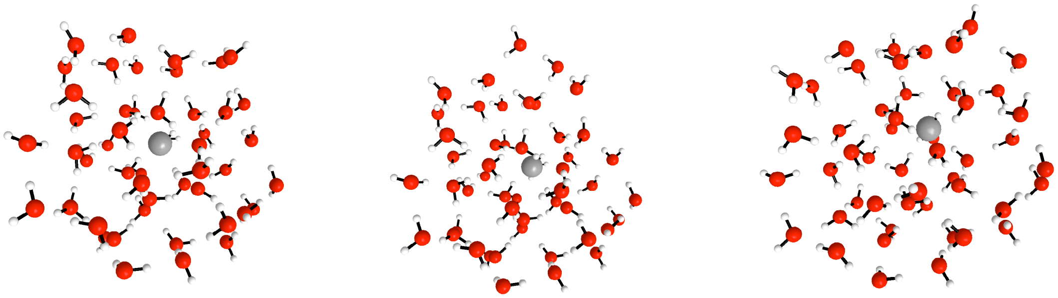

50 H_2O 3.4 D [3.14 D] 3.44 D [3.22 D] 3.17 D [2.84 D]
0.0 0.3 5.2 kcal/mol

Figure 3.5. Sample minima for n=41, 50 H_2O water molecules. The same format and labeling used in Figure 4 is used here.

The most energetically favorable structures for 26 water molecules are similar to those found for n=20; that is two planar "sheets" of molecules stacked on top of each other (see structure 26B in Figure 3.6). For larger clusters (32, 41, and 50), the lowest energy structures are spherical as expected for bulk water, rather than the higher energy stacked planar sheets (structures 32A, 41A and 50A in Figure 3.6). The structures which have one water molecule solvated by other water molecules evenly distributed throughout its three dimensional surroundings are considered to be completely solvated. At n=32, the completely

www.manaraa.com

solvated structure (32A) is lower in energy than the sheet structure (32B) and this trend is followed for n=41 and 50. The energy difference between the approximately spherical structure (global minimum) and the planar sheet structure increases from 14.3 to 18.1 to 29.1 kcal/mol as n increases from 32 to 41 to 50.

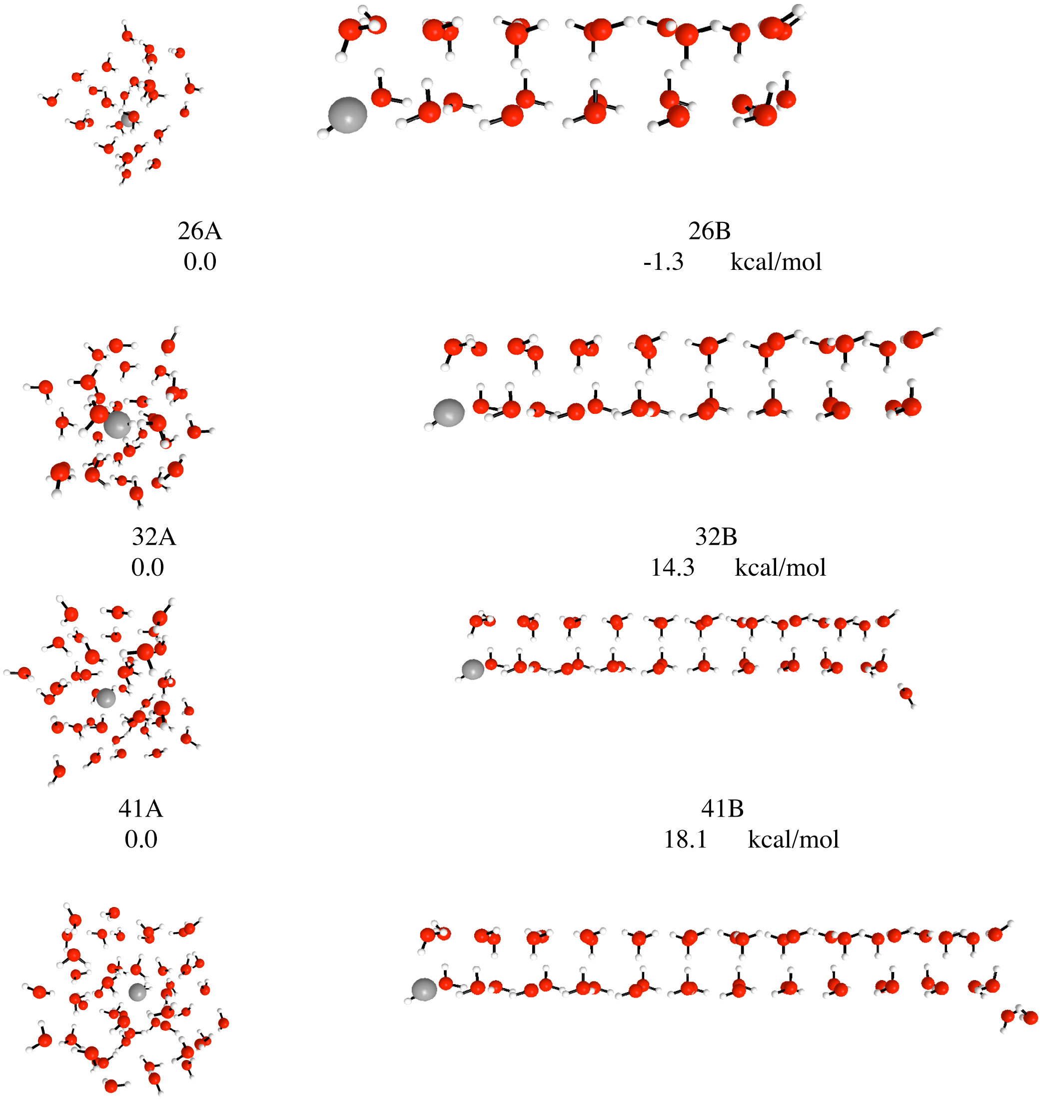
26A
0.0

26B
-1.3 kcal/mol

32A
0.0

32B
14.3 kcal/mol

41A
0.0

41B
18.1 kcal/mol

50A
0.0

50B
29.1 kcal/mol

Figure 3.6. Symmetric structures formed from minima for n=26,32,41 and 50. These structures involve parallel planes of 4 water molecules hydrogen bonded to each other. The 4 water molecules in each parallel plane hydrogen bond to each either and form the shape of a square. Relative energies are compared to the lowest energy structure which is comprised of one central water molecule completely solvated and surrounded by the rest of the cluster.

www.manaraa.com

The Boltzmann averaged dipole moments of an MP2 water molecule placed approximately at the center of 26, 32, 41 and 50 water molecule clusters are given in Table 3.3. The Boltzmann averaged dipole moments for the four values of n are similar to each other and slightly fluctuate within the experimental error bars given by Badyal et al[3] (2.9 ± 0.6). As observed for the smaller water clusters, MP2/aug-cc-pVTZ predicts a smaller dipole moment for each cluster size than MP2/DH(d,p) and using the larger basis set yields dipole moments that are closer to the experimental value.

Table 3.3. Boltzmann averaged dipole moments of all structures found for 32, 41 and 50 water molecules, using the DH(d,p) and aug-cc-pVTZ basis sets, and placing the MP2 water at the approximate center of the cluster.

Cluster size	DH (d,p) Avg. Dipole	aug-cc-pVTZ Avg. Dipole
26	3.3	3.1
32	3.3	2.9
41	3.5	3.3
50	3.4	3.2

D. Origin of the dipole moment

In order to sample the dipole moment of a single water molecule in various hydrogen bonding environments throughout water clusters containing n=32 and 41 molecules, an MP2/aug-cc-pVTZ calculation was done at every EFP position in the global minimum structure for each value of n. The location of the MP2 water molecule was moved about the cluster until all positions had been sampled, with the n-1 waters represented by EFPs. The Boltzmann averaged dipole moments are presented in Table 3.4. The range presented by the minimum and maximum dipole moments (~0.7D) is similar to the experimental uncertainty (± 0.6D)[3].

المنارة للاستشارات

www.manaraa.com

Table 3.4. Boltzmann averaged MP2/aug-cc-pVTZ dipole moment (in Debye) for $(H_2O)_{32}$ and $(H_2O)_{41}$. The largest dipole moment found in the cluster is given in the column Max. Value while the smallest value is listed in the Min. Value column.

Cluster Size	Avg. Dipole	Max. Value	Min. Value
32	3.1	3.43	2.67
41	3.3	3.37	2.72

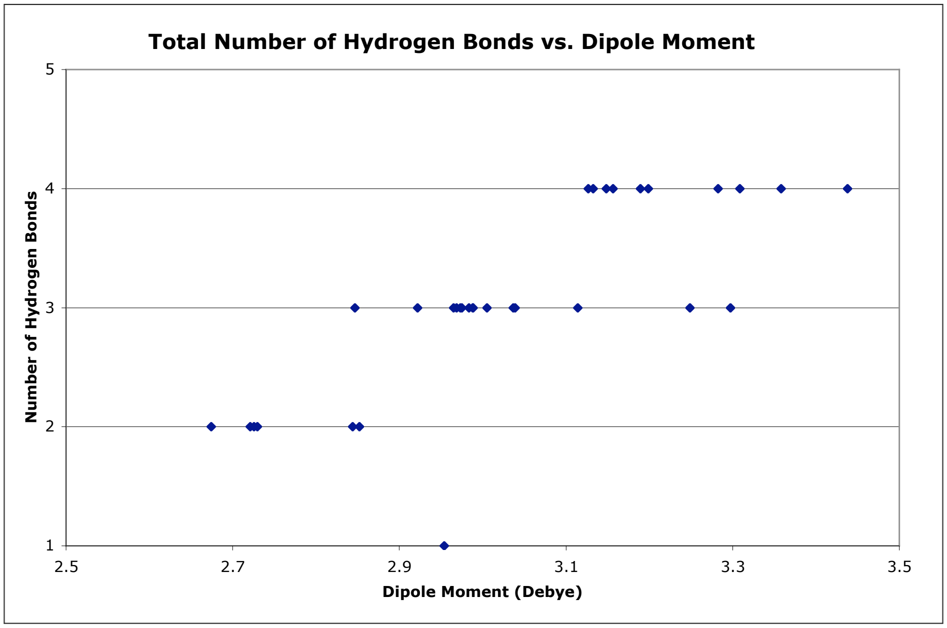

Figure 3.7. The dipole moment of each water molecule was calculated in the global minimum structure for n=32. The number of hydrogen bonds for each molecule is plotted against the dipole moment for the molecule. In general, increasing the number of hydrogen bonds increases the dipole moment of the molecule.

Figure 3.7 presents a graph that depicts the dependence of the computed dipole moment on the number of hydrogen bonds formed by the MP2 water as it is moved to various positions in the global minimum 32-water cluster. In general, the dipole moment

www.manaraa.com

increases as the number of hydrogen bonds increases up to 4 (in which case the water molecule donates 2 and accepts 2 hydrogen bonds). This suggests that the dipole moment of a water molecule that is internal in a water cluster will tend to be larger than the dipole moments of a water molecule that resides at or near the surface and forms fewer hydrogen bonds.

Additional analysis shows that hydrogen bonds in which a lone pair on the MP2 water interacts with EFP OH bonds play the most significant role in dipole moment enhancement. This will be referred to in this discussion as a hydrogen bond accepting arrangement, as opposed to hydrogen bond donating in which the MP2 OH bond is interacting with lone pairs on EFP waters. Figure 3.8 plots the number of hydrogen bond *donors* against the predicted dipole moment of each water molecule within the global minimum structure for n=32. It is clear that the dipole moment is enhanced as the number of donating OH hydrogen bonds on the MP2 water increases from 1 to 2. However, the dipole moment is not significantly enhanced when the number of donating hydrogen bonds increases from 0 to 1. For the ranges of dipole moments for which the number of hydrogen bond donors is 1 or 2, the lower half of each range has one hydrogen bond acceptor, while the upper half corresponds to structures in which the MP2 water lone pairs *accept* two hydrogen bonds. Also, note that in the line in Figure 3.8 that corresponds to zero MP2 OH hydrogen bond donors, there are two cases with greatly enhanced dipole moments, ~2.85D and 2.95D. In these cases, the participation of the MP2 water in hydrogen bonding comes from two hydrogen bond acceptors by the two lone pairs on the MP2 water. This indicates that the lone pair orbitals on the MP2 water, which participate in accepting hydrogen bonds, play an important role in the dipole moment enhancement.

www.manaraa.com

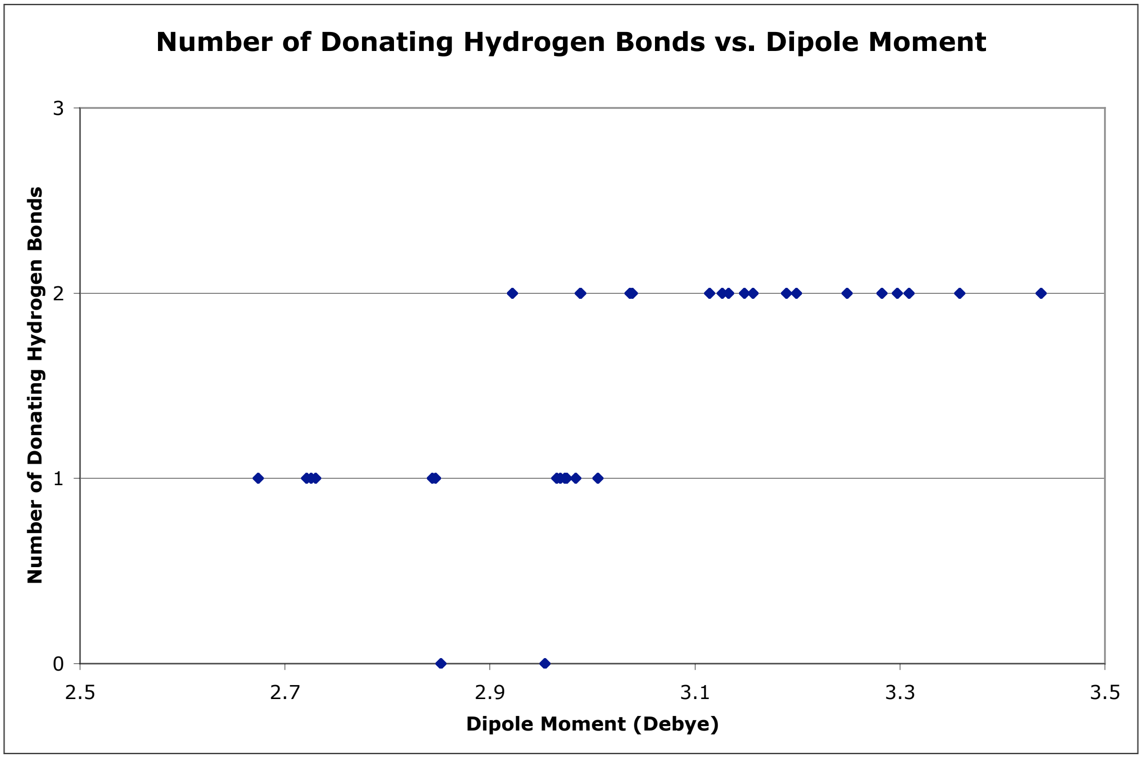

Figure 3.8. The number of donating hydrogen bonds of each molecule in the $(H_2O)_{32}$ global minimum is plotted against that molecule's predicted dipole moment. Dipole moment enhancement is very large for the two cases where only accepting hydrogen bonds are present.

Localized molecular orbitals (LMOs) provide an opportunity to understand the origin of the dipole moment enhancement in a chemically intuitive manner. As noted by Pople[80,81], a bond orbital resembles a quadrupole[80], with positive centers (nuclei) at each end and a negative charge distribution (electrons) in between. Lone pairs, on the other hand, resemble dipoles, with a positive nucleus at one end and electron density at the other, giving rise to a charge separation. This suggests that the water dipole moment will largely arise from the oxygen lone pairs. This notion can be examined by decomposing the dipole moment of a water molecule into a vector sum of the dipole moments that arise from its bond and lone pair orbitals. Such an analysis is facilitated by using charge neutral localized charge distributions (LCDs)[73,74]. Since LMOs and LCDs are only available at the Hartree Fock (HF)

المنارة للاستشارات

www.manaraa.com

level of theory, dipole moments in this section are reported at this level of theory using the aug-cc-pVTZ basis set. Of course, the HF water dipole moment calculated with a given atomic basis is larger than that predicted by MP2 with the same basis set, and therefore larger than the experimental value as well. As will be seen below, the HF dipole moment for a water molecule in an EFP cluster is also higher than the corresponding MP2 dipole moment. However, the trends exhibited by the HF dipole moments as the number of EFP water molecules in the cluster increases is the same as those for an MP2 water molecule. So, the following analysis is reasonable. Though this scheme ultimately divides electron density into LMOs, this is not done until the final step.

Of course, any analysis in which an observable (e.g., water dipole moment) is divided into non-observable components (e.g., OH bond and lone pair dipole moments) is inherently arbitrary and cannot be directly verified experimentally. Nonetheless, such interpretations in terms of commonly used chemical concepts can be very useful. The OH and lone pair LMO orbitals in an isolated (HF) water molecule are modified when this HF water molecule is placed in a cluster of EFP waters, because the orthogonal linear combinations of atomic orbitals in the HF water are modified by the field of the EFP waters via the polarizability term that is iterated to self-consistency within the HF interations.

Now, consider the water monomer and the global minimum for the 32-water cluster, examined in terms of LCDs in Table 3.5. As noted above, although the HF dipole moments in Table 3.5 are larger than the corresponding MP2 dipole moments, the trend and the magnitude of the increase in dipole moment is captured by the HF level of theory. As expected based on the previous discussion, the largest contribution to the magnitude of the water monomer dipole moment comes from the two lone pair LMOs (see Figure 3.9). There

www.manaraa.com

is only a small contribution from the two O-H bond orbitals and virtually no contribution from the oxygen inner shell LMO. Since the net dipole moment is the *vector sum* of the five contributions (two lone pairs, two OH bond pairs, and the inner shell), and since the *magnitudes* of the lone pair dipole moments are greater than the net molecular dipole moment, it is clear from the top half of Table 3.5 that the OH dipole moments are oriented in the opposite direction from the lone pair dipole moments and therefore diminish the net dipole moment. Since the *magnitudes* of the OH bond dipole moments are rather smaller than the lone pair dipole moments, the net water monomer dipole moment is dominated by the lone pair contributions. Nonetheless, the OH bond dipole vectors do play an important quantitative role in determining the overall dipole moment. The same is true for the HF water molecule in a 32-water cluster discussed in the following paragraphs.

Table 3.5. Dipole moments for each LMO for the monomer and for the center-most molecule of the global minimum for n=32. The first column numbers each LMO. The second column describes the type of LMO. The next column gives (in Debye) dipole vector magnitudes and the molecular dipole moment. The angles between lone pair dipole vectors are given in the last column.

monomer

orbital no.	orbital type	dipole	Lone pair angle
1	core	0	
2	lp	2.88	124.6
3	lp	2.88	
4	bonded	0.39	
5	bonded	0.39	
		1.99	

32 GM

orbital no.	orbital type	dipole	Lone pair angle
1	core	0	
2	lp	3.07	116.8
3	lp	3.12	
4	bonded	0.16	
5	bonded	0.08	
		3.3	

www.manaraa.com

Now, consider the analogous analysis for the “central” (most fully solvated) water in the global minimum for $(H_2O)_{32}$. The *ab initio* water is again represented by HF/aug-cc-pVTZ, while the remaining water molecules are DFT-based EFPs.

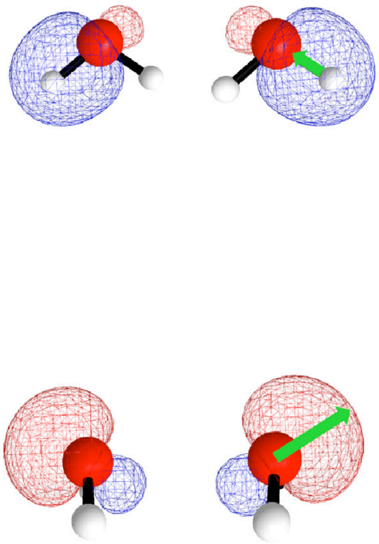

Figure 3.9. Illustrations of localized molecular orbitals and the dipole moments along each orbital. The two green arrows illustrate a dipole moment vector lying along a oxygen-hydrogen bond orbital and along an oxygen lone pair.

As for the water monomer, the dipole moment for the central water molecule in $(H_2O)_{32}$ is dominated by the contributions from the lone pair LMOs (see Table 3.5). Importantly, the magnitude of the lone pair dipole moments do not change significantly relative to those of the monomer, nor do those of the bonding LMOs. So, the dipole moment enhancement does not originate from any significant change of the magnitude of the LMO dipole moments. Rather, the dipole moment enhancement is driven by changes in the

www.manaraa.com

orientation of the lone pair dipole moments upon solvation. As shown in Table 3.5, the angle between these lone pair LMO vectors decreases from 124.6° in the monomer to ~117° when solvated by 31 EFPs. This decrease in the angle between the lone pair dipole vectors, expected in a highly hydrogen bonded environment encountered in liquid or solid water, results in a greater resultant net dipole moment. Once again, the net molecular dipole moment is smaller in magnitude than the lone pair dipole moments because of the opposing OH bond pair dipole moments. Even though the OH dipole moments are much smaller in magnitude, they again have a non-trivial attenuating affect. This behavior is also apparent for n=41 and 50, as may be seen in Table 3.6. The observed decrease in the angle between the lone pair LMOs arises from the formation of the hydrogen bonds to these lone pairs, thereby increasing the bonding character of these orbitals.

Table 3.6. Localized orbital dipoles and angles between the localized dipole vectors for the global minimum structures for n=41,50.

41 GM

orbital no.	orbital type	Dipole	Lone pair angle
1	core	0	
2	lp	3.08	117.5
3	lp	3.08	
4	bonded	0.16	
5	bonded	0.12	
		3.3	

50 GM

orbital no.	orbital type	dipole	Lone pair angle
1	core	0	
2	lp	3.05	117.5
3	lp	3.08	
4	bonded	0.15	
5	bonded	0.09	
		3.21	

المنارة للاستشارات

www.manaraa.com

IV. Conclusions

The dipole moment of water has been examined starting with the monomer and systematically adding effective fragment potential water molecules to the cluster. Even a small number of water molecules serves to significantly increase the dipole moment of the quantum water. Clusters as small as 6-20 water molecules reproduce the experimentally observed dipole moment enhancement, and clusters with 26, 32, 41 and 50 water molecules agree with each other and with the experimentally observed dipole moment in bulk water.

Numerous papers cite polarization[18,23,24,32,36,41,42,44,51] due to the hydrogen bonding in the liquid environment as a reason for the dipole moment enhancement. Larger induced dipoles have been proposed to be the result of larger polarization effects due to hydrogen bonding. The present work has employed a localized charge distribution analysis to illustrate that the dipole moment of both an isolated water molecule and a water molecule in the presence of a cluster of EFP waters is derived primarily from the water lone pairs, attenuated by opposing OH dipole vectors. It then follows that the enhancement of the dipole moment of a water molecule in the presence of other water molecules arises primarily from decreases in the angles between the lone pair dipole vectors. This angle decrease arises in turn from the increased participation of these lone pairs in hydrogen bonds when a water molecule is surrounded by other waters. This analysis is based on an interpretation of an observable (the water dipole moment) in terms of non-observable components (OH bond and lone pair dipole moments). Even though such approaches are difficult to verify experimentally, such interpretations in terms of commonly used chemical concepts can be very useful.

www.manaraa.com

Acknowledgements

Funding for this study was provided by the Ames Laboratory and the Department of Energy. The authors thank Dr. Paul Day and Dr. Heather Netzloff for providing initial cluster geometries, and Professor Hans Stauffer for interesting and helpful discussions.

References

1. Shostak, S. L.; Ebenstein, W. L.; Muenter, J. S. *J. Chem. Phys.*, **1991**, *94*, 5875.

2. Shostak, S. L.; Ebenstein, W. L.; Muenter, J. S. *J. Chem. Phys.*, **1991**, *94*, 5883.

3. Badyal, Y. S.; Saboungi, M.-L.; Price, D. L.; Shastri, S. D.; Haeffner, D. R.; Soper, A. K. *J. Chem. Phys.*, **2000**, *112*, 9206.

4. Dyke, T. R.; Mack, K. M.; Muenter, J. S. *J. Chem. Phys.,* **1977**, *66*, 498.

5. Clough, S. A.; Beers, Y.; Klein, G. P.; Rotham, L. S.; *J. Chem. Phys.*, **1973**, *59*, 2254.

6. Dyke, T. R.; Muenter, J. S. *J. Chem. Phys.*, **1973**, *59*, 3125.

7. Xantheas, S. S.; Dunning, T. H. Jr. *J. Chem. Phys.*, **1993**, *99*, 8774.

8. Swanton, D. J.; Bacskay, G. B.; Hush, N. S. *J. Chem. Phys.*, **1986**, *84*, 5715.

9. Gregory, J. K.; Clary, D. C.; Liu, K.; Brown, M. G.; Saykally, R. J. *Science,* **1997**, *275*, 814.

10. Niesar, U.; Corongiu, G.; Clementi, E.; Kneller, G. R.; Bhattacharya, D. K. *J. Phys. Chem.*, **1990**, *94*, 7949.

11. Dang, L. X. *J. Phys. Chem. B*, **1998**, *102*, 620.

12. Rick, S. W.; Stuart, S. J.; Berne, B. J. *J. Chem. Phys.*, **1994**, *101*, 614.

13. Stillinger, F. H.; Rahman, A. *J. Chem. Phys.*, **1974**, *60*, 1545.

14. Ahlstrom, P.; Wallqvist, A.; Engstrom, S.; Jonsson, B. *Mol. Phys.*, **1989**, *68*, 563.

المنارة للاستشارات

www.manaraa.com

15. Caillol, J. M.; Levesque, D.; Weis, J. J.; Kusalik, P. G.; Patey, G. N. *Mol. Phys*., **1985**, *55*, 65.

16. Fois, E.S., Sprik, M. Parrinello, M. *Chem. Phys. Lett*., 223, **1994**, 411-415.

17. B. Wei, D.R. Salahub, *Chem. Phys. Lett*., 224, **1994**, 291.

18. Tu, Y.; Laaksonen, A. *Chem. Phys. Lett*., **2000**, *329*, 283.

19. Tu, Y.; Laaksonen, A. *J. Chem. Phys*., **1999**, *111*, 7519.

20. Gatti, C., Silvi, B., Colonna, F. *Chem. Phys. Lett*., 247, **1995**, 135-141.

21. Heggie, M.I., Latham, C. D., Maynard, S.C.P., Jones, R. *Chem. Phys. Lett*., 249, **1996**, 485-490.

22. Reis, H., Raptis, S. G., Papadopoulos, M. G., *Chem. Phys*., 263, **2001**, 302-316.

23. Coulson, C. A.; Eisenberg, D. *Proc. Roy. Soc. London*, **1966**, *291*, 445.

24. Chialvo, A. A.; Cummings, P.T. *J. Chem. Phys*., **1996**, *105*, 8274.

25. Bursulaya, B. D.; Jeon, J.; Zichi, D. A.; Kim, H. J. *J. Chem. Phys*., **1998**, *108*, 3286.

26. Delle Site, L.; Alavai, A.; Lynden-Bell, R. M. *Mol. Phys*., **1999**, *96,* 1683.

27. Rick, S. W. *J. Chem. Phys*., **2001**, *114*, 2276.

28. Svishchev, I.M.; Kusalik, P.G.; Wang, J.; Boyd, R. J. *J. Chem. Phys*., **1996**, *105*, 4742.

29. Batista, E. R.; Xantheas, S. S.; Jonsson, H. *J. Chem. Phys*., **2000**, *112*, 3285.

30. Whalley, E. *Chem. Phys. Lett*., **1978**, *53*, 449.

31. Liu, K.; Brown, M. G.; Saykally, R. J. *J. Chem. Phys. A,* **1997**, *101*, 8995.

32. Dang, L. X.; Chang, T.-M. *J. Chem. Phys*., **1997**, *106*, 8149.

33. Sprik, M.; Klein, M. L.; *J. Chem. Phys*., **1988**, *89*, 7556.

34. Whalley, E. *Chem. Phys. Lett*., **1978**, *53*, 449.

35. Xantheas, S. S. *J. Chem. Phys*., **1995**, *102*, 4505.

المنارة للاستشارات

www.manaraa.com

36. Batista, E. R.; Xantheas, S. S.; Jonsson, H. *J. Chem. Phys.*, **1998**, *109*, 4546.

37. Bernardo, D. N.; Ding, Y.; Krogh-Jespersen, K.; Levy, R. M. *J. Phys. Chem.*, **1994**, *98*, 4180.

38. Xantheas, S. S.; Dunning, T. H. Jr. *J. Chem. Phys.*, **1993**, *98*, 8037.

39. Kozack, R. E.; Jordan, P. C. *J. Chem. Phys.,* **1992**, *92*, 3120.

40. Zhu, S.-B.; Sing, S.; Robinson, G. W. *J. Chem. Phys.,* **1991**, *95*, 2791.

41. Cieplak, P.; Kollman, P.; Lybrand, T. *J. Chem. Phys.*, **1990**, *92*, 6755.

42. Silvestrelli, P. L.; Parrinello, M. *Phys. Rev. Lett.*, **1999**, *82*, 3308.

43. Sprik, M. *J. Chem. Phys.* **1991**, *95*, 6762.

44. Gubskaya, A. V.; Kusalik, P. G. *J. Chem. Phys.*, **2002**, *117*, 5290.

45. Brodholt, J.; Sampoli, M.; Vallauri, R. *Mol. Phys.*, **1995**, *85*, 81.

46. Rocha, W. R.; Coutinho, K.; de Almeida, W. B.; Canuto, S. *Chem. Phys. Lett.*, **2001**, *335*, 127.

47. Carnie, S. L.; Patey, G. N. *Mol. Phys.*, **1982**, *47,* 1129.

48. Field, M. J. *Mol. Phys.*, **1997**, *91*, 835.

49. Caldwell, J.; Dang, L. X.; Kollman, P. A. *J. Amer. Chem. Soc.,* **1990**, *112*, 9144.

50. Batista, E. R.; Xantheas, S. S.; Jonsson, H. *J. Chem. Phys.*, **1999**, *111*, 6011.

51. Barnes, P.; Finney, J. L.; Nicholas, J. D.; Quinn, J. E. *Nature,* **1979**, *282*, 459.

52. Kusalik, P. G.; Svishchev, I. M. *Science,* **1994**, *265*, 1219.

53. M. J. McGrath; J. I. Siepmann; I.-F. W. Kuo; C. J. Mundy, **2007**, *10*, 1411.

Laasonen, K.; Sprik, M.; Parrinello, M.; Car, R. *J. Chem. Phys.*, **1993**, *99*, 9080.

54. Day, P. N.; Jensen, J. H.; Gordon, M. S.; Webb, S. P.; Stevens, W. J.; Krauss, M.; Garmer, D.; Basch, H.; Cohen, D. *J. Chem. Phys.* **1996**, *105*, 1968.

المنارة للاستشارات

www.manaraa.com

55. Gordon, M. S.; Freitag, M. A.; Bandyopadhyay, P.; Jensen, J. H.; Kairys, V.; Stevens, W. J. *J. Phys. Chem. A* 2001, *105*, 293.

56. Schmidt, M. W.; Baldridge, K. K.; Boatz, J. A.; Jensen, J. H.; Koseki, S.; Matsunaga, N.; Gordon, M. S.; Ngugen, K. A.; Su, S.; Windus, T. L.; Elbert, S. T.; Montgomery, J.; Dupuis, M. *J. Comput. Chem.* 1993, *14*, 1347.

57. Gordon, M.S.; Schmidt, M.W. Advances in Electronic Structure Theory: GAMESS a Decade Later, *Theory and Applications of Computational Chemistry,* Dykstra, C. E., Frenking, G., Kim, K.S., Scuseria, G.E., Eds.; Elsevier: Boston, **2005;** Ch. 41.

58. Adamovic, I.; Freitag, M. A.; Gordon, M. S. *J. Chem. Phys.*, **2003**, *118*, 6725.

59. Webb, S.P.; Gordon, M. S. *J. Phys. Chem. A*, **1999**, *103*, 1265.

60. Adamovic, I.; Gordon, M. S. *J. Phys. Chem. A*, **2005**, *109*, 1629.

61. Day, P. N.; Pachter, R.; Gordon, M. S.; Merrill, G. N. *J. Chem. Phys.*, **2000**, *112*, 2063.

62. Pople, J. A.; Binkley, J. S.; Seeger, R. *Int. J. Quantum Chem. Sym.* **1976,** *10,* 1.

63. Frisch, M. J.; Head-Gordon, M.; Pople, J. A. *Chem. Phys. Lett.* **1990,** *166,* 275.

64. Fletcher, G. D.; Schmidt, M. W.; Gordon, M. S. *Adv. Chem. Phys.* **1999,** *110,* 267.

65. Aikens, C. M.; Webb, S. P.; Bell, R. L.; Fletcher, G. D.; Schmidt, M. W.; Gordon, M. S. *Theor. Chem. Acc.,* 2003, *110,* 233.

66. Dunning, T. H.; Hay, P. J. "Methods of Electronic Structure Theory", Shaefer, H. F. III, Ed. Plenum Press, N. Y. 1977, pp. 1-27.

67. Dunning, T.H. Jr. J. Chem. Phys. 90, 1007 (1989)

68. Kendall, R. A.; Dunning, T. H. Jr.; Harrison, R.J. J. Chem. Phys. 96, 6769, 1992.

69. Metropolis, N.; Rosenbluth, A.; Tellor, A. *J. Chem. Phys.* 1953, *21,* 1089.

70. Kirkpatrick, S.; Gelatt, C. D.; Vecchi, M. P. *Science* 1983, *220*, 671.

المنارة للاستشارات

www.manaraa.com

71. Parr, R. G.; Yang, W. "Density Functional Theory of Atoms and Molecules", Oxford Scientific, 1981.

72. Koch, W.; Holthausen, M. C. "A Chemist's Guide to Density Functional Theory", Wiley-VCH, 2001.

73. Jensen, J. H.; Gordon, M. S. *J. Phys. Chem.*, **1995**, *99*, 8091.

74. Remer, L. C.; Jensen, J. H. *J. Phys. Chem.*, **2000**, *104*, 9266.

75. Boys, S. F. "Quantum Science of Atoms, Molecules, and Solids" P.O. Lowdin, Ed, Academic Press, NY, 1966, 253-262.

76. Edmiston, C.; Ruedenberg, K. *Rev. Mod. Phys.*, **1963,** *35,* 457.

77. Bader, R. F. W.; Nguyen-Dang, T. T. *Adv. Quantum Chem.,* **1981**, *14*, 63-124.

78. Day, P. N.; Pachter, R.; Gordon, M. S.; Merrill, G. N. *J. Chem. Phys.*, **2000**, *112*, 2063.

79. Bode, B. M.; Gordon, M. S. *J. Mol. Graphics Mod.*, **1998**, *16,* 133-138.

80. Pople, J. A. *Proc. Roy. Soc. London;* **1951**, *A205*, 155.

81. Pople, J. A. *Proc. Roy. Soc. London;* **1950**, *A202*, 323.

المنارة للاستشارات

www.manaraa.com

CHAPTER 4. AQUEOUS SOLVATION OF BIHALIDE ANIONS

A paper accepted for publication to the Journal of Physical Chemistry A

Daniel D. Kemp and Mark S. Gordon

Abstract

Second order Møller-Plesset perturbation theory (MP2) is used to perform geometry optimizations on $XHX^{-}\cdot(H_2O)_n$, for X = Br, I, with n = 1-6 water molecules. Of particular interest is the manner in which the solvent molecules orient themselves around the solute and which configurations are lowest in energy. Although for most values of n water molecules may donate all of their hydrogen atoms for hydrogen bonding to the solute, this type of structure is the lowest in energy only for n = 0-2, and only a local minimum for n = 3,4,6. For n = 5 this type of structure is a saddle point. Coupled cluster single point calculations at the MP2 geometries are used to obtain accurate relative energies for all stationary points.

Introduction

Bihalide anions[1-8] XHX^- are linear anions with a hydrogen atom placed between two halide atoms X. Interest in bihalide anions stems from the fact that they form strong intramolecular hydrogen bonds [7-10] and they are useful for studying transition states in the corresponding neutral species via photodetachment experiments[11,12]. Using this experimental technique, bihalide anions can, for example, be used to study transition states for the prototypical H exchange reactions X + HX → XH + H, because the minimum energy geometries of the anions are very similar to the transition state geometries of their neutral counterparts. So, photodetachment of an electron from the anion minimum energy geometry

المنارة للاستشارات

www.manaraa.com

places the system close to the neutral transition state. This facilitates the study of the vibrational spectroscopy of the neutral transition state by photodetachment spectroscopy.

If solvent molecules are included in the experiments, one can systematically investigate the effects of increasing numbers of solvent molecules on the transition state dynamics[12,13]. Both computational and experimental methods have been employed to study the effects of solvent molecules on bihalide systems.

Recently, Neumark et al performed a combined experimental and theoretical study of bihalide anions ($BrHBr^-$, IHI^- and $BrHI^-$)[12], in which they solvated these ions with small numbers of solvent molecules, including water, with only one solute molecule present. The experimental spectrum of the ion hydrogen bonded to one water showed little change compared to the spectrum of the bare ion. The computations of Neumark et al[12] predicted two energy minima; one with the water molecule donating each of its hydrogen atoms to the solute for hydrogen bonding (labeled **3** in Figure 4.1) and another with the water molecule placed such that only one hydrogen atom will hydrogen bond to the anion (labeled **4** in Figure 4.1). This latter structure distorts the ion geometry by pulling one halogen atom closer to the water molecule to maximize the hydrogen bonding interaction. Neumark et al concluded that the experimental spectrum of the solvated species corresponds to structure **3**. This conclusion was based on the observation that the water molecule in structure **3** donates both of its hydrogen atoms to hydrogen bonds and that this arrangement does not significantly alter the geometry of the solute from the unsolvated (gas phase) geometry. Therefore, the experimental spectrum should not change significantly compared to the spectrum of the gas phase anion, as is observed. The distorted structure **4** in Figure 4.1 is therefore less likely to be the one observed in the experiments.

www.manaraa.com

BrHBr-

1

IHI-

2

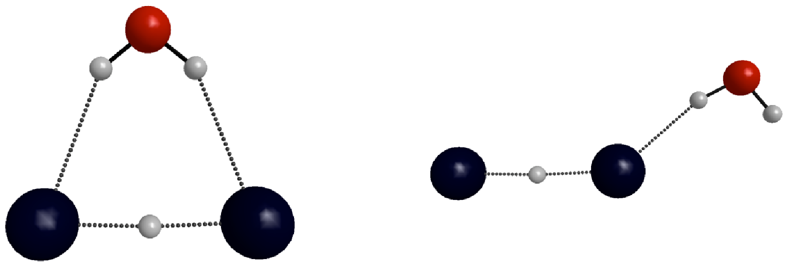

BrHBr-(H_2O)

3

BrHBr-(H_2O)

4

Figure 4.1. MP2-optimized symmetric geometries of both $BrHBr^-$ and IHI^- bihalide anions **1** and **2**. Structures **3** and **4** illustrate the minima found by Newmark et al[12] for n=1.

The present work describes calculations on both $BrHBr^-(H_2O)_n$ and $IHI^-(H_2O)_n$ with n=1-6 water molecules. Geometry optimizations have been performed to search for the lowest energy structure for each value of n. The motivation for this study is to determine the preferred solvated structures for the solvated anions, in order to provide insight for the interpretation of the spectra for these more complex species.

المنارة للاستشارات

www.manaraa.com

Computational Methods

Second order Møller-Plesset perturbation theory (MP2)[14-17] was employed in geometry optimization searches for $XHX^-(H_2O)_n$ (X = Br, I and n = 1-6). The 6-31++G(d,p)[18-20] basis set was used for oxygen and hydrogen atoms in the $BrHBr^-(H_2O)_n$ calculations, while the Binning-Curtiss version of this basis set[21] was used for Br. This same basis set was also used for the oxygen and hydrogen atoms during the $IHI^-(H_2O)_n$ geometry optimizations, while the Stevens, Basch, Krauss, Jasien and Cundari (SBKJC) basis set[22] and the related effective core potentials (ECPs) were used to describe the iodine atoms. The General Atomic and Molecular Structure System (GAMESS)[23,24] was used for all calculations. All structures in the figures were viewed with MacMolPlt[25].

When a stationary point was reached during a geometry optimization, the matrix of energy second derivatives with respect to the atomic positions (Hessian) was calculated and diagonalized to verify that the stationary point was indeed an energy minimum (no negative eigenvalues) rather than a saddle point (one or more negative eigenvalues). If a negative Hessian eigenvalue (force constant) was found, the geometry optimization was restarted at that geometry with a tightened optimization convergence criterion of $1x10^{-05}$ hartree/bohr (default value is $1x10^{-4}$ hartree/bohr). This was followed by a new Hessian calculation. The Hessian eigenvalues also provide the zero point energies that have been added to the calculated energy differences.

To obtain accurate relative energies, single point energies were calculated, at the MP2 minimum energy geometries, with coupled-cluster theory using single, double and perturbative triple excitations[26] (CCSD(T)) for each local minimum. For all CCSD(T) calculations, the all-electron 6-311++G(df,p)[27-29] basis set was used for the anion as well as

www.manaraa.com

for the solvent molecules. The MP2 zero point energies were added to the CCSD(T) single point energies to obtain 0K enthalpy differences.

Results

A. $BrHBr^-(H_2O)_n$

The geometry of the gas phase anion (n=0) is found to be linear and symmetric ($D_{\infty h}$) with an H-Br distance of 1.70 Å. This is in good agreement with Neumark et al[12], and the relatively short Br-H distances illustrate why bihalide anions are considered to be examples of strong hydrogen bonds.

For n=1, MP2 predicts that in the lowest energy structure, both hydrogen atoms of the water molecule participate in hydrogen bonds with the anion. This C_{2V} structure, **Br1A** in Figure 4.2, has a 4.9 kcal/mol lower energy than **Br1B** (C_s symmetry), in which the solvent water molecule acts as a hydrogen donor in just one hydrogen bond to the anion. These predictions are in good agreement with both the previous calculations and the experimental evidence[12]. Structure **Br1B** in Figure 4.2 has an essentially linear arrangement of O-H-Br-H atoms, whereas the hydrogen bond in the higher energy species in the Neumark work (**4** in Figure 4.1) is nonlinear. Despite this small difference, both studies agree upon the global minimum structure.

Now consider structures with more than one water molecule. In the global minimum structure for n = 2, **Br2A** in Fig. 2, each water molecule donates both of its hydrogen atoms to hydrogen bonds to the anion. If one arranges the two waters and the solute so that all atoms lie in a common plane and both water molecules donate both of their hydrogen atoms in hydrogen bonds to the solute (**Br2C**), there is an imaginary vibrational mode that leads to structure **Br2A.**

المنارة للاستشارات
www.manaraa.com

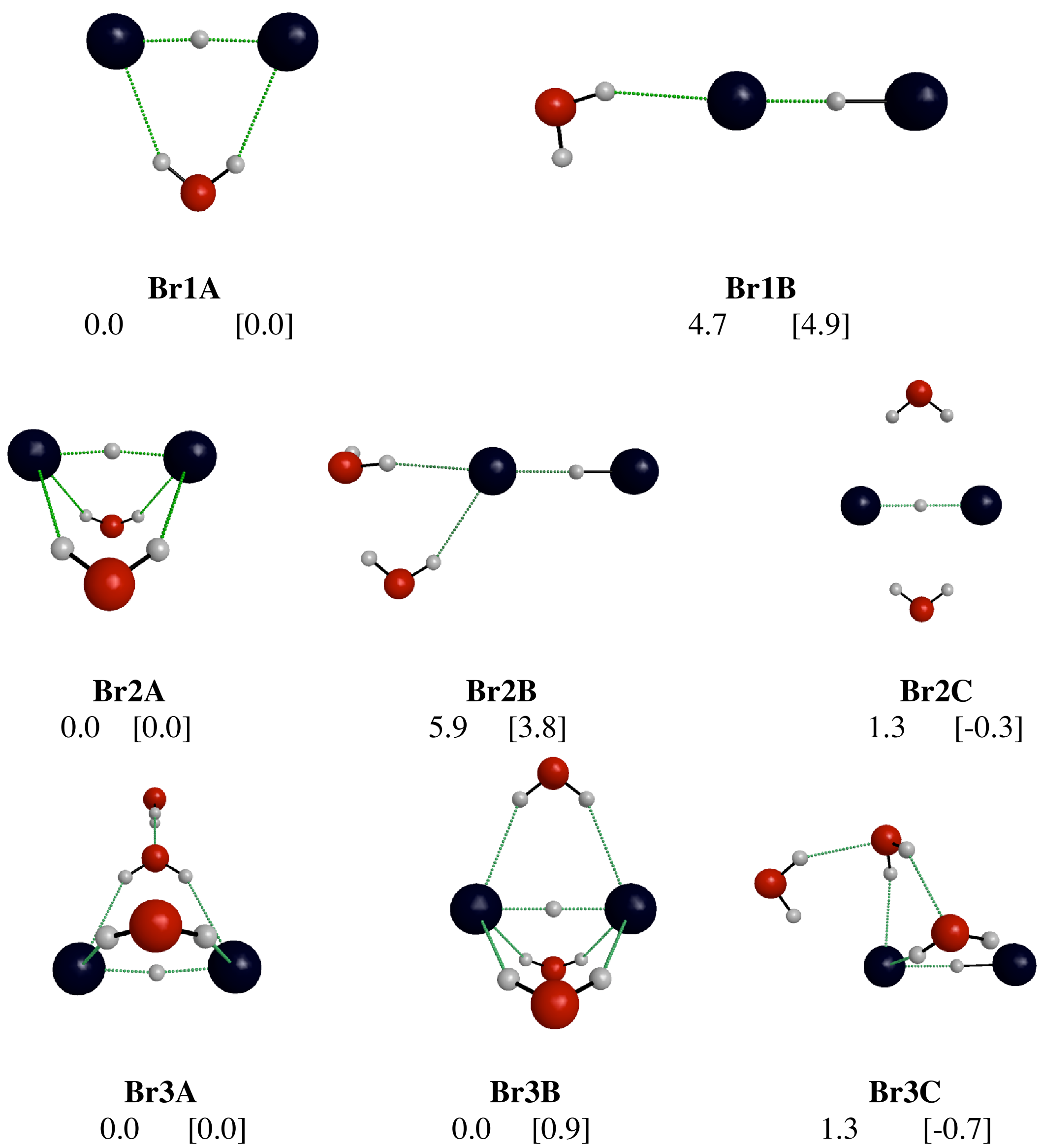

Figure 4.2. The lowest energy structure and other low-lying minima for $BrHBr^-(H_2O)_n$, n=1-3. Each row contains one more water molecule than the preceding row. The MP2 lowest energy structure found for each value of n is given first in each row. The two other structures in each row are examples of higher-energy species. Relative MP2 [CCSD(T)] energies are given in kcal/mol. A dotted green line denotes hydrogen bonding.

Symmetry adapted perturbation theory (SAPT) calculations[30] were performed on the solvent molecules in their **Br2A** and **Br2C** orientation, but without the anion present, in order to analyze the interactions among the solvent molecules. These calculations suggest

www.manaraa.com

(see Table 4.1) that although the solvent-solvent electrostatic energy is more positive (less attractive) for the structure resulting from the re-optimization in the presence of the solute, the solvent-solvent dispersion energy has become slightly more negative (more attractive). This leads to the stabilization of the global minimum (**Br2A**) relative to the planar structure (**Br2C**). The increase in the electrostatic energy occurs because the two water molecules are much closer to each other than they would be without the presence of the anionic solute but it should not be a concern if the negatively charged solute is present. Note that CCSD(T) single point energies calculated at the MP2 optimized geometries slightly favor Br2C relative to Br2A. It is possible that fully optimized structures at the CCSD(T) level of theory would agree better with the SAPT predictions than do the CCSD(T) single point energies.

Table 4.1. SAPT energies in kcal/mol for structure **Br2C** and Br2A in Figure 4.2, without the solute anion present.

	Br2C	Br2A
Electrostatic enegy	0.65	1.10
Exchange energy	0.00	0.01
Dispersion energy	-0.01	-0.05
Induction energy	-0.01	-0.02
Final Energy	0.63	1.07

For n = 3, a minimum energy structure, **Br3B** (Figure 4.2), can be found in which all three solvent molecules orient themselves symmetrically around the solute, such that each water donates both hydrogen atoms in hydrogen bonds to the solute anion. However, **Br3B** is not the lowest energy structure. MP2 predicts that in the lowest energy structure, **Br3A** in Figure 4.2, the third water molecule hydrogen bonds to another water molecule rather than to the solute. However, CCSD(T) single point energies at the MP2 geometries predict that the

www.manaraa.com

lowest energy structure is, in fact, a third structure, **Br3C**, in which one water molecule donates two hydrogen bonds to the solute and accepts one hydrogen bond from another water molecule; the other two water molecules hydrogen bond to both the solute and to each other. Since this CCSD(T) predicted global minimum uses all hydrogen atoms in hydrogen bonding, it does seem reasonable that **Br3C** is the global minimum. Nonetheless, **Br3A** and **Br3B** are only 0.7 kcal/mol and 1.6 kcal/mol, respectively, higher in energy than **Br3C** at this level of theory.

For n = 4, a local minimum (**Br4B** in Figure 4.3) can be found that features four waters placed symmetrically around the solute, with each donating two hydrogen bonds to the solute. Not surprisingly, **Br4B** is not the global minimum for n = 4. The global minimum predicted by MP2, and confirmed by CCSD(T), is labeled **Br4A** in Figure 4.3. In this structure, two water molecules each donate both hydrogen atoms in hydrogen bonds to the solute, while simultaneously accepting a hydrogen bond from (the same) third water molecule. The fourth water donates one hydrogen bond to the water cluster and a second hydrogen bond to one halide atom. Structure **Br4A** is 8.4 kcal/mol lower in energy than **Br4B** at the CCSD(T) level of theory, but only 1.7 kcal/mol lower than a third species, **Br4C**, that exhibits three symmetrically displaced waters about the anion, with the fourth water hydrogen bonding to two of the other waters. This observation suggests the existence of steric hindrance among the water molecules that prevents too many waters from directly interacting with the solute. Placing three water molecules in such a symmetric arrangement (e.g., **Br4C**) is energetically competitive, but more than three waters does not appear to be favorable. Note that only the three lowest-energy structures are shown in the figures. Other, higher energy isomers, can be found, but are not shown in the figures.

المنارة للاستشارات
www.manaraa.com

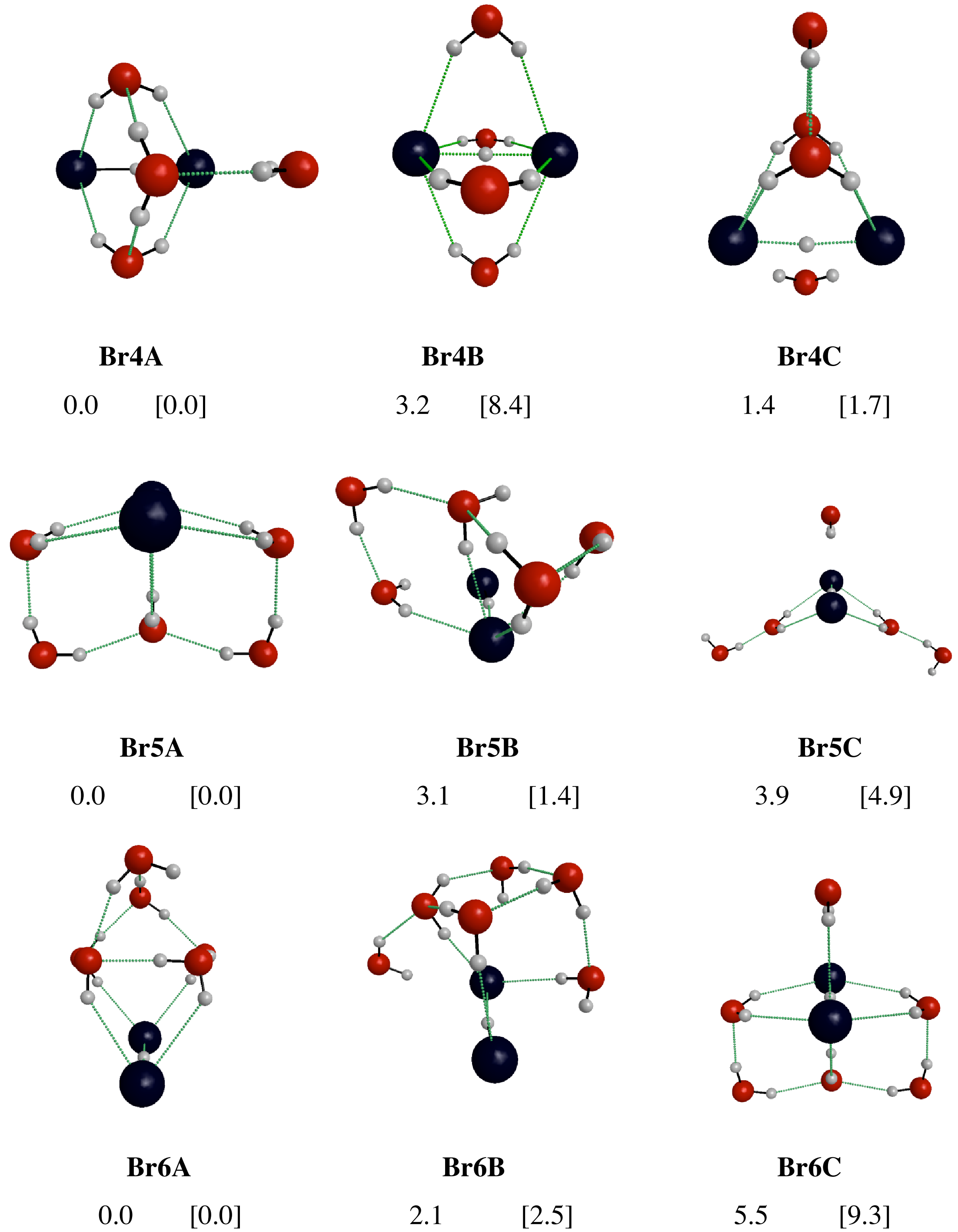

Br4A 0.0 [0.0]

Br4B 3.2 [8.4]

Br4C 1.4 [1.7]

Br5A 0.0 [0.0]

Br5B 3.1 [1.4]

Br5C 3.9 [4.9]

Br6A 0.0 [0.0]

Br6B 2.1 [2.5]

Br6C 5.5 [9.3]

Figure 4.3. Global minima and several additional minima are given for $BrHBr^{-}(H_2O)_n$ n=4-6. The same notation is used as that in Figure 4.2.

A symmetric structure for n=5 in which all five water molecules donate both hydrogen atoms in hydrogen bonds to the solute cannot be found as a minimum on the

المنارة للاستشارات

www.manaraa.com

potential energy surface. All attempts to find such a structure result in optimizations to other, less symmetric species. If symmetry is used to constrain the geometry of the water molecules so that such a structure is found, one imaginary frequency exists. Observing the mode of this imaginary frequency shows that following it would break the symmetry of the structure.

Structure **Br5A**, the predicted global minimum shown in Figure 4.3, has three symmetrically displaced water molecules that donate both hydrogen atoms to hydrogen bonds to the halides of the solute (similar to **Br4C**), while the remaining two water molecules donate both of their hydrogen atoms in such a way as to connect all of the solvent molecules in a hydrogen bonding network. This structure uses all hydrogen atoms in hydrogen bonding.

The global minimum structure for n=6 (**Br6A** in Figure 4.3) arranges the solvent molecules such that all six water molecules form a network of hydrogen bonds that resembles a prism. Four of the water molecules hydrogen bond to the solute and to other water molecules, while the remaining two waters hydrogen bond exclusively with other water molecules. In contrast to n=5, for n = 6 a symmetric structure in which all water hydrogen atoms donate hydrogen bonds to the solute was found without imaginary frequencies. However, this structure is 20.0 kcal/mol higher in energy than the global minimum structure. Structure **Br6C** has four waters symmetrically displaced about the solute, with the remaining two waters forming hydrogen bonds that connect symmetrically displaced water molecules. However, **Br6C** is more than 9 kcal/mol higher in energy than **Br6A**. This is consistent with the notion that four or more waters arranged symmetrically about the solute causes too much steric hindrance, thereby raising the energy relative to other isomers.

المنارة للاستشارات

www.manaraa.com

B. IHI-$(H_2O)_n$

The gas phase IHI^- anion (n=0, **2** in Figure 4.1) is linear, with hydrogen-halide distances of 1.9Å, compared with the $BrHBr^-$ distances of 1.7Å due to the presence of the larger halide atoms.

For n = 1, the global minimum structure (**I1A** in Figure 4.4) and another higher-energy structure (**I1B**) look very similar to those found for the $BrHBr^-$ solute. In **I1A**, the water molecule donates two hydrogen atoms in hydrogen bonds to the solute, in good agreement with the structure predicted both experimentally and theoretically by Neumark et al. One difference between structure **I1B** and **Br1B** (Figure 4.2) is that the water molecule in **I1B** seems to direct both of its hydrogen atoms towards the solute, rather than just one.

The two structures found for n=2 (Figure 4.4) closely resemble the two structures found for $BrHBr^-(H_2O)_2$. The global minimum (**I2A**) is not planar and is very similar to **Br2A**. A structure can be found which is entirely planar (**I2B**), but this structure has one imaginary frequency. Tighter optimization of **I2B** leads to **I2A**. **I2A** and **I2B** are very close in energy at both the MP2 and CCSD(T) levels of theory; unlike $BrHBr^-$, both levels of theory agree that the planar structure is not the lowest energy structure. Though both levels of theory did not agree qualitatively about the global minimum for $BrHBr^-(H_2O)_2$, the relative energies for these structures is very small and often less than 1.0 kcal/mol. This may explain why MP2 and CCSD(T) disagree regarding the planarity of $BrHBr^-(H_2O)_2$, but agree for IHI-$(H_2O)_2$.

www.manaraa.com

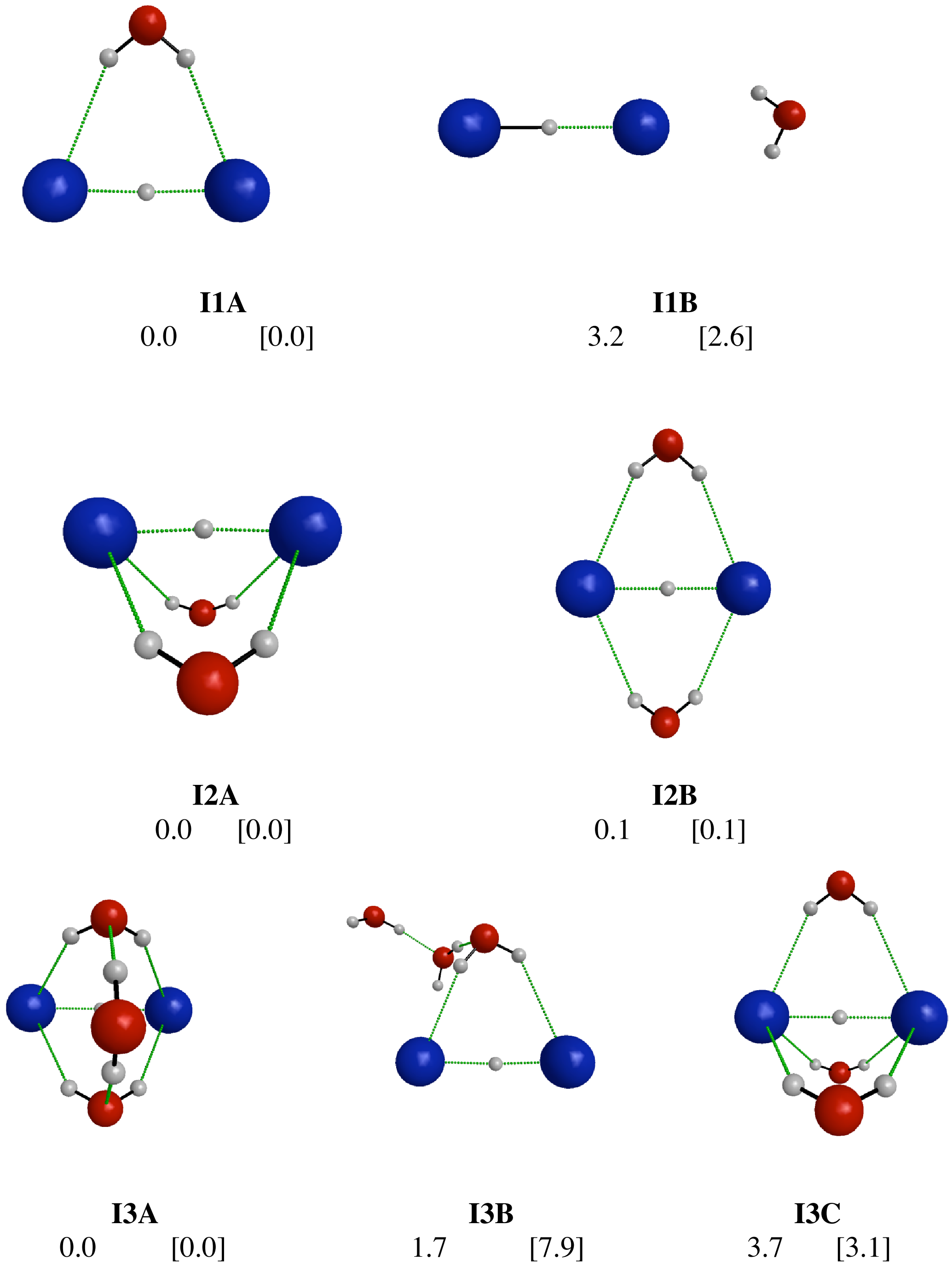

I1A
0.0 [0.0]

I1B
3.2 [2.6]

I2A
0.0 [0.0]

I2B
0.1 [0.1]

I3A
0.0 [0.0]

I3B
1.7 [7.9]

I3C
3.7 [3.1]

Figure 4.4. Structures and global minima for $IHI^-(H_2O)_n$ n=1-3. MP2 and [CCSD(T)] relative energies are given relative to the MP2 global minimum in kcal/mol.

For n=3, a structure in which the three water molecules are symmetrically displaced about the solute (Figure 4.4, **I3C**) with all six hydrogen atoms participating as donors in

المنارة للاستشارات
www.manaraa.com

hydrogen bonds, is a local minimum, but it is higher in energy than the global minimum by 3.1 kcal/mol at the CCSD(T) level of theory. The n = 3 global minimum structure (**I3A** in Figure 4.4) is very similar to that found for BrHBr$^-$(H$_2$O)$_3$, with two waters donating hydrogen bonds and accepting hydrogen bonds from the third water molecule.

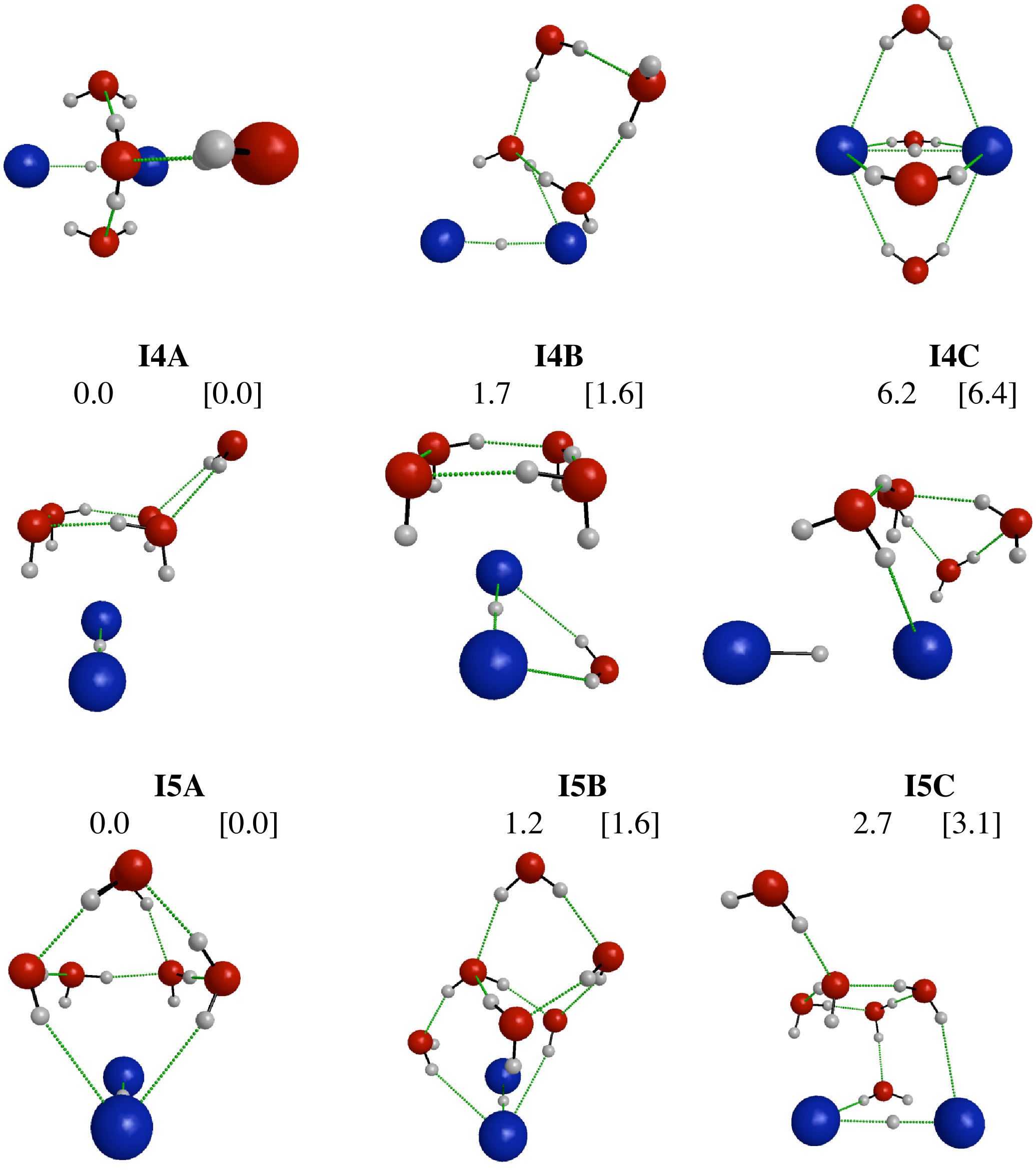

I4A 0.0 [0.0]
I4B 1.7 [1.6]
I4C 6.2 [6.4]

I5A 0.0 [0.0]
I5B 1.2 [1.6]
I5C 2.7 [3.1]

I6A 0.0 [0.0]
I6B 3.0 [1.8]
I6C 3.0 [2.6]

Figure 4.5. Global minima and sample structures for the IHI- solute solvated by n=4-6 water molecules.

المنارة للاستشارات

www.manaraa.com

Calculations on n=4 (see Figure 5) predict that a symmetric structure with all water hydrogen atoms donated in hydrogen bonds to the solute is a local minimum (no imaginary frequencies), but not the global minimum. This structure (**I4C**) is 6.4 kcal/mol higher in energy that the global minimum structure **(I4A**). **I4A** is similar to the n=3 global minimum, except that the fourth water molecule hydrogen bonds to the water cluster via one hydrogen bond.

Just as for $BrHBr^-$, the n=5 symmetric IHI^- structure with all water molecules donating their hydrogen atoms to the solute for hydrogen bonding, could not be located as a local minimum without imaginary frequencies. For IHI^-, the symmetric structure has four imaginary frequencies. Examining these normal modes shows that they will break the symmetry of the molecule if they are followed. The global minimum structure (Figure 5, **I5A**) favors hydrogen bonding between water molecules rather than multiple interactions with the solute. None of the I-H-O angles between the solute halide atoms, and the hydrogen and oxygen atoms of a water molecule are above 150°.

The predicted global minimum for $IHI^-(H_2O)_6$ (Figure 5, **I6A**) is very similar to that for $BrHBr^-(H_2O)_6$. This global minimum has four water molecules donating one hydrogen atom each to the solute for hydrogen bonding, while the other hydrogen atoms are donated to form another hydrogen bond with a different water molecule. The remaining two water molecules participate in water-water hydrogen bonds. It is possible for four water molecules to donate all of their hydrogen atoms for hydrogen bonding with the solute, as shown by structure **I6F** (Supporting Materials Figure 4.4). However, this structure is 8.2 kcal/mol higher in energy than the global minimum. As for $BrHBr^-$, a symmetric structure can be

www.manaraa.com

found as a local minimum but it is 22.1 kcal/mol higher in energy than the global minimum structure.

Discussion

For clusters with more than two water molecules, for X = Br, I, all water molecule hydrogen atoms may be donated to the solute for hydrogen bonding. However, such structures do not generally correspond to the global minimum geometries. An analysis of this observation can be analyzed in part by examining the Mulliken charge[31-34] distribution on both the solvated and unsolvated solute.

Table 4.2 shows the Mulliken charges for the $BrHBr^-$ solute solvated by n=0-4 water molecules. The structures in Table 4.2 are those in which the waters are arranged symmetrically about the solute and in which each water donates both of its hydrogen atoms to hydrogen bonds with the solute. Specifically, the species in the table are structure $BrHBr^-$ in Figure 4.1, structures **Br1A**, **Br2A**, **Br3B** in Figure 4.2, and structure **Br4B** in Figure 4.3. As additional solvent molecules are added to the solute, the total Mulliken charge on the solute itself does not change significantly from the gas phase value of -1. So, the total Mulliken charge on the solute is not the driving force for the structural arrangement of the solvent molecules.

Table 4.2. Mulliken charges for $BrHBr^-$ solvated by n=0-4 symmetrically arranged water molecules which donate all hydrogen atoms to the solute for hydrogen bonding.

n	Br	H	Total Charge
0	-0.78	+0.56	-1.00
1	-0.75	+0.53	-0.96
2	-0.72	+0.50	-0.94
3	-0.68	+0.42	-0.94
4	-0.58	+0.20	-0.97

www.manaraa.com

The individual Mulliken charges on the Br and H atoms do change significantly as the number of water molecules present increases. In particular, the absolute values of the charges on both the Br and H atoms all decrease. The Br charge increases from the unsolvated value of –0.78 to -0.58 when n=4. Concomitantly, the solute H atom charge decreases from +0.56 for the unsolvated solute to +0.20 for n=4. So, as solvent molecules are added, the excess electron density on the Br atoms delocalizes onto the H atom. This delocalization is likely to diminish the strong electrostatic (ion-molecule) attraction between the solute and the solvent molecules. This undoubtedly contributes to the reluctance of the solute to accommodate more than a small number of solvent molecules in an arrangement in which each solvent molecule contributes both of its hydrogen atoms to hydrogen bonds. As the electron density on the solute delocalizes, the waters also tend to form more water-water H-bonds

Analysis of IHI^- produces a similar qualitative picture, as illustrated in Table 4.3. The structures chosen for this analysis are **I1A**, **I2A**, and **I3C** in Figure 4.4 and **I4C** in Figure 5. The total Mulliken charge on the solute molecule remains close to the gas phase value of -1 as water molecules are added. Also, the charges on the individual I and H atoms in the solute remain approximately at their gas phase values as the number of water molecules increases from 0-3. Of course, these charges are already much smaller than those in $BrHBr^-$ (cf., Table 4.2). However, when a 4th water molecule is added, the charge on each I atom decreases to an absolute value of ~0.45, and the charge on the H atom becomes -0.18. So, as for $BrHBr^-$, there is substantial delocalization of the electron density as the number of associated solvent molecules increases. As noted above, this electron density delocalization very likely

www.manaraa.com

contributes to the inability of the solute to accommodate more than a small number of water molecules.

Table 4.3. Mulliken charges for the IHI^- molecule solvated by n=0-4 symmetrically arranged water molecules.

n	I	H	Total Charge
0	-0.50	+0.01	-1.00
1	-0.51	+0.03	-0.99
2	-0.52	+0.05	-1.00
3	-0.51	+0.02	-1.00
4	-0.45	-0.18	-1.07

Steric hindrance might also play a role in the relatively high energy of the larger symmetric structures. The O-O distances (in Angstroms) within the symmetric structures are given in Table 4.4 for $BrHBr^-(H_2O)_n$. The value for n=2 is smaller than that for n=3 because of the favorable dispersion interaction discussed previously. After n=3, the O-O distance decreases for each successive value of n as would be expected, as the structures become more crowded. While the symmetric structure for n=6 is free of imaginary frequencies, it is 20 kcal/mol higher than the global minimum, and the O-O distance is only 3.39Å Angstroms. So, in addition to the charge delocalization noted above, steric interactions also play a role in destabilizing the symmetric structures.

Table 4.4. O-O internuclear distances within the symmetric displaced $BrHBr\text{-}(H_2O)_n$ structures are given in Angstroms as a function of the number of water molecules, n.

n	O-O Distance
2	4.79
3	5.39
4	4.39
5	3.73
6	3.39

www.manaraa.com

Table 4.5. Total (TBE) and differential (DBE) binding energies for $BrHBr^{-}(H_2O)_n$ as a function of the number of water molecules n, at the MP2 and CCSD(T) levels of theory. Energies in kcal/mol.

n	MP2 TBE	MP2 DBE	CCSD(T) TBE	CCSD(T) DBE
1	-12.5	-12.5	-12.2	-12.2
2	-24.1	-11.6	-22.9	-10.7
3	-34.1	-10.0	-33.5	-10.6
4	-46.7	-12.7	-46.5	-13.0
5	-56.3	-9.6	-56.2	-9.7
6	-70.5	-14.2	-71.0	-14.9

Total binding energies (TBE) and differential binding energies (DBE) are given in kcal/mol for $BrHBr^{-}(H_2O)_n$ in Table 4.5 and for $IHI^{-}(H_2O)_n$ in Table 4.6. These binding energies were calculated by first obtaining a Boltzmann-averaged energy for each value of n. The total binding energy is the energy difference between the bound cluster, and the bare anion plus n individual water molecules. The differential binding energy is the predicted energy difference as an additional water molecule is added to the cluster.

Table 4.6. MP2 and CCSD(T) total (TBE) and differential (DBE) binding energies for $IHI^{-}[H_2O]_n$, as a function of the number of waters, n. Energies in kcal/mol.

n	MP2 TBE	MP2 DBE	CCSD(T) TBE	CCSD(T) DBE
1	-8.8	-8.8	-9.5	-9.5
2	-16.9	-8.1	-17.8	-8.3
3	-27.9	-11.1	-28.0	-10.2
4	-37.2	-9.2	-37.3	-9.3
5	-47.4	-10.3	-47.0	-9.7
6	-59.6	-12.1	-58.3	-11.4

Excellent qualitative and quantitative agreement exists between the binding energies predicted by MP2 and CCSD(T) for $XHX^{-}(H_2O)_n$, for both X = Br, I. The largest difference in the DBE between the two levels of theory is only 0.9 kcal/mol. It is clear from the structures displayed in Figures 3 and 5 that the first solvation shell is not complete for the n=6 global minimum structure. Indeed, none of the low-energy n = 6 structures are fully

www.manaraa.com

solvated. It is likely that the DBEs will not settle to a uniform value until the first solvation shell is complete.

Table 4.7. The predicted IR frequency of the antisymmetric X-H-X stretch vibrational mode is provided for every MP2 and CCSD(T) global minimum structure. All frequencies are given in units of cm^{-1}. When more than one antisymmetric vibrational mode was predicted, the range of values is given along with the total number of modes in the range and the frequency of the mode which is predicted to have the greatest intensity. All structures are given separately in the Figures.

Structure	IR Freq.	# of frequencies	Most Intense
BrHBr-	680.0	1	680.0
Br1A	686.9	1	686.9
Br2A	688.6	1	688.6
Br2C	709.3	1	709.3
Br3A	692.9	1	692.9
Br3C	1453.8	1	1453.8
Br4A	695.1, 852.2	1	695.1
Br5A	695.5, 754.0	2	754.0
Br6A	678.8-789.5	4	789.5
IHI-	632.8	1	632.8
I1A	649.6	1	649.6
I2A	662.9	1	662.9
I3A	661.1, 754.4	2	661.1
I4A	679.2, 824.3	2	679.2
I5A	610.4, 668.7, 699.0	3	699.0
I6A	591.1-763.1	5	656.4,685.8

Antisymmetric X-H-X stretch infrared (IR) vibrational frequencies are provided for every global minimum structure in Table 4.7. These frequencies were obtained from the MP2 Hessian calculations. For instances in which MP2 and CCSD(T) predict two different global minimum structures, the MP2 IR frequencies are reported for both minima (**Br2C** and **Br3C**). The unsolvated anions only have one IR-active mode. As the number of water solvent molecules increases, the number of frequencies with an antisymmetric X-H-X

www.manaraa.com

vibration increase. This corresponds to a broadened experimental IR peak as the cluster size grows. When multiple frequencies with an antisymmetric stretch characteristic are predicted in the Hessian, they often lie very close to each other and they are much more intense than any of the nearby peaks in the IR spectrum. Though the quantitative frequency values may be different experimentally, it seems that the X-H-X antisymmetric vibrational mode should be relatively easy to identify based on the predicted frequencies from the Hessians.

When studying the vibrational mode with the most intense peak (Table 4.7), it is clear that most of the reported $BrHBr^-(H_2O)_n$ frequencies lie between 680-800 cm^{-1} and most of the $IHI^-(H_2O)_n$ frequencies lie between 630-800 cm^{-1}. The one exception is **Br3C** which has a predicted X-H-X anti-symmetric stretch at 1453.8 cm^{-1}. Closely examining **Br3C** in Figure 4.2 reveals that the bihalide hydrogen atom lies closer to one bromine atom. The hydrogen is 1.9 angstroms from the bromine on the left and 1.5 angstroms from the bromine on the right. Because the hydrogen atom is not at an equal distance between the two bromine atoms, the force constant is different and the frequency is more like a hydrogen-bromine stretch than a Br-H-Br anti-symmetric stretch.

Conclusion

$BrHBr^-(H_2O)_n$ and $IHI^-(H_2O)_n$ geometries were optimized for n=1-6 at the MP2 level of theory. The water molecules prefer to donate all of their hydrogen atoms to the solute for n=1,2. However, although this type of structure is a local minimum for n=3,4 it is not a global minimum. For n=5,6 this type of structure is not a minimum on the potential energy surface. This is due in part to charge delocalization in the solute anion and in part to the increasing steric interactions among the water molecules with increasing n.

www.manaraa.com

Acknowledgements

This work was supported by a grant from the Chemistry Division, Basic Energy Sciences, Department of Energy, administered by the Ames Laboratory. The authors thank Professor Dan Neumark for useful discussions and comments.

References

1. Milligan, D. E.; Jacox, M. E. *J. Chem. Phys.*, **1971**, *55*, 2550.

2. Martin, J. S.; Fujiwara, F. Y. *J. Chem. Phys.*, **1972**, *56*, 4098.

3. Jiang, G. J.; Anderson, G. R. *J. Chem. Phys.*, **1973**, *60*, 3258.

4. Räsänen, M.; Seetula, J. *J. Chem. Phys.,* **1992**, *98*, 3914.

5. Lugez, C. L.; Jacox, M. E.; Thompson, W. E. *J. Chem. Phys.*, **1996**, *105*, 3901.

6. Rauk, A.; Armstrong, D. A. *J. Phys. Chem.*, **2000**, *104*, 7651.

7. Pivonka, N. L.; Kaposta, C.; von Helden, G.; Meijer, G.; Wöste, L.; Neumark, D. M.; Asmis, K. R. *J. Chem. Phys.*, **2002**, *117*, 6493.

8. Pivonka, N. L.; Kaposta, C.; Brümmer, M.; Meijer, G.; Wöste, L.; Neumark, D. M.; Asmis, K. R. *J. Chem. Phys.*, **2003**, *118*, 5275.

9. Caldwell, G.; Kebarle, P. *Can. J. Chem.,* **1985**, *63*, 3863.

10. McDaniel, D. H.; Vallée, R. E. *Inorg. Chem.*, **1963**, *2*, 2550.

11. Metz, R. B.; Neumark, D. M. *J. Chem. Phys.,* **1992**, *97*, 962.

12. Gómez, H.; Meloni, G.; Madrid, J.; Neumark, D. M. *J. Chem. Phys.*, **2003**, *119,* 872.

13. Fujiwara, F. Y.; Martin, J. S. *J. Chem. Phys.*, **1972**, *56,* 4091.

14. Pople, J. A.; Binkley, J. S.; Seeger, R. *Int. J. Quantum Chem. Sym.* **1976,** *10,* 1.

15. Frisch, M. J.; Head-Gordon, M.; Pople, J. A. *Chem. Phys. Lett.* **1990,** *166,* 275.

16. Fletcher, G. D.; Schmidt, M. W.; Gordon, M. S. *Adv. Chem. Phys.* **1999,** *110,* 267.

المنارة للاستشارات

www.manaraa.com

17. Aikens, C. M.; Webb, S. P.; Bell, R. L.; Fletcher, G. D.; Schmidt, M. W.; Gordon, M. S. *Theor. Chem. Acc.,* 2003, *110,* 233.

18. Ditchfield, R.; Hehre, W. J.; Pople, J. A. *J. Chem. Phys.*, **1971**, *54*, 724.

19. Pietro, W. J.; Levi, B. A.; Hehre, W. J.; Stewart, R. F. *Inorg. Chem.*, **1980**, *19*, 2225.

20. Hariharan,, P. C.; Pople, J. A. *Theoret. Chim. Acta*, **1973**, *28*, 213.

21. Binning, R.C. Jr.; Curtis, L.A. *J. Comput. Chem.*, **1990**, *11*, 1206.

22. Stevens, W. J.; Krauss, M.; Basch, H.; Jasien, P. G. *Can. J. Chem.*, **1992**, *70*, 612.

23. Schmidt, M. W.; Baldridge, K. K.; Boatz, J. A.; Jensen, J. H.; Koseki, S.; Matsunaga, N.; Gordon, M. S.; Ngugen, K. A.; Su, S.; Windus, T. L.; Elbert, S. T.; Montgomery, J.; Dupuis, M., *J. Comput. Chem.* **1993**, *14*, 1347.

24. Schmidt, Michael W., Gordon, Mark S. Theory and Applications of Computational Chemistry: The First Fourty Years. Elsevier, 2005, 1167-1189.

25. Bode, B. M. and Gordon, M. S. *J. Mol. Graphics Mod.*, **1998**, *16,* 133.

26. Piecuch, P.; Kucharski, S. A.; Kowalski, K.; Musial, M. *Comp. Phys. Commun.*, **2002**, *149*, 71.

27. Krishnan, R.; Binkley, J. S.; Seeger, R.; Pople, J. A. *J. Chem. Phys.*, **1980**, *72*, 650.

28. Curtiss, L. A.; McGrath, M. P.; Blaudeau, J.-P.; Davis, N. E.; Binning, R. C. Jr.; Radom, L. *J. Chem. Phys.*, **1995**, *14*, 6104.

29. Glukhovtsev, M. N.; Pross, A.; McGrath, M. P.; Radom, L. *J. Chem. Phys.*, **1995**, *103*, 1878.

30. Jeziorski, R.; Moszynski, R.; Szalewicz, K. *Chem. Rev.*, **1994**, *94*, 1887.

31. Mulliken, R. S. *J. Chem. Phys.*, **1955**, *23*, 1833.

32. Mulliken, R. S. *J. Chem. Phys.*, **1955**, *23*, 1841.

المنارة للاستشارات

www.manaraa.com

33. Mulliken, R. S. *J. Chem. Phys.*, **1955**, *23*, 2338.

34. Mulliken, R. S. *J. Chem. Phys.*, **1955**, *23*, 2343.

المنارة للاستشارات

www.manaraa.com

CHAPTER 5. STRUCTURE OF LARGE NITRATE-WATER CLUSTERS AT AMBIENT TEMPERATURES: SIMULATIONS WITH EFFECTIVE FRAGMENT POTENTIALS AND FORCE FIELDS WITH IMPLICATIONS FOR ATMOSPHERIC CHEMISTRY

A paper to be submitted to the *Journal of American Chemical Society*

Daniel D. Kemp[a], Mark S. Gordon,[a]

Yifat Miller[b], R. Benny Gerber[b],

Jennie L. Thomas[c], Douglas J. Tobias[c]

Barbara Finlayson-Pitts[c]

[a]Iowa State Univeristy

[b]Hebrew University

[c]Univeristy of California, Irvine

Abstract

Structural properties of large $NO_3^{-}\cdot(H_2O)_n$ (n = 15–500) clusters are studied by Monte Carlo simulations using Effective Fragment Potentials (EFPs), and by classical molecular dynamics simulations using a polarizable empirical force field. The simulation results are analyzed with a focus on the description of hydrogen-bonding and solvation in the clusters. In addition, a comparison between the electronic structure-based EFP and the classical force field description of the 32 water cluster system is presented. The EFP simulations, which focused on the cases of n = 15 and 32, show an internal, fully solvated structure and a “surface adsorbed” structure for the 32-water cluster at 300 K, with the latter configuration

www.manaraa.com

being more probable. The internal solvated structure and the "surface adsorbed" structure differ considerably in their hydrogen-bonding coordination numbers. The force field-based simulations agree qualitatively with these results, and the local geometry of NO_3^- and solvation at the surface-adsorbed site in the force field simulations are similar to those predicted using EFPs. Differences and similarities between the description of hydrogen-bonding of the anion in the two approaches are discussed. Extensive classical force field-based simulations at 250 K predict that long timescale stability of "internal" NO_3^-, which is characteristic of extended bulk aqueous interfaces, emerges only for $n > 300$. Møller-Plesset perturbation theory is used to test the geometries of selected surface and interior anions for $n=32$ and the results are compared to the EFP and MD simulations. Quantitatively, all approaches agree that surface structures are preferred over the interior structures for clusters of this size. The relatively large aqueous clusters of NO_3^- studied here are of comparable size to clusters that lead to new particle formation in air. Nitrate ions on the surface of such clusters may have significantly different photochemistry than the internal species. The possible implications of surface-adsorbed nitrate ions for atmospheric chemistry are discussed.

I. Introduction

The nitrate anion (NO_3^-) is one of the most abundant ions in the atmosphere.[1,2] It plays an important role in many atmospheric chemical[1,2] and biological[3,4] processes. The chemistry and the photochemistry of NO_3^- ions in aqueous aerosols may strongly depend on whether the ions are solvated in the bulk or present at the surface of the aerosol.[5] Therefore,

www.manaraa.com

understanding the solvation of NO_3^- and its propensity for the surface of aqueous solutions is important.

The behavior of nitrate ions at the air-solution interface of aqueous nitrate solutions has been the subject of a growing number of experimental investigations in recent years. Nonlinear vibrational spectroscopic measurements that probe environments lacking inversion symmetry, specifically, vibrational sum frequency generation (SFG) and second harmonic generation (SHG), have been used to study the interfaces of aqueous nitrate solutions. SFG spectra covering the range of frequencies of water O–H stretching vibrations have provided indirect evidence for the presence of nitrate ions in the vicinity of the air-water interface signaled by their perturbation of the water hydrogen bonding network.[6,7] The presence of nitrate in the interfacial region has also been demonstrated by direct SFG detection of the nitrate symmetric stretching mode.[8] However, SFG measurements are not capable of determining the precise location and details of the solvation of the ions, nor their relative concentration in the interfacial region vs. the bulk. UV-SHG experiments have also been employed to directly probe the presence of nitrate at the air-water interface.[9] The concentration dependence of the SHG intensity could be fit to a Langmuir adsorption isotherm, consistent with nitrate adsorption at the interface, but the free energy of adsorption could not be determined precisely from the fits. Thus, as in the case of the SFG data, the SHG data do not permit the amount of nitrate in the interfacial region to be accurately quantified. Electrospray ionization mass spectrometry measurements suggest that the affinity of nitrate for the air-water interface is slightly greater than that of bromide,[10] an ion that is generally considered to adsorb to the interface.[11] In contrast, analysis of surface tension data based on a thermodynamic partitioning model has led to the conclusion that the concentration

المنارة للاستشارات
www.manaraa.com

of nitrate at the air-water interface is the same as in the bulk.[12] Very recently, depth-resolved x-ray photoemission measurements were used to directly measure the concentration profile of nitrate ions at the air-solution interface.[13] These experiments clearly showed that nitrate is present in the interfacial region, but at a substantially lower concentration than in the bulk.

The first molecular dynamics (MD) simulation study of the behavior of nitrate at the air-solution interface suggested that nitrate has a propensity to adsorb to the air-water interface.[13,14] This conclusion was reached based on the observation that the nitrate ion remained at the interface for several hundred ps when a polarizable force field was employed. The force field results were corroborated by a density functional theory (DFT) MD simulation of a $NO_3^-\cdot(H_2O)_{10}$ cluster, in which the forces were obtained from the electronic structure computed via DFT with the BLYP exchange-correlation functional, that demonstrated the preference of the ion for the surface of the cluster.[14] Although the cluster results have not yet been called into question, subsequent more extensive force field-based studies of nitrate at extended bulk solution-air interfaces have consistently predicted that, while the nitrate ion is capable of visiting the interface, its concentration in the interfacial region is substantially depleted relative to the bulk solution,[15-17] in contrast to the original suggestion of a pronounced interfacial propensity.[13,14] A careful comparison with x-ray photoemission data has demonstrated semi-quantitative agreement between the depth-dependence of the nitrate concentration extracted from the experimental data and predicted by one of the more recent MD simulations employing a polarizable force field.[13]

A full understanding of the role of the interfacial environment in determining the reactivity of nitrate ions at aqueous surfaces in the atmosphere requires a more detailed description of the microsolvation of nitrate in interfacial settings over a range of atmospheric

www.manaraa.com

conditions. Electronic structure calculations and spectroscopic measurements have provided insight into the solvation of nitrate in small clusters containing up to six water molecules at low temperatures,[18-22] but data on larger clusters at ambient temperatures is lacking.

We focus here on the solvation of NO_3^- in relatively large water clusters, which are of interest for several reasons. First, while clusters are small compared to bulk systems, they may nevertheless provide insights into the behavior in the condensed phase and at extended bulk interfaces. Second, small to modest-sized clusters can be modeled realistically by more rigorous methods, and such systems can therefore serve as a proving ground for tools used for larger clusters and extended interfacial systems. Finally, the investigation of the dependence of various properties on cluster size may provide new fundamental insights into the bulk vs. interfacial solvation of nitrate ions.

One of the main challenges in theoretical investigations of ion solvation is the development of an accurate description of ion-solvent interactions. One can gain insight into ion-water interactions at the molecular level by using a quantum mechanical description of the forces. Molecular anions have complex charge distributions, so that electronic structure-based methods have unique advantages. However, an obvious disadvantage is the prohibitive increase in cost as the cluster size grows. Thus, empirical force fields are presently the most practical tool available for the theoretical investigation of the solvation of anions in very large water clusters and in bulk solution. Comparison of the two approaches for clusters of intermediate sizes is therefore of considerable value for establishing the accuracy of force fields.

In this paper we report a theoretical study of the solvation of NO_3^- in water clusters, $NO_3^-\cdot(H_2O)_n$, with n = 32–500, that employed three approaches. The first is Monte Carlo

المنارة للاستشارات

www.manaraa.com

(MC) simulations based on an electronic structure-based potential called the “Effective Fragment Potential” (EFP). The EFP method is feasible for cluster sizes of up to 32 or more water molecules, and can be used to test the empirical force field. The second is classical MD simulations based on an empirical polarizable force field. The third method is second order Møller-Plesset perturbation theory (MP2), which is used to optimize selected structures for n=32. The empirical force field is computationally applicable to larger clusters and bulk solutions. Thus, we present EFP results for n = 15 and n = 32, and use n = 32 for detailed comparisons with the force field-based simulations and MP2. We also investigate the dependence of the surface propensity of NO_3^- on cluster size using force field-based simulations of clusters with n = 100, 300, and 500 water molecules. Both the EFP and force field-based simulations predict that NO_3^- strongly prefers to reside on the surface of the cluster with n = 32, while MP2 predicts that surface structures are slightly preferred over the interior structures. The force field-based simulations predict that the surface propensity persists in clusters as large as n = 300, and that the preference of NO_3^- for the interior that has been demonstrated by both simulation and experimental investigations of bulk solutions[13,15-17] does not set in until n > 300 water molecules. The implications of the surface preference for NO_3^- in large clusters (n = 15–300) for atmospheric chemistry.

II. Methods

II. A. Effective Fragment Potential (EFP) calculations

المنارة للاستشارات

The Effective Fragment Potential (EFP) method, developed by Gordon and coworkers,[23,24] is a semi-classical model potential, derived from electronic structure theory, for computing intermolecular interactions between solutes and solvents or between solvent molecules. Central to the EFP is the evaluation of the charge distribution within the molecules based on first principles algorithms. The EFP approach has been successfully applied to the solvation of atomic anions in water clusters ($X^{-}\cdot(H_2O)_n$).[25,26] This paper presents the first application of the EFP approach to a solvated molecular anion, NO_3^-.

Global minimum energy structure searches were performed using the MP2 level of theory and the DH(d,p)[27] basis set for the NO_3^- anion. All of the water molecules were treated within the EFP framework. The general atomic and molecular electronic structure system GAMESS[28] was used for all of the EFP-based calculations.

Searches for the minimum energy structures, including the global minimum on the $NO_3^-\cdot(H_2O)_{32}$ potential energy surfaces, used a MC[29]/simulated annealing (SA)[30] code. The utilization of MC with EFP and the use of EFP itself have several advantages over electronic-structure methods and force field potentials. First, the EFP method can be used directly with MC simulations, and thus is applicable to sampling an equilibrium thermodynamic distribution of structures, while with *ab initio* electronic structure methods, only optimized structures can usually be obtained, due to the limitations of computer resources. For the calculation of room-temperature properties of floppy systems such as ion-water clusters, thermal fluctuations are clearly essential. Second, the energies of the equilibrium structures have been corrected with zero-point-energies, while in classical MD simulations, quantum effects are not taken into account. Finally, the EFP is not subject to the potential fitting and

www.manaraa.com

parameterization errors that could affect the accuracy of empirical force field-based descriptions of NO_3^-/water interactions.

MC/SA was used to initiate structure searches at 600 K and then to slowly cool the systems to 300 K. Geometry optimizations (at 0 K) were performed after every 10 steps in the MC simulations. All of the energies reported here include zero point energy (ZPE) corrections obtained from the Hessian, which is the matrix of the second derivative of the potential energy with respect to the nuclear coordinates. The total number of local minimum structures collected from the simulations for $NO_3^-\cdot(H_2O)_{32}$ is 35. All of the structures that were sampled in the simulations were verified to be local minima by ensuring that no negative eigenvalues (corresponding to imaginary frequencies) were present in the Hessian.

The population, P_j, of each structure j extracted from the simulations is computed using Eq. (1):

$$P_j = \frac{e^{-\Delta E_j / k_B T}}{\sum_j e^{-\Delta E_j / k_B T}}, \qquad (1)$$

ΔE_j is the energy difference between the jth structure and the global minimum structure of a given cluster, $T = 300$ K, and k_B is the Boltzmann constant. Average energies are computed using Eq. (2):

$$\langle E \rangle = \sum_j P_j E_j, \qquad (2)$$

in which the sum runs over the structures in a given class (e.g., structures with NO_3^- on the surface or in the interior of the cluster).

www.manaraa.com

II. B. Polarizable force field-based MD simulations

Simulations of clusters containing one NO_3^- ion and a given number of water molecules (n = 32, 100, 300, and 500) were performed using classical molecular dynamics. In order to obtain stable clusters, the velocities were reassigned periodically during the simulation to provide an average temperature of 250 K. For the cluster containing 32 waters the velocities were reassigned every 100 time steps, while for the larger clusters the velocities were reassigned every 1000 time steps. All simulations were carried out using the Amber 8 suite of programs.[31] The internal degrees of freedom of the water molecules were constrained using the SHAKE algorithm.[32] All of the simulations consisted of 500 ps equilibration followed by 3 ns production runs using a time step of 1 fs. For clusters containing up to 300 waters, all pair interactions were calculated explicitly (i.e., the nonbonded interactions were not truncated). For the 500-water cluster, periodic boundary conditions were employed and the electrostatic interactions were calculated using the Particle Mesh Ewald method[33,34] with a neutralizing background and a real space cutoff of 12 Å. The 500-water cluster was placed in a large cubic box with an edge length of 150 Å to approximate an isolated cluster.

A polarizable force field was used for both water and NO_3^-. Water molecules were modeled using the POL3 water model.[35] The force field for nitrate, adapted from the model used by Salvador and coworkers,[14] represents the polarizability by equal contributions from each NO_3^- oxygen ($\alpha = 1.49$ Å^3). The nitrate ion geometry is fixed using artificial O-O bonds in the simulations. The nitrate force field parameters used in the present study are summarized in Table 5.1. In order to avoid the polarization catastrophe,[36] induced dipoles

www.manaraa.com

have been calculated using a method developed previously with the scaling chosen to preserve the properties of neat water.[37] The force field employed here has been shown to perform well at reproducing the thermodynamic properties and composition of bulk interfaces of concentrated nitrate solutions.[13,17]

Table 5.1: Polarizable force field parameters for NO_3^- used in the present study given in the Amber[31] convention.

Atom	q (e)	α (Å^3)	R_m (Å)	ε (kcal/mol)
N (nitrate)	+0.950	0.000	1.880	0.170
O (nitrate)	–0.650	1.490	1.800	0.160

II. C. Møller-Plesset perturbation theory (MP2)

To examine the structures obtained from EFP simulations, MP2 single point energies were calculated for all n=32 structures. Then, three structures were chosen from the EFP simulations at n=32 for further optimization using MP2: the global minimum structure (a surface anion) and the two lowest-energy interior anion structures. All water molecules were expressed with MP2, rather than EFP potentials. The DH(d,p) basis set used to describe the anion in the EFP simulations was used for every atom in the MP2 optimizations.

III. Results and Discussion

المنارة للاستشارات

www.manaraa.com

III. A. Simulations with Effective Fragment Potentials: Structural Properties of $NO_3^{-}\cdot(H_2O)_{32}$

1. Distribution of Structures with NO_3^{-} in the Interior and on the Surface

In this section we characterize the solvation of NO_3^{-} both in the interior and on the surface of water clusters using configurations generated with the EFP method. The total number of different structures collected from the simulation of $NO_3^{-}\cdot(H_2O)_{32}$ is 35. Among these, NO_3^{-} is in the interior in 6 of the configurations and on the surface in 29 configurations. All of the structures sampled in the simulation are either local minima or the global minimum.

Two surface structures with relatively high population probabilities were predicted, using MP2 energies at the EFP geometries. The global minimum, which is statistically the most important structure found in the simulations, predicts that NO_3^{-} will reside on the surface of the cluster (Figure 5.1a). The surface structure shown in Figure 5.1b is nearly isoenergetic with the global minimum, with only ~0.01 kcal/mol separating them. The populations of the structures are computed using Eq. (1). These two structures (Figures 1a and 1b) are fairly similar and the percentage of population for each of these two structures is 45%, i.e., together they represent 90% of the population. Another surface adsorbed structure that constitutes a smaller population (9%) is shown in Figure 5.1c. This surface structure differs from the other two lower energy surface structures primarily with respect to the arrangement of the water molecules. The energy difference between the surface structure shown in Figure 5.1c and the global minimum surface structure is only ~1 kcal/mol. The

www.manaraa.com

population of each of the other 26 surface structures obtained in the simulations (not shown here) is much less than 1%, and the energy differences of these structures from the global minimum are in the range of 3–20 kcal/mol. The sum of the populations of all of these other structures is only ~2%.

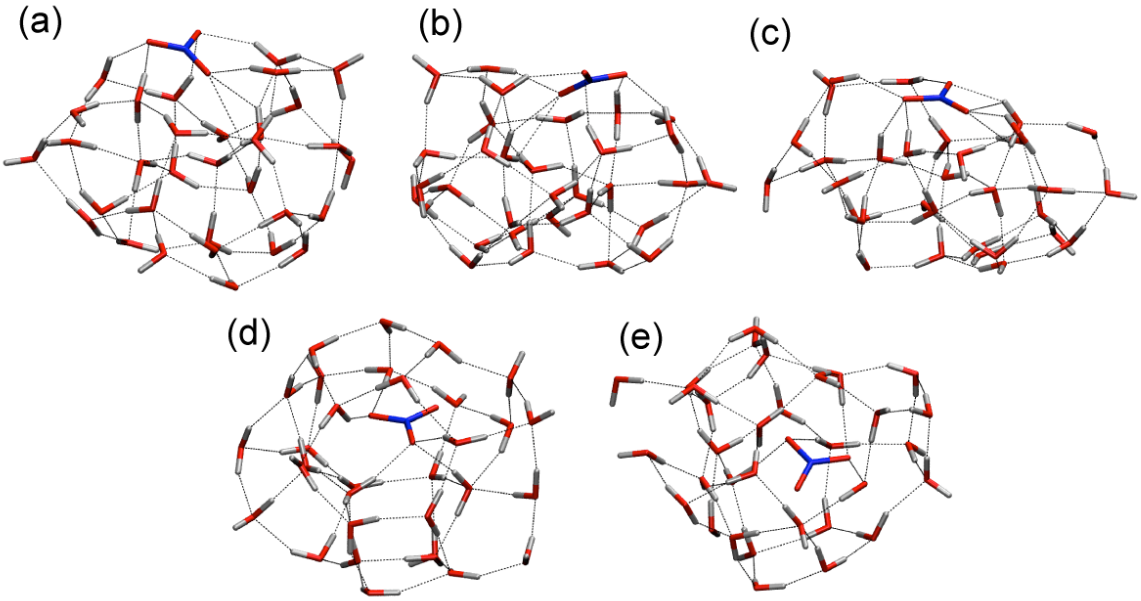

Figure 5.1. EFP minimum energy structures for $NO_3^- \cdot (H_2O)_{32}$: (a) nitrate on the surface, global minimum structure; (b) and (c) nitrate on the surface, local minima; (d) nitrate inside the cluster, local minimum (e) second lowest-energy interior anion structure. Coloring scheme used throughout the paper: O, red; N, blue; H, light gray.

Six interior structures were obtained in the simulations, but there is only one significant interior structure due to its greater stability than the other interior structures. The population of the lowest energy interior structure, shown in Figure 5.1d, is only ~ 4×10^{-4} %. The energy difference between this structure and the global minimum surface structure is 7 kcal/mol. The contribution of each of the other 26 surface structures obtained in the

المنارة للاستشارات
www.manaraa.com

simulations (not shown here) is much less than 1% and the energy difference of these structures from the global minimum is relatively high. For example, the energy difference between the second-lowest energy interior structure (Figure 5.1e) to the global minimum (Figure 5.1a) is 12.8 kcal/mol. The population ratio between surface and interior structures is 99.9996:0.0004. Thus, it is safe to say that, in the relatively small n=32 cluster, the NO_3^- is almost always on the surface and almost never inside the cluster at the MP2/EFP1 level of theory.

The average energies of both the surface and the interior structures of $NO_3^-\cdot(H_2O)_{32}$ were computed using equation (2). The difference between the average energy of the interior structures and the average energy of the surface structures [Se Eq. (2)], 7 kcal/mol, is a measure of the stability of the surface versus interior of NO_3^- in a cluster of 32 water molecules at the MP2/EFP level of theory.

2. Structure and Solvation of NO_3^- at the Surface and in the Interior

The structural properties of both surface and interior structures are characterized using the following four properties: the number of solvated O atoms of the NO_3^-, the number of water molecules that have hydrogen bonds with the three O atoms in NO_3^-, lengths of hydrogen bonds between NO_3^- and water molecules, and the NOH angle, defined as the angle between the N atom of NO_3^- and the O–H bond of a solvating H_2O molecule.

We define the number of solvated O atoms as the number of O atoms of NO_3^- that are hydrogen bonded to water molecules. The criterion used to define a hydrogen bond is distance less than 2Å. The number of solvated O atoms in NO_3^- for the surface structures of

المنارة للاستشارات www.manaraa.com

$NO_3^-{\cdot}(H_2O)_{32}$ is predominately one (~43%) or two (~47%). Only a few structures (~10%) have all three oxygen atoms in NO_3^- hydrogen bonded to water molecules. In a few cases, one O atom in NO_3^- has more than one hydrogen bond. For the interior structures, the number of solvated O atoms in NO_3^- is either two (~55%) or three (~45%).

The coordination number is defined as the number of water molecules that hydrogen bond with the O atoms in NO_3^-. There may be more than one water molecule that participates in hydrogen bonding with an individual O atom in NO_3^-. The coordination numbers predicted for the surface structures of $NO_3^-{\cdot}(H_2O)_{32}$ are in the range of 1-4, with the most probable number of water molecules around the ion being 2–3. For interior structures, the coordination numbers are predominantly 3 and 4 (86% of the structures), and 5 in relatively few cases (14% of the structures). As expected, the coordination numbers for the interior structures are larger than those for the surface structure.

Additional information on the solvation of nitrate in $NO_3^-{\cdot}(H_2O)_{32}$ is provided by the distribution of the distances between each of the nitrate O atoms and the H atoms of coordinating water molecules. It is found that 48% of the structures with nitrate on the surface have $O_{nitrate}$–H_{water} distances of 1.95–2.00 Å, 36% have distances of 1.90–1.95 Å, and only 16% have distances of 1.85–1.90 Å. In the interior structures, the most probable value of the hydrogen bond distance is in the range 1.85–1.90 Å. Thus, the distribution is shifted to shorter distances, and this indicates that the NO_3^-/water hydrogen bonding is stronger for the interior structures. The fact that the interior site is much higher in total energy than the surface is most likely due to the disruption of the water-water hydrogen-bonded network in the interior sites. Thus, while NO_3^- can make reasonably strong hydrogen bonds with water

www.manaraa.com

molecules, these do not sufficiently compensate for the disruption of water-water hydrogen bonds, at least in small clusters.

The $N_{nitrate}$–$O_{nitrate}$–H_{water} (NOH) angle provides a metric for discriminating between interior and surface solvation of NO_3^-. The preferred angle for both interior and surface structures lies in the range 90–110°; 38% of the interior structures have an angle of 90–100°, while 46% of the surface structures have an angle of 100–110°. The interior structures have a small population (~4%) of angles in the range of 140–150°, while none of the surface structures have NOH angles in this range.

III. B. Cluster Size Effect in the Small Cluster Regime: $NO_3^-\cdot(H_2O)_{15}$ versus $NO_3^-\cdot(H_2O)_{32}$

In contrast to n = 32, for which there is a stable local minimum with the nitrate ion in the interior of the cluster (albeit with very low population), there is (based on the EFP calculations) no stable interior site for n = 15. There are, however, several distinct surface structures. The global minimum, which is statistically the most important structure found in the simulations (58% population), is the surface adsorbed structure shown in Figure 5.2a. The surface structure that is depicted in Figure 5.2b is a local minimum with a population of 38%, which is ~0.25 kcal/mol higher in energy than the global minimum structure. While the first solvation shell of 2a and 2b are very similar, the structures do differ in the arrangements of the water molecules and the orientation of their hydrogen atoms. The populations of the other surface structures obtained in the simulations (not shown here) are 1% or smaller, and the energy differences of these structures from the global minimum are in the range of 2–10 kcal/mol.

المنارة للاستشارات

www.manaraa.com

The number of solvated nitrate O atoms for the $NO_3^-\cdot(H_2O)_{15}$ surface structures is predominately one or three (33% for one solvated O atom and 33% for three solvated O atoms). However, 18% of the structures have two nitrate O atoms hydrogen bonded to water molecules. As noted earlier, the number of solvated nitrate O atoms in $NO_3^-\cdot(H_2O)_{32}$ surface structures is predominately one or two. Only a few structures (~10%) have three NO_3^-oxygen atoms that are hydrogen bonded to water molecules.

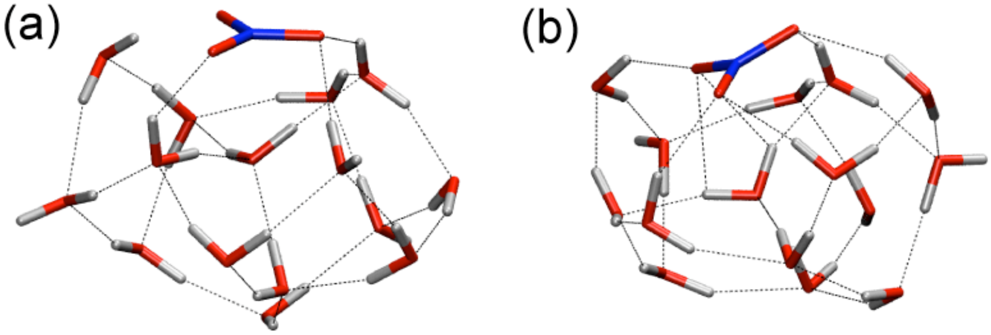

Figure 5.2. EFP minimum energy structures for $NO_3^-\cdot(H_2O)_{15}$: (a) nitrate on the surface, global minimum; (b) nitrate on the surface, local minimum.

The coordination numbers predicted for the $NO_3^-\cdot(H_2O)_{15}$ surface structures are in the range of 1–3, with the most probable number of water molecules around the ion being 1–2 (~84% of the population). This can be compared to the coordination numbers predicted for the surface structures of $NO_3^-\cdot(H_2O)_{32}$, which are in the range of 1–4, with the most probable number of water molecules around the ion being 2–3.

For the $NO_3^-\cdot(H_2O)_{15}$ surface structures, 45% have hydrogen bond distances of 1.95-2.00 Å, 37% have hydrogen bond distances of 1.90–1.95 Å, 16% have hydrogen bond distances of 1.85–1.90 Å, and only 2% have hydrogen bond distances of 1.80–1.85 Å. This is very similar

www.manaraa.com

to that found for the cluster with 32 water molecules, indicating that the hydrogen bond distances are not very sensitive to cluster size.

The preferred NOH angle for $NO_3^-{\cdot}(H_2O)_{32}$ surface structures lies between 90-110°, as 48% of the surface structures have an angle of 100–110°. For the smaller $NO_3^-{\cdot}(H_2O)_{15}$ cluster the preferred angle in surface structures also lies in the range 90–110°; 31% of the surface structures have an angle of 100–110°. However, 24% of the surface structures of $NO_3^-{\cdot}(H_2O)_{15}$ have angles lying between 120–130°.

To summarize the results of the EFP calculations reported thus far, the n = 15 and n = 32 clusters differ somewhat in their structural properties, insofar as the location of the NO_3^- ion is concerned. The n = 15 cluster has more than one important surface-like structure. This cluster may be more "floppy" and structureless because it is very small. However, for n = 32, both well-defined surface and internal structures are predicted, although the surface location is overwhelmingly more favorable energetically, and one can describe the solvating water molecules as forming a "droplet" shape.

III. C. Structure and Ion Solvation in $NO_3^-{\cdot}(H_2O)_{32}$: Force Field-based MD Simulations vs. EFP

The relatively minor computational cost of the empirical force field permits extensive sampling of the ion position and solvation in large nitrate-water clusters during a MD simulation at 250 K. The MD simulation of $NO_3^-{\cdot}(H_2O)_{32}$ was initiated with the ion in the center of the cluster. The ion rapidly went to the surface of the cluster during the equilibration, and never returned to the interior during the 3 ns production run. The water O radial density profile, $\rho(r)$, and the probability of finding the nitrate N atom at a distance r

www.manaraa.com

from the cluster center-of-mass, are plotted in Figure 5.3a. The water density is consistent with a diffuse droplet shape with an average radius of ~5 Å. The NO_3^- probability distribution shows that the ion is exclusively located on the surface of the cluster, on average ~4.5 Å from the center-of-mass. The representative snapshot from the MD simulation depicted in Figure 5.3b shows that cluster shape and the ion arrangement on the cluster are similar to the corresponding attributes of the highest probability clusters generated by the EFP (Figure 5.1a-c). Thus, both the force field and EFP predict that the predominant structures of $NO_3^-\cdot(H_2O)_{32}$ have the nitrate ion sitting on the surface with its plane parallel to the water-vacuum "interface".

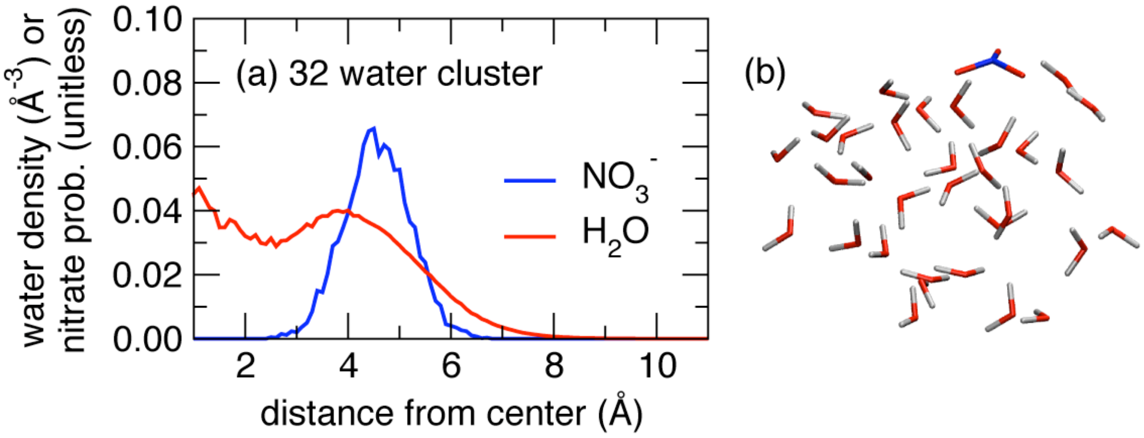

Figure 5.3. (a) Water density profile (red curve) and radial probability distribution of the nitrate N atom (blue curve) plotted vs. the distance from the center-of-mass in the force field-based MD simulation of $NO_3^-\cdot(H_2O)_{32}$. (b) Snapshot from the MD simulation of $NO_3^-\cdot(H_2O)_{32}$.

Although the force field and EFP agree that NO_3^- predominantly resides on the surface of $NO_3^-\cdot(H_2O)_{32}$, there are some noteworthy discrepancies in the details of the ion solvation predicted by the two methods. For example, the $O_{nitrate}$–H_{water} radial distribution

www.manaraa.com

functions $g(r)$ plotted in Figure 5.4 reveal subtle differences in differences in hydrogen bonding. The EFP result was computed by only considering configurations in which the NO_3^- ion is on the surface of the cluster. While the $g(r)$ computed from the EFP-generated configurations is noisier due to limited sampling, both the EFP and the force field results display sharp first and relatively broad second peaks, indicating the existence of a tight first and diffuse second solvation shell. The positions of the first and second peaks from the force field-based simulation, 1.8 Å and 2.1 Å, respectively, are significantly smaller than the corresponding values from the EFP calculations, 2.1 Å and 3.4 Å, respectively. Thus, the force field predicts shorter nitrate-water hydrogen bonds than the EFP.

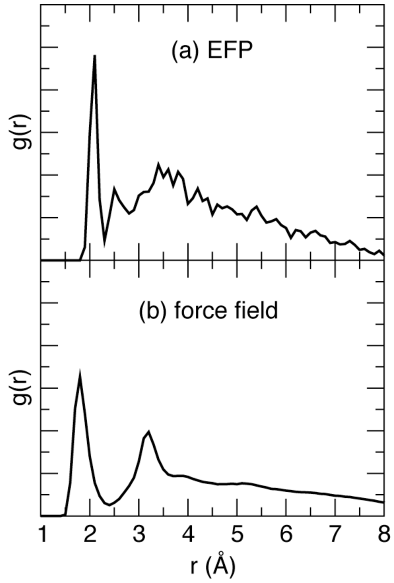

Figure 5.4. Radial distribution functions of water H atoms around nitrate O atoms in $NO_3^-{\cdot}(H_2O)_{32}$ clusters computed from: (a) minimum energy configurations from ELP calculations with the nitrate ion on the surface of the cluster; (b) configurations from the force field-based MD simulation. Due to the lack of a well-defined reference density to normalize $g(r)$ for these small cluster systems, the absolute scale is arbitrary and has therefore been omitted.

www.manaraa.com

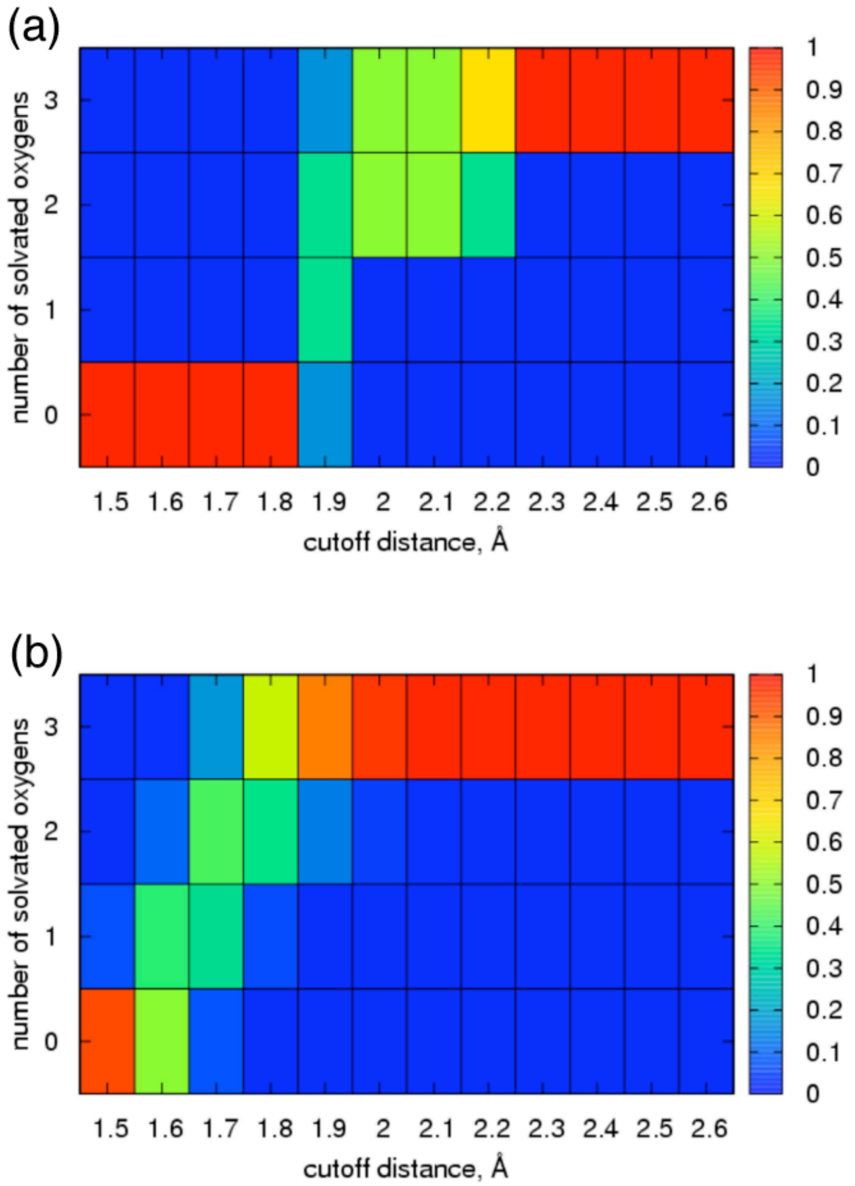

Figure 5.5. The probability of observing a specific number of solvated nitrate oxygen atoms as a function of the $O_{nitrate}$-H_{water} hydrogen bonding cutoff distance in $NO_3^-\cdot(H_2O)_{32}$ clusters. (a) Minimum energy configurations from EFP calculations with the nitrate ion on the surface of the cluster. (b) Configurations from the force field-based MD simulation.

Additional details on the nitrate-water interactions are provided by the histograms of the number of nitrate O atoms that are solvated by water molecules, plotted in Figure 5.5 as a

www.manaraa.com

function of the $O_{nitrate}$–H_{water} cutoff distance used to define a nitrate-water hydrogen bond. Overall, these plots are consistent with the conclusion from the $g(r)$ data that the force field predicts shorter hydrogen bonds than does the EFP method, in the sense that more hydrogen bonds are counted at short cutoff distances in the force field results vs. the EFP. In the discussion of liquid structure, the position of the first minimum in $g(r)$ is used to define the spatial extent of the first solvation shell. If the hydrogen bond cutoff is defined by the position of the first minimum in the $O_{nitrate}$–H_{water} $g(r)$, which occurs at 2.3–2.4 Å, then both the EFP and force field-based simulations consistently predict that all three nitrate O atoms are solvated essentially all the time when the ion is on the surface of the cluster.

Overall, the preferred nitrate ion location and solvation in $NO_3^-\cdot(H_2O)_{32}$ predicted by the empirical polarizable force field used in this work compares favorably with the more accurate, but computationally costly, electronic structure-based EFP method. In addition to validating the qualitative predictions of the force field, the fact that a consistent picture emerges from both approaches testifies to the robustness of the results.

III. D. Classical Polarizable Force Field Simulations of $NO_3^-\cdot(H_2O)_n$, n = 100, 300, and 500: Evolution of Structural Properties with Cluster Size

The strong surface propensity of nitrate in modest-sized (15–32 water) clusters is qualitatively different from the behavior of nitrate near extended interfaces of bulk aqueous solutions. The consensus that has emerged recently from both theoretical and experimental studies is that nitrate approaches the air-solution interface, but does not strongly adsorb, in concentrated bulk solutions.[9,13-17] It is therefore expected that a crossover in the preference from surface to interior solvation should be observed in clusters at some point as the cluster

www.manaraa.com

size is increased. We have investigated the cluster size-dependence of nitrate solvation by performing additional simulations of nitrate-water clusters with n = 100, 300, and 500 water molecules. These larger clusters were investigated with empirical force field-based MD simulations only.

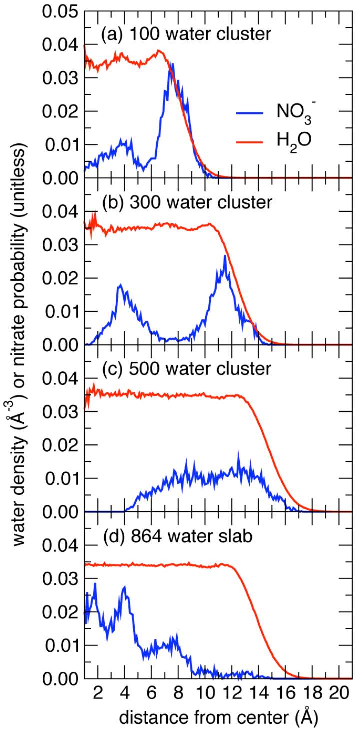

Figure 6. Water density profiles (red curves) and probability distributions of the nitrate N atom (blue curves) plotted vs. the distance from the center-of-mass in the force field-based MD simulations of (a) $NO_3^-\cdot(H_2O)_{100}$ cluster; (b) $NO_3^-\cdot(H_2O)_{300}$ cluster; (c) $NO_3^-\cdot(H_2O)_{500}$ cluster; (d) 864 water slab (bulk).

Water radial density profiles that define the extent of the cluster are plotted in Figure 6 along with the probability of finding the nitrate N atom at a distance *r* from the center-of-mass of clusters with n = 100, 300, and 500 water molecules. For comparison, the water density profile and nitrate distribution obtained from a simulation of a single nitrate ion in a

www.manaraa.com

slab of 864 water molecules with periodic boundary conditions that generate an extended bulk air-water interface are shown in Figure 6d. The data plotted in Figure 6d confirm that the nitrate ion prefers the interior and avoids the surface of the solution in an extended interfacial setting. In the 100 and 300 water clusters, the nitrate probability distribution displays two peaks, corresponding to interior and surface locations of the ion. In the 100 water cluster, the population at the surface is about three times greater than the interior, while in the 300 water cluster the surface is only slightly favored over the interior. In the 500 water cluster, a distinct surface population is no longer discernable, and population of nitrate that is well-solvated in the interior of the cluster clearly exceeds that near the surface of the cluster. Snapshots depicting the preferred location of nitrate in clusters with n = 100, 300, and 500 water molecules are shown in Figure 7.

In summary, this study shows that the nitrate anion in water clusters prefers to lie on the surface of the smaller clusters considered here (n = 15, 32, 100, and 300 water molecules). However, this preference decreases with an increase in the cluster size. For a relatively large cluster consisting of 500 water molecules, the nitrate anion no longer displays strong surface adsorption, and it spends the majority of the time well-solvated in the interior of the cluster. This decrease in surface propensity is presumably driven, in part, by entropy due to an increase in the ratio of interior sites to surface sites as the size of the cluster increases. There could also be an energetic component associated with the organization of the solvent shells around the ion.

المنارة للاستشارات

www.manaraa.com

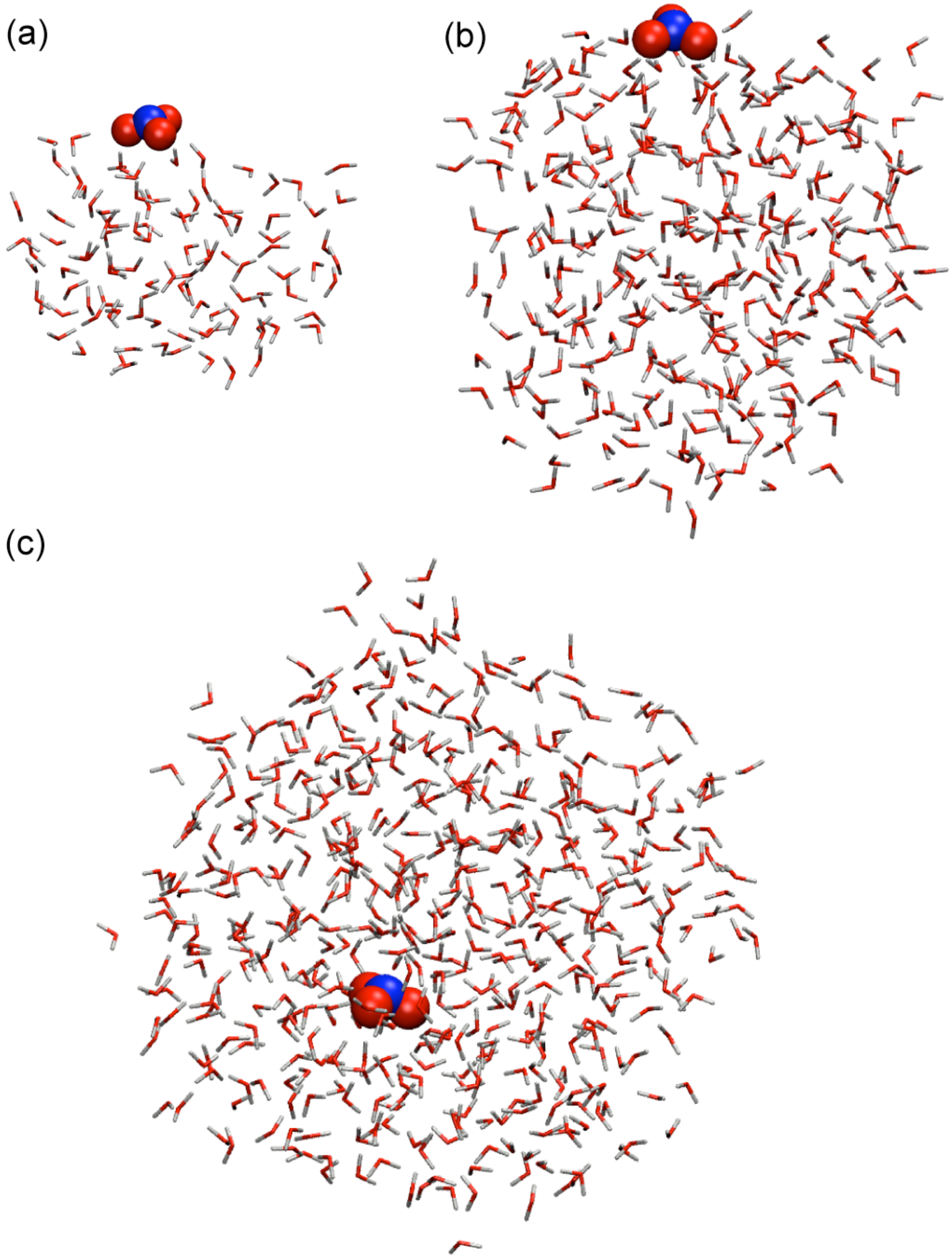

Figure 7. Representative snapshots from the force field-based MD simulations of (a) $NO_3^-\cdot(H_2O)_{100}$; (b) $NO_3^-\cdot(H_2O)_{300}$; (c) $NO_3^-\cdot(H_2O)_{500}$. The snapshots depict the preferred surface location of nitrate in the 100 and 300 water clusters, and the preferred interior location in the 500 water cluster.

المنارة للاستشارات
www.manaraa.com

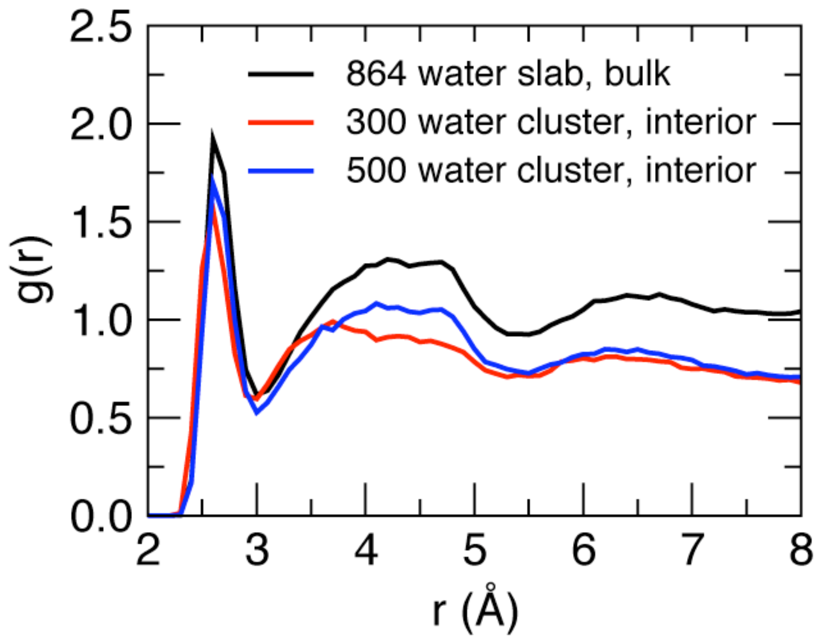

Figure 8. Radial distribution functions of water O atoms around nitrate O atoms from force field-based MD simulation configurations in which the nitrate ion is in the interior of clusters or a bulk water slab: red, $NO_3^-\cdot(H_2O)_{300}$; blue, $NO_3^-\cdot(H_2O)_{500}$; black, 864 water slab.

Analysis of nitrate solvation using MD simulations of bulk solutions reveals a diffuse solvent shell around nitrate, which is manifested as a broad split first peak in the $N_{nitrate}$–O_{water} radial distribution function, that contains ~18 water molecules and extends to ~5 Å from the N atom.[17] A reasonable hypothesis is that the interior location of the nitrate ion is disfavored in the smaller clusters due to the inability to support the complex solvent organization around the ion that is preferred in bulk solution. This hypothesis is supported by the $O_{nitrate}$–O_{water} radial distribution functions plotted in Figure 8, which display two prominent peaks. Except for a disparity in scale due to the difference in the normalization of bulk and cluster radial distribution functions, the $g(r)$ for nitrate on the interior of the 500 water cluster is essentially

www.manaraa.com

identical to that of nitrate in the interior of the extended slab. Thus, the interior of the 500 water slab supports the solvation environment preferred by nitrate in dilute bulk solution. In contrast, the second peak in the *g*(*r*) for nitrate on the interior of the 300 water cluster is suppressed, indicating, remarkably, that the complex solvation environment preferred by nitrate in bulk solution cannot be fully accommodated in this large cluster. Evidently, the full development of the solvent shells provides additional energetic stabilization that favors the bulk environment in the 500 water cluster and extended slab.

III. E. Optimization of surface and interior structures by MP2 level of theory

MP2 single point energies were computed for all n=32 structures obtained from MP2/EFP simulations and the energy differences between the structures were computed as well. To assess the accuracy of the predicted structures obtained from the MP2/EFP simulations, we optimized the structures with the MP2 level of theory, computed the energy differences between the structures and compared the results to the MP2/EFP level of theory. Since optimization with the MP2 level of theory including the Hessian calculations is computationally expensive, optimization without Hessian calculations were performed for only three selected structures obtained from the MP2/EFP simulations: the global minimum (Figure 5.1a) and the two lowest-energy interior anion structures (shown in Figs. 1d and 1e). For the $(H_2O)_{32}{\bullet}NO_3^-$ cluster, both MP2/EFP and MP2 predict that the nitrate prefers to “sit” on the surface rather than be in a bulk solvated environmental. Further, MP2/EFP predicts that the population probabilities of the surface structures are much higher than that of the

المنارة للاستشارات
www.manaraa.com

population probabilities of the interior structures, which are so small that they can be neglected.

However, quantitatively, there are differences between the prediction of the MP2/EFP method and the MP2 method in the relative energies between the structures. Table 5.2 summarizes the differences in the relative energies for the structures shown in Figure 5.1. For example, while in the MP2/EFP simulations the energy difference between the surface structure (global minimum) (Figure 5.1a) and the most stable interior structure (Figure 5.1d) is 6.9 kcal/mol, after MP2 optimization, the energy difference between these two structures is only 0.5 kcal/mol.

Table 5.2: Comparison of the relative energies of surface and interior structures for $NO_3^-{\cdot}(H_2O)_{32}$ and of the averaged hydrogen bonding distances for the MP2/EFP1 method and MP2 level of theory. Average hydrogen bond distances between water molecules that are connected to the nitrate ion and other water molecules are provided.

Structure Type	MP2/EFP1 relative energy	MP2 single point relative energy	MP2 optimized relative energy	MP2/EFP1 $O_{nitrate}$-H_{water} distance	MP2 $O_{nitrate}$-H_{water} bond distance	MP2/EFP1 average H-bond distance	MP2 average H-bond distance	Figure
Surface	0.00	2.5	0	1.99	1.91	1.74	1.83	1a
Surface	0.01	2.5	-	-	-	-	-	1b
Surface	1.0	2.8	-	-	-	-	-	1c
Interior	6.9	0	0.5	1.86	1.83	1.78	2.21	1d
Interior	12.8	8.3	6.9	2.03	1.83	1.74	1.84	1e

These results suggest that even though the global minimum structure is a surface anion, interior anion structures may be nearly isoenergetic with the global minimum. Contrary to the results of many studies utilizing inexpensive empirical potentials, it is possible that n=32 is approaching a sufficiently large enough cluster to complete the first solvation shell around the nitrate anion and form an interior anion. This also suggests that

www.manaraa.com

the hydrogen bonding environment of aqueous nitrate solutions may be too complex to quantitatively study with inexpensive model potentials. Though the quantitative agreement with MP2 is not as good as one would like, it is important to point out that the MP2/EFP simulations did find energetically relevant interior anions. The relatively inexpensive MP2/EFP level of theory is able to obtain energetically relevant minima at much smaller computational cost compared to MP2 calculations. When the structures are obtained with MP2/EFP and the relative energies are calculated with MP2, the most accurate relative energies available for systems of this size can be obtained for a broad sample of structures.

Comparison of the averaged hydrogen bond distances of each of the three selected structures obtained in MP2/EFP simulations and their optimized structures by MP2 level of theory is summarize in Table 5.2. The average $O_{nitrate}$-H_{water} distance differs between the two methods by only 0.08 Å for the lowest energy surface anion (Figure 5.1a), while the average hydrogen bond distance differs by 0.9 Å. The average hydrogen bonding distances of the interior structures shown in Figures 1d and 1e differ between the two methods by 0.43 Å and 0.1 Å, respectively. Visual inspection of the structures reveals that the internal geometries of the water molecules change more than the placement of the solvent molecules with respect to the whole cluster. Despite the structural changes which occur during optimization, the relative energies of the optimized structures do not differ much from the MP2 single points.

The quantitative differences between the relative energies at the MP2/EFP and the relative energies at the MP2 level of theory may be due to dispersion. EFP does not include dispersion effects while MP2 does. The charge distribution of the nitrate anion may be complex enough that the dispersion forces between the solute and the solvent molecules may play a key role in determining whether or not the anion is completely solvated. A general

www.manaraa.com

potential model, called EFP2, has been developed and includes dispersion. However, it has not yet been fully interfaced with *ab initio* calculations. Studying the importance of dispersion will be the focus of a future study when the EFP2/*ab initio* interface is complete.

These results show that solely relying on model potentials may not always provide accurate quantitative results for every cluster size and checking the results with *ab initio* methods is necessary. This serves as a reminder of the importance of *ab initio* calculations and verifying results with the highest level of theory that is computationally feasible.

IV. Atmospheric Relevance of Nitrate-Water Clusters

The formation and growth of new particles in air is important for understanding and predicting their effects on visibility, health and climate.[38-40] Elucidating the species involved in nucleation in particular has been difficult due to the small size of the clusters and the lack of analytical methods to probe such small amounts of material. While it is clear that sulfuric acid is often responsible for new particle formation, there are intriguing hints that nitrogen may also play a role. For example, nitrogen and organics have often both been found in sub-10 nm-sized particles in some studies, with the organic being more closely associated with nitrogen than with sulfate.[41,42] The form of nitrogen in the particles is not well known but appears to be at least in part, nitrate ions.

The photochemistry of nitrate ions in bulk solution is well known:[43,44,45]

$$NO_3^- + h\nu \rightarrow NO_2 + O^- \xrightarrow{H_2O} NO_2 + OH + OH^- \qquad (3)$$

المنارة للاستشارات

www.manaraa.com

$$\rightarrow \; NO_2^- + O(^3P) \qquad (4)$$

The overall quantum yields for production of OH and $O(^3P)$ in bulk solutions are $\phi_3 = 0.009$ and $\phi_4 = 0.001$, respectively, at 305 nm.[43-45] This photochemistry is important under some conditions in the atmosphere, since nitrate is a ubiquitous component of atmospheric aerosols, snowpacks and urban surfaces.[1] For example, photochemical production of NO_x in snowpacks has been attributed primarily to reactions 3 and 4.[46-53]

There is reason to believe that the photochemistry of nitrate ions may be quantitatively, and perhaps qualitatively, different when the nitrate ion is on the surface compared to the bulk. At the interface, there is an incomplete solvent cage so that one would expect less recombination of NO_2 with O^- and of NO with $O(^3P)$, leading to larger overall quantum yields.[54] A particularly intriguing result from the present study is the high percentage of surface structures that have only one O atom in NO_3^- that is solvated compared to none in the bulk, where either two or all three O atoms are solvated. In addition, a large percentage of the surface nitrate ions have only one or two water molecules that are hydrogen bonded to O atoms in the nitrate, whereas none in the bulk are so under-coordinated. This significant difference in the interaction of nitrate ions with surrounding water molecules may change the overall quantum yields for OH and $O(^3P)$ production, and potentially also the relative importance of these two pathways. For example, enhanced production of gas phase NO_2 seems likely if the nitrate photolyzes while only one of the oxygen atoms is hydrogen-bonded to water, compared to the situation in the bulk where two or three of the nitrate oxygen atoms are hydrogen-bonded.

www.manaraa.com

Enhanced production of the oxidants OH and O(^{3}P) at the interface may result in unique, and as yet unrecognized, photochemistry in the atmosphere. For example, some atmospherically important organic gases such as α-pinene[55] and napthalene[16,56-58] have significant residence times on aqueous surfaces. If there is generation of highly reactive OH and O(^{3}P) nitrate at the interface by nitrate ion photolysis, then there is the potential for oxidation of the organics adsorbed at the surface. If the volatility of the organic oxidation products is small and/or they are soluble, they will remain associated with the particle. This new mechanism of formation of organics in particles would lead to an association between nitrate and organics, especially in the smallest particles where nitrate is predicted from the current work to reside at the interface. Clusters of 32–300, where the nitrate ion prefers the surface, correspond to particles with diameters of the order of 1–2.5 nm in the atmosphere, where nucleation and growth is in the early stages. Such a mechanism may contribute to the finding of nitrogen and organics in the smallest particles observed in Mexico City by Smith and coworkers.[41,42] In addition, the possibility should be considered that when nitrate begins to favor the interior for larger clusters, oxidants will continue to be generated at the surface via formation in the bulk followed by diffusion to the interface.

Finally, thin films of water exist on surfaces in the tropospheric boundary layer.[59] Gaseous nitric acid undergoes rapid deposition on such surfaces,[1] and is formed on them via heterogeneous chemistry such as the hydrolysis of adsorbed NO_2/N_2O_4.[60] Nitrate is also taken up on urban surfaces by the deposition of nitrate-containing particles. Such surfaces are known to adsorb organics from air.[61-63] Depending on the nature of water on these surfaces, which is currently not well understood,[64] nitrate ions may also prefer the interface in these thin films as well, leading to enhancement of the photochemical oxidations of co-adsorbed

www.manaraa.com

organics. Relevant to this possibility is recent work on films of organics and nitric acid by Handely et al[65] in which photochemical loss of HNO_3 was observed and attributed to photoreduction of the HNO_3. Such chemistry on urban surfaces is not currently included in urban airshed models due to the lack of data on such processes, but is clearly an area that is potentially important for accurate modeling of urban airsheds and application to development of effective control strategies.

V. Concluding Remarks

The structural properties of nitrate-water clusters, $NO_3^-\cdot(H_2O)_n$, were explored for a large range of cluster sizes, from n = 15 to nanodroplets containing several hundred water molecules. For the smallest cluster sizes considered, with n = 15 and n = 32, the electronic structure-based effective fragment potential method was used to compute the structural properties. The fact that the predictions of this method are in good qualitative agreement with polarizable force field-based MD simulations lends strong support to the main conclusion of this study, namely, that the nitrate ions have a strong preference for the surface in relatively small water clusters. Even though relatively low-energy interior anions are predicted, MP2 optimizations confirm that the lowest energy structure for n=32 is likely to be a surface anion. This surface preference for small clusters persists, albeit more weakly, for clusters containing hundreds of water molecules approaching nm size droplets. A crossover from a preference for surface solvation to the predominance of interior solvation that is characteristic of bulk solution interfaces is observed to occur between n = 300 and n = 500 water molecules. The photochemistry of nitrate anions could be significantly altered by their

المنارة للاستشارات
www.manaraa.com

presence at the surfaces of such water clusters, films and other systems compared to the bulk, and this may play a role in new particle formation in the atmosphere as well as in the chemistry and photochemistry of nitrate in thin water films on surfaces. Experimental and additional theoretical studies are underway to explore this possibility.

Acknowledgments

RBG, BJFP and DJT acknowledge the support of the AirUCI Environmental Molecular Science Institute (Grant # CHE-0431312) funded by the National Science Foundation. BJFP is also grateful to the U.S. Department of Energy (Grant # DE-FG02-05ER64000) for partial support of this work. DDK and MSG acknowledge the support of the Department of Energy Chemical Physics program at the Ames Laboratory, administered by Iowa State University.

References

(1) Finlayson-Pitts, B. J.; Pitts, J. N. *Chemistry of the Upper and the Lower Atmosphere*; Academic: San Diego, 2000.

(2) Wayne, R. P. *Chemistry of Atmospheres*; Oxford university Press: Oxford, 2000.

(3) Frank, H. *Chemical Physics of ionic Solutions*; John Wiley and Sons: New York, 1956.

(4) Williams, R. J. P. *Bio-inorganic Chemistry*; American Chemical Society: Washington, DC, 1971.

المنارة للاستشارات

www.manaraa.com

(5) Nissenson, P.; Knox, C. J. H.; Finlayson-Pitts, B. J.; Phillips, L. F.; Dabdub, D. *Physical Chemistry Chemical Physics* 2006, *8*, 4700.

(6) Schnitzer, C.; Baldelli, S.; Shultz, M. J. *J. Phys. Chem. B* 2000, 585.

(7) Xu, M.; Spinney, R.; Allen, H. C. *J. Phys. Chem. B* 2009, *113*, 4102.

(8) Xu, M.; Tang, C. Y.; Jubb, A. M.; Chen, X.; Allen, H. C. *J. Phys. Chem. C* 2009, *113*, 2082.

(9) Otten, D. E.; Petersen, P. B.; Saykally, R. J. *Chem. Phys. Lett.* 2007, *449*, 261.

(10) Cheng, J.; Vecitis, C. D.; Hoffmann, M. R.; Colussi, A. J. *J. Phys. Chem. B* 2006, *110*, 25598.

(11) Jungwirth, P.; Tobias, D. J. *Chem. Rev.* 2006, *106*, 1259.

(12) Pegram, L. M.; Record Jr., M. T. *Proc. Natl. Acad. Sci. USA* 2006, *103*, 14278.

(13) Brown, M. A.; Winter, B.; Faubel, M.; Hemminger, J. C. *J. Am. Chem. Soc.* 2009, *ASAP*, XXX.

(14) Salvador, P.; Curtis, J. E.; Tobias, D. J.; Jungwirth, P. *Physical Chemistry Chemical Physics* 2003, *5*, 3752.

(15) Dang, L. X.; Chang, T. M.; Roeselova, M.; Garrett, B. C.; Tobias, D. J. *Journal of Chemical Physics* 2006, *124*.

(16) Minofar, B.; Vacha, R.; Wahab, A.; Mahiuddin, S.; Kunz, W.; Jungwirth, P. *Journal of Physical Chemistry B* 2006, *110*, 15939.

(17) Thomas, J. L.; Roeselova, M.; Dang, L. X.; Tobias, D. J. *Journal of Physical Chemistry A* 2007, *111*, 3091.

www.manaraa.com

(18) Waterland, M. R.; Stockwell, D.; Kelley, A. M. *Journal of Chemical Physics* 2001, *114*, 6249.

(19) Shen, M. Z.; Xie, Y. M.; Schaefer, H. F.; Deakyne, C. A. *Journal of Chemical Physics* 1990, *93*, 3379.

(20) Howell, J. M.; Sapse, A. M.; Singman, E.; Synder, G. *Journal of Physical Chemistry* 1982, *86*, 2345.

(21) Wang, X. B.; Yang, X.; Wang, L. S.; Nicholas, J. B. *Journal of Chemical Physics* 2002, *116*, 561.

(22) Goebbert, D. J.; Garand, E.; Wende, T.; Bergmann, R.; Meijer, G.; Asmis, K. R.; Neumark, D. M. *J. Phys. Chem. A* 2009, *ASAP*, XXX.

(23) Day, P. N.; Jensen, J. H.; Gordon, M. S.; Webb, S. P.; Stevens, W. J.; Krauss, M.; Garmer, D.; Basch, H.; Cohen, D. *Journal of Chemical Physics* 1996, *105*, 1968.

(24) Gordon, M. S.; Freitag, M. A.; Bandyopadhyay, P.; Jensen, J. H.; Kairys, V.; Stevens, W. J. *Journal of Physical Chemistry A* 2001, *105*, 293.

(25) Merrill, G. N.; Webb, S. P. *Journal of Physical Chemistry A* 2003, *107*, 7852.

(26) Kemp, D. D.; Gordon, M. S. *Journal of Physical Chemistry A* 2005, *109*, 7688.

(27) Dunning, J., T.H. ; Hay, P. J. *Methods of Electronic Structure Theory*New York, 1977.

(28) Schmidt, M. W.; Baldridge, K. K.; Boatz, J. A.; Elbert, S. T.; Gordon, M. S.; Jensen, J. H.; Koseki, S.; Matsunaga, N.; Nguyen, K. A.; Su, S. J.; Windus, T. L.; Dupuis, M.; Montgomery, J. A. *Journal of Computational Chemistry* 1993, *14*, 1347.

المنارة للاستشارات

www.manaraa.com

(29) Metropolis, N.; Rosenbluth, A. W.; Rosenbluth, M. N.; Teller, A. H.; Teller, E. *J. Chem. Phys.* 1953, *21*, 1087.

(30) Kirkpatrick, S.; Gelatt, C. D.; Vecchi, M. P. *Science* 1983, *220*, 671.

(31) Case, D. A.; Darden, T. A.; Cheatham, T. E., III; Simmerling, C. L.; Wang, J.; Duke, R. E.; Luo, R.; Merz, K. M.; Wang, B.; Pearlman, D. A.; Crowley, M.; Brozell, S.; Tsui, V.; Gohlke, H.; Mongan, J.; Hornak, V.; Cui, G.; Beroza, P.; Schafmeister, C.; Caldwell, J. W.; Ross, W. S.; Kollman, P. A. AMBER 8 University of California, San Francisco, 2004.

(32) Ryckaert, J. P.; Ciccotti, G.; Berendsen, H. J. C. *Journal of Computational Physics* 1977, *23*, 327.

(33) Darden, T.; York, D.; Pedersen, L. *Journal of Chemical Physics* 1993, *98*, 10089.

(34) Essmann, U.; Perera, L.; Berkowitz, M. L.; Darden, T.; Lee, H.; Pedersen, L. G. *Journal of Chemical Physics* 1995, *103*, 8577.

(35) Caldwell, J. W.; Kollman, P. A. *Journal of Physical Chemistry* 1995, *99*, 6208.

(36) Thole, B. T. *Chemical Physics* 1981, *59*, 341.

(37) Petersen, P. B.; Saykally, R. J.; Mucha, M.; Jungwirth, P. *Journal of Physical Chemistry B* 2005, *109*, 10915.

(38) Kulmala, M.; Vehkamaki, H.; Petaja, T.; Dal Maso, M.; Lauri, A.; Kerminen, V. M.; Birmili, W.; McMurry, P. H. *Journal of Aerosol Science* 2004, *35*, 143.

(39) Ghan, S. J.; Schwartz, S. E. *Bulletin of the American Meteorological Society* 2007, *88*, 1059.

المنارة للاستشارات

www.manaraa.com

(40) *Climate Change 2007: The Physical Science Basis. IPCC Secretariat*Geneva, 2007.

(41) Smith, J. N.; Dunn, M. J.; Van Reken, T. M.; Iida, K.; Stolzenburg, M. R.; McCurdy, P. H.; Huey, L. G. *Geophys. Res. Lett., submitted* 2007.

(42) Smith, J. N.; Moore, K. F.; MuCurdy, P. H.; Eisele, F. L. *Aerosol Sci. Technol*. 2004, *38*, 100.

(43) Mack, J.; Bolton, J. R. *Journal of Photochemistry and Photobiology a-Chemistry* 1999, *128*, 1.

(44) Warneck, P.; Wurzinger, C. *Journal of Physical Chemistry* 1988, *92*, 6278.

(45) Herrmann, H. *Physical Chemistry Chemical Physics* 2007, *9*, 3935.

(46) Honrath, R. E.; Peterson, M. C.; Guo, S.; Dibb, J. E.; Shepson, P. B.; Campbell, B. *Geophysical Research Letters* 1999, *26*, 695.

(47) Dubowski, Y.; Colussi, A. J.; Hoffmann, M. R. *Journal of Physical Chemistry A* 2001, *105*, 4928.

(48) Jones, A. E.; Weller, R.; Anderson, P. S.; Jacobi, H. W.; Wolff, E. W.; Schrems, O.; Miller, H. *Geophysical Research Letters* 2001, *28*, 1499.

(49) Zhou, X. L.; Beine, H. J.; Honrath, R. E.; Fuentes, J. D.; Simpson, W.; Shepson, P. B.; Bottenheim, J. W. *Geophysical Research Letters* 2001, *28*, 4087.

(50) Dubowski, Y.; Colussi, A. J.; Boxe, C.; Hoffmann, M. R. *Journal of Physical Chemistry A* 2002, *106*, 6967.

(51) Boxe, C. S.; Colussi, A. J.; Hoffmann, M. R.; Tan, D.; Mastromarino, J.; Case, A. T.; Sandholm, S. T.; Davis, D. D. *Journal of Physical Chemistry A* 2003, *107*, 11409.

www.manaraa.com

(52) Chu, L.; Anastasio, C. *Journal of Physical Chemistry A* 2003, *107*, 9594.

(53) Jacobi, H. W.; Annor, T.; Quansah, E. *Journal of Photochemistry and Photobiology a-Chemistry* 2006, *179*, 330.

(54) Wingen, L. M.; Moskun, A. C.; Johnson, S. N.; Thomas, J. L.; Roeselová, M.; Tobias, D. J.; Kleinman, M. T.; Finlayson-Pitts, B. J. *Phys. Chem. Chem. Phys.* 2008, *10*, 5668.

(55) Yu, Y.; Ezell, M. J.; Zelenyuk, A.; Imre, D.; Alexander, M. L.; Ortega, J.; Thomas, J. L.; Gogna, K.; Tobias, D. J.; D'Anna, B.; Harmon, C. W.; Johnson, S.; Finlayson-Pitts, B. J. *submitted for publication* 2007.

(56) Raja, S.; Valsaraj, K. T. *Journal of the Air & Waste Management Association* 2005, *55*, 1345.

(57) Chen, J.; Ehrenhauser, F. S.; Valsaraj, K. T.; Wornat, M. J. *Journal of Physical Chemistry A* 2006, *110*, 9161.

(58) Raja, S.; Valsaraj, K. T. *Atmospheric Research* 2006, *81*, 277.

(59) Sumner, A. L.; Menke, E. J.; Dubowski, Y.; Newberg, J. T.; Penner, R. M.; Hemminger, J. C.; Wingen, L. M.; Brauers, T.; Finlayson-Pitts, B. J. *Physical Chemistry Chemical Physics* 2004, *6*, 604.

(60) Finlayson-Pitts, B. J.; Wingen, L. M.; Sumner, A. L.; Syomin, D.; Ramazan, K. A. *Physical Chemistry Chemical Physics* 2003, *5*, 223.

(61) Diamond, M. L.; Gingrich, S. E.; Fertuck, K.; McCarry, B. E.; Stern, G. A.; Billeck, B.; Grift, B.; Brooker, D.; Yager, T. D. *Environmental Science & Technology* 2000, *34*, 2900.

المنارة للاستشارات

www.manaraa.com

(62) Gingrich, S. E.; Diamond, M. L. *Environmental Science & Technology* 2001, *35*, 4031.

(63) Simpson, A. J.; Lam, B.; Diamond, M. L.; Donaldson, D. J.; Lefebvre, B. A.; Moser, A. Q.; Williams, A. J.; Larin, N. I.; Kvasha, M. P. *Chemosphere* 2006, *63*, 142.

(64) S. G. Moussa, T. M. M., M. Szori, M. Roeselová,; D. J. Tobias, R. L. G., J. C. Hemminger, B. J. Finlayson-Pitts. *J. Phys. Chem. A* 2009, *113*, 2060.

(65) Handley, S. R.; Clifford, D.; Donaldson, D. J. *Environmental Science & Technology* 2007, *41*, 3898.

للاستشارات المنارة

www.manaraa.com

CHAPTER 6. DEVELOPMENT OF AN OPEN SHELL EFFECTIVE FRAGMENT POTENTIAL

A paper to be submitted to *Theoretical Chemistry Accounts*

Daniel D. Kemp and Mark S. Gordon

Abstract

The effective fragment potential method has been extended to study systems containing open shell molecules using the restricted open-shell Hartree-Fock level of theory. The present implementation models intermolecular interactions with electrostatics, static polarization and exchange-repulsion. The Coulomb and static polarization terms only required modest modifications from the closed shell case, but the exchange repulsion term required a derivation from first principles. The analytic gradients for each interaction energy has also been derived and implemented. The relevant energy terms and several examples involving open-shell molecules are presented.

I. Introduction

The first implementation of the effective fragment potential (EFP) method into the General Atomic and Molecule Electronic Strucutre System (GAMESS)[1,2] was exclusively for the water molecule (EFP1)[3]. The EFP1 model was originally based upon the Hartree-Fock (HF)[3] level of theory, but a density functional theory (DFT)[4] based model has also been developed. The EFP1 method was implemented with three different intermolecular interaction energies: electrostatics (Coulomb), static polarization and a combined exchange-repulsion/charge transfer term. The Coulomb term is based upon the Stone distributed multipolar analysis[5,6] expanded through octopoles, and the static polarization is expressed in

www.manaraa.com

terms of a tensor sum of localized molecular orbital (LMO) polarizability tensors. The exchange repulsion/charge transfer term was fitted to a set of calculations (at the appropriate level of theory) on the water dimer at several orientations and intermolecular distances.

The EFP1 method has been successfully applied to various problems, ranging from small water clusters to mixed *ab inito*/EFP1 studies of reaction mechanisms[7], solvation effects[8] and solvated structures[9,10]. Due to the success of the water-specific EFP1 method, the EFP2[11] method was developed so that one could study any closed-shell solvent or solute molecule with no empirically fitted parameters. The original EFP2 implementation included the same intermolecular energy interaction terms as EFP1, except that the exchange repulsion interaction energy and analytic gradient were derived from first principle, and the corresponding charge transfer term was only derived much later.[12] The newly derived exchange repulsion term depends upon the intermolecular overlap integrals expressed in terms of frozen LMOs[13,14]. Dispersion[15] and charge transfer[12] have also been derived and coded. Damping expressions for Coulomb, polarization, and dispersion terms have also been implemented.[16]

In the present work, the contributions to the open shell EFP2 method are presented in Section II. Several applications are presented in Section III, and conclusions are summarized in Section IV.

II. Interaction Energy Terms

The open shell EFP2 method is based upon spin restricted open shell Hartree-Fock (ROHF)[17] method, in which all unpaired electrons have parallel spins. In the following each contribution to EFP2 is discussed.

www.manaraa.com

A. Electrostatics

The Coulomb term is expanded in a distributed multipole expansion, in terms of monopoles, dipoles, quadrupoles and octopoles at all atom centers and bond midpoints[6]. The EFP-EFP Coulomb interactions are modified by a damping term as noted above. Because the distributed multipole analysis is based upon the density matrix of the system, it is applicable to any wavefunction, open or closed shell[6], so no explicit modification of this term is required for open shells.

B. Polarization

The polarization interaction energy is calculated from the polarizability tensors obtained using a finite field approach, by applying the coupled perturbed Hartree Fock (CPHF) equations[18] to each LMO. The localized orbital polarizabilities have the following form:

$$\alpha^{l}_{xy} = \lim_{Fy \to 0} \frac{\mu^{l}_{x}\left(F_{y}\right) - \mu^{l}_{x}(0)}{F_{y}} \tag{1}$$

where α^{l}_{xy} is the xy component of the polarizability for the lth LMO of a particular EFP and F is the electric field. μ^{l}_{x} is the x-component of LMO l in the presence (F_y) or absence (0) of the field. The induced dipole field vectors are related via the polarizablity tensor:

$$\vec{\mu}_i = \widetilde{\alpha}_i \vec{F}_i \tag{2}$$

In Eq. (2) $\vec{\mu}_i$ is the induced dipole vector, $\vec{F}_i$ is the electric field vector and $\widetilde{\alpha}_i$ is the polarizability tensor at point i. The polarization interaction energy between fragments is defined as

$$E_{pol} = E_{\text{int}} + E_{sol} \tag{3}$$

المنارة للاستشارات
www.manaraa.com

where

$$E_{\text{int}} = -\sum_i \vec{\mu}_i \vec{F}_i^{efp} - \sum_i \sum_{j>i} \vec{\mu}_i \cdot \vec{F}_i^{\mu j} \quad \textbf{(4)}$$

$$E_{sol} = \frac{1}{2} \sum_i \vec{\mu}_i \cdot \left(\vec{F}_i^{efp} + \vec{F}_i^{\mu} \right) \quad \textbf{(5)}$$

$\vec{F}_i^{efp}$ is the field at the polarizable point i due to the static multipoles in the other fragments, $\vec{F}_i^{\mu j}$ is the field at point i due to the induced dipole j when j and i are not in the same fragment and $\vec{F}_i^{\mu}$ is the field at i due to the induced dipoles in all the other fragments.

The polarizable points are taken to be the LMO centroids. This dipole-induced dipole interaction is iterated to self-consistency within the SCF procedure. No new code is required to extend this term to open shell species. To demonstrate this, the polarizability tensors of the water molecule were calculated with the ROHF EFP2 code and found to be identical to those obtained using the RHF code.

C. Exchange Repulsion

The EFP2 exchange repulsion[19] is obtained from the interactions between LMOs on two fragments A and B. or open shells, three types of interactions must be considered: 1) Fragments A and B are both closed shell species, 2) Fragment A is an open shell species and B is a closed shell species, 3) both fragments A and B are open shell species. All of these orbital subspaces are discussed below.

1. A and B are both closed shell EFPs

When A and B are both closed shell EFPs, the equation for the RHF-based EFP2 method applies. The exchange repulsion energy is given by Eq. (6):

www.manaraa.com

$$
\begin{aligned}
E_{exch}(V) &= -2\sum_{i\in A}\sum_{j\in B}\left\langle i\,|\,K_j\,|\,i\right\rangle \\
&-2\sum_{i\in A}\sum_{j\in B}S_{ij}\left(V_{ij,A}+V_{ij,B}+\sum_{k\in A}\left(\left\langle i\,|\,2J_k\,|\,j\right\rangle-\left\langle i\,|\,K_k\,|\,j\right\rangle\right)+\sum_{l\in B}\left(\left\langle i\,|\,2J_l\,|\,j\right\rangle-\left\langle i\,|\,K_l\,|\,j\right\rangle\right)\right) \\
&+2\sum_{i\in A}\sum_{j\in B}S_{ij}\left[\sum_{k\in A}S_{kj}\left(V_{ik,B}+\sum_{l\in B}\left\langle i\,|\,2J_l\,|\,k\right\rangle\right)+\sum_{l\in B}S_{il}\left(V_{jl,A}+\sum_{k\in A}\left\langle j\,|\,2J_k\,|\,l\right\rangle\right)-\sum_{k\in A}\sum_{l\in B}S_{kl}\left\langle ik\,|\,lj\right\rangle\right]
\end{aligned}
\tag{6}
$$

The four different types of integrals in Eq. (1) are defined below:

$$\left\langle i\,|\,K_j\,|\,i\right\rangle = \iint dr_1 dr_2 \phi_i^*(1)\phi_j(1) r_{12}^{-1}\phi_j^*(2)\phi_i(2) \tag{7}$$

$$\left\langle i\,|\,2J_l\,|\,j\right\rangle = 2\iint dr_1 dr_2 \phi_i^*(1)\phi_j(1) r_{12}^{-1}\phi_l^*(2)\phi_l(2) \tag{8}$$

$$V_{ij,B} = \left\langle i\,|\,\frac{-Z_B}{R_{1B}}\,|\,j\right\rangle = -\int dr_1 \phi_i^*(1)\frac{-Z_B}{R_{1B}}\phi_j(1) \tag{9}$$

$$S_{ij} = \left\langle i\,|\,j\right\rangle = \int dr_1 \phi_i^*(1)\phi_j(1) \tag{10}$$

2. A is an open shell EFP and B is a closed shell EFP

Starting with Eq. (18) in Ref. 17:

$$
\begin{aligned}
E_{exch}(V) &= \int \gamma_{exch}^{A}(1)\left(U_B(1)+\int\frac{\gamma_0^B(2)}{r_{12}}d\tau_2\right)d\tau_1 \\
&+\int \gamma_{exch}^{B}(1)\left(U_A(1)+\int\frac{\gamma_0^A(2)}{r_{12}}d\tau_2\right)d\tau_1 \\
&+\iint\left(\frac{\gamma_{exch}^{A}(1\,|\,2)\gamma_{exch}^{B}(2\,|\,1)}{r_{12}}\right)d\tau_1 d\tau_2 \\
&-\iint\left(\frac{\gamma_{\mathrm{int}}^{A}(1\,|\,2)\gamma_{\mathrm{int}}^{B}(2\,|\,1)}{r_{12}}\right)d\tau_1 d\tau_2
\end{aligned}
\tag{11}
$$

Since A is an open shell species, some orbitals have single occupancy. Taking this into account leads to[17] (see Eq. (6)):

$$\gamma_{\mathrm{int}}^{A}(1\,|\,2) = \gamma_0^{A}(1\,|\,2) + \gamma_{exch}^{A}(1\,|\,2) \tag{12}$$

$$\gamma_0^{A}(1\,|\,2) = \sum_{m\in A}\phi_m^*(1)\phi_m(2)\left[\alpha(1)\alpha(2)\right] \tag{13}$$

$$\gamma_{exch}^{A}(1\,|\,2) = -\sum_{m\in a}\sum_{j\in b}S_{mj}\left(\phi_m^*(1)\phi_j(2)-\sum_{o\in A}S_{oj}\phi_m^*(1)\phi_o(2)\right)\left[\alpha(1)\alpha(2)\right] \tag{14}$$

www.manaraa.com

$$\gamma_{\text{int}}^{A}(1|2)=\sum_{m\in A}\phi_m^*(1)\phi_m(2)\left[\alpha(1)\alpha(2)\right]-\sum_{m\in a}\sum_{j\in b}S_{mj}\left(\phi_m^*(1)\phi_j(2)-\sum_{o\in A}S_{oj}\phi_m^*(1)\phi_o(2)\right)\left[\alpha(1)\alpha(2)\right] \quad \textbf{(15)}$$

$$\gamma_0^{A}(2)=\sum_{q\in A}\phi_q^*(2)\phi_q(2)\left[\alpha(2)\alpha(2)+\beta(2)\beta(2)\right] \quad \textbf{(16)}$$

$$\gamma_0^{B}(2)=\sum_{l\in B}\phi_l^*(2)\phi_l(2)\left[\alpha(2)\alpha(2)+\beta(2)\beta(2)\right] \quad \textbf{(17)}$$

$$\gamma_{exch}^{B}(2|1)=-\sum_{q\in A}\sum_{l\in B}S_{ql}\left(\phi_q^*(2)\phi_l(1)-\sum_{p\in B}S_{pq}\phi_l^*(2)\phi_p(1)\right)\left[\alpha(2)\alpha(1)\right] \quad \textbf{(18)}$$

$$\gamma_{exch}^{B}(1)=-\sum_{q\in A}\sum_{l\in B}S_{ql}\left(\phi_q^*(1)\phi_l(1)-\sum_{p\in B}S_{pq}\phi_l^*(1)\phi_p(1)\right)\left[\alpha(1)\alpha(1)\right] \quad \textbf{(19)}$$

$$\gamma_{\text{int}}^{A}(2|1)=\sum_{l\in B}\phi_l^*(2)\phi_l(1)\left[\alpha(2)\alpha(1)\right]-\sum_{q\in A}\sum_{l\in B}S_{ql}\left(\phi_q^*(2)\phi_l(1)-\sum_{p\in B}S_{pq}\phi_l^*(2)\phi_p(1)\right)\left[\alpha(2)\alpha(1)\right] \quad \textbf{(20)}$$

In these equations, U_A is the potential due to the nuclei in fragment A and all sums are over the LMOs on A or B. Substituting Eqs. (7) – (15) into Eq. (2) and collecting terms based on their power dependence on the intermolecular overlap matrix S, leads to:

$$\begin{aligned}
E_{exch}(V) &= -\sum_{m\in A}\sum_{j\in B}<m|K_j|m> \\
&-\sum_{m\in A}\sum_{j\in B}S_{mj}\left(V_{mj,B}+V_{mj,A}+\sum_{l\in B}\left(\langle m|2J_l|j\rangle-\langle m|K_l|j\rangle\right)+\sum_{o\in A}\left(\langle m|2J_o|j\rangle-\langle m|K_o|j\rangle\right)\right) \\
&+\sum_{m\in A}\sum_{j\in B}S_{mj}\left(\sum_{o\in A}S_{oj}\left(V_{mo,B}+\sum_{l\in B}\langle m|2J_l|o\rangle\right)+\sum_{l\in B}S_{ml}\left(V_{jl,A}+\sum_{o\in A}\left(\langle j|2J_o|l\rangle\right)\right)-\sum_{l\in B}\sum_{o\in A}S_{ol}\langle mo|lj\rangle\right)
\end{aligned} \quad \textbf{(21)}$$

Eq. (21) differs from the closed shell case only by the orbital indices on the sums and the integer coefficients in front of the integrals. The orbital summations on fragment A span only the open-shell orbitals while the orbital sums on B span the closed shell orbitals on fragment B.

3. Fragment A and B are open shell species

Here, there are open shell orbitals on both A and B that must be accounted for. The resulting exchange repulsion is given in the equation below:

المنارة للاستشارات

www.manaraa.com

$$\begin{aligned}
E_{exch}(V) = &-\sum_{m\in A}\sum_{n\in B}\langle m \mid K_n \mid m\rangle \\
&-\sum_{m\in A}\sum_{n\in B} S_{mn}\left(V_{mn,B}+V_{mn,A}+\sum_{p\in B}\left(\langle m \mid J_p \mid n\rangle-\langle m \mid K_p \mid n\rangle\right)-\sum_{o\in A}\left(\langle m \mid J_o \mid p\rangle-\langle m \mid K_o \mid p\rangle\right)\right) \\
&+\sum_{m\in A}\sum_{n\in B} S_{mn}\left(\sum_{o\in A} S_{on}\left(V_{om,B}+\sum_{p\in B}\langle o \mid J_p \mid m\rangle\right)+\sum_{p\in B} S_{mp}\left(V_{np,A}+\sum_{o\in A}\langle n \mid J_o \mid p\rangle\right)-\sum_{q}\sum_{r} S_{qr}\langle mq \mid rn\rangle\right)
\end{aligned} \qquad \textbf{(22)}$$

Finally, the total exchange repulsion between all pairs of fragments is obtained by appropriately summing the contributions from Eqs. (6), (21), and (22).

In order to perform geometry optimizations, one needs to derive and implement expressions for the analytic energy gradient. The gradient of the electrostatic and polarization energies are the same as for closed shells, since the corresponding energy expressions are the same. The energy expressions for the exchange repulsion are similar to those for the closed shell case[20,21], so the corresponding gradient expressions are easily obtained and coded. All of the changes discussed here have been incorporated into the GAMESS (General Atomic and Molecular Electronic Structure System)[1,2] electronic structure program.

III. Examples

A glycyl radical ROHF EFP2 was generated using the 6-311++G(d,p)[22,23] basis set. The EFP glycyl radical was then solvated with a closed-shell EFP2 water molecule generated using the same basis set. Since the Kitaura-Morokuma[24] and Reduced Variational Space (RVS)[25] analyses are apparently not available for open shell systems, comparisons are made to fully ab initio ROHF and Z-Averaged Perturbation Theory (ZAPT)[26,27] calculations.

In order to test the EFP2 method against higher level *ab initio* methods, the intramolecular bond lengths and bond angles of all molecules were frozen during the *ab initio* optimizations. This provides a fair test against the EFP2 method which freezes each internal fragment geometry at the monomer geometry. Each molecule was allowed to freely

المنارة للاستشارات
www.manaraa.com

move and rotate relative to the other fragments during the optimizations. Figure 6.1 illustrates the intermolecular geometry of the glycyl-water calculations. All calculations were run on an IBM 1200 Mhz Power4+.

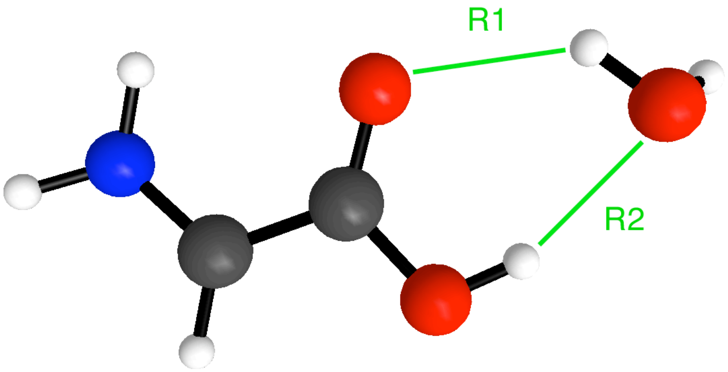

Figure 6.1. The equilibrium geometry of the glycyl radical solvated by one water molecule is given at the ROHF EFP2, full ROHF and ZAPT levels of theory. Oxygen atoms are expressed in the color red, carbon atoms are in gray, nitrogen is blue and all hydrogen atoms are white. The R1 and R2 distances illustrate the intermolecular distances of the two hydrogen bonds.

The EFP2 geometry, binding energy predictions and CPU times are compared with the ROHF and ZAPT levels of theory in Table 6.1. The hydrogen bond lengths between fragments at the EFP2 level of theory are a bit longer than those predicted by ZAPT, by ~0.1-0.2 angstroms. The EFP2 and ROHF distances are in excellent agreement with each other.

www.manaraa.com

Table 6.1. Intermolecular distances (in Angstroms), binding energies (in kcal/mol) and CPU time (in seconds) are given for the glycyl-water calculation at three levels of theory. The R1 and R2 distances correspond to the illustrated distances in Figure 6.1.

Method	R1 (angs)	R2 (angs)	B.E. kcal/mol	Time (sec)
EFP2	2.15	2.09	-8.7	6
ROHF	2.17	1.98	-8.2	1097
ZAPT	2.04	1.9	-9.7	8053

The binding energies (Table 6.1) for the *ab initio* levels of theory were obtained by subtracting the energies of each individual molecule from the energy of the supermolecule. This subtracts out the internal energies of the separate molecules from the energy of the supermolecule. There are no internal energies within the EFP2 fragments. The EFP2 binding energy lies between those predicted by ROHF and ZAPT, with energy differences on the order of 1 kcal/mol or less. Since second order perturbation theory includes dispersion energy, while ROHF does not, it is likely that when dispersion is included in EFP2, the agreement with ZAPT would improve. The EFP2 structure and binding energy are in excellent agreement with *ab initio* calculations and are obtained at orders of magnitude less computational cost.

Now, consider Figure 6.2, in which the weak interaction between an allyl radical and a water molecule is illustrated. The EFP2 R1 and R2 distances lie between those predicted by ROHF and ZAPT (Table 6.2). The EFP2 binding energy of –1.2 kcal/mol is in close agreement with the ROHF value of –1.1 kcal/mol. Whether the molecules are more strongly bound (e.g., glycyl-water), or weakly bound (e.g., allyl-water), the ROHF EFP2 method does reasonably well at reproducing *ab inito* results at a fraction of the computational cost.

المنارة للاستشارات

www.manaraa.com

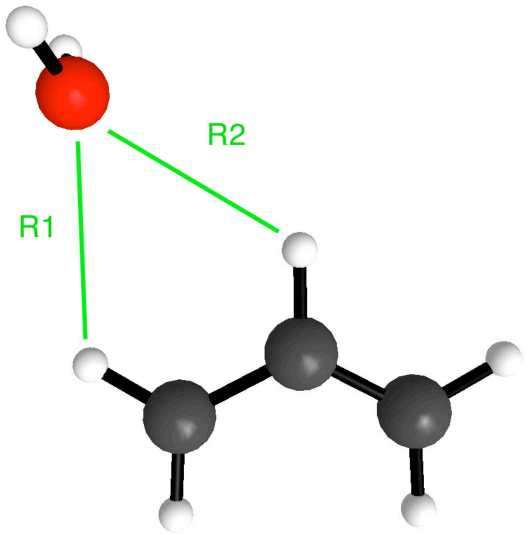

Figure 6.2. The equilibrium geometry of one water molecule and the allyl radical is given at the ROHF EFP2, ROHF and ZAPT levels of theory. All atoms are colored as they were in Figure 6.1.

Table 6.2. Intermolecular distances (in Angstroms) and binding energies (in kcal/mol) for the allyl-water equilibrium geometries are provided for three levels of theory. The R1 and R2 distances are illustrated in Figure 6.2.

Method	R1 (angs)	R2 (angs)	B.E. kcal/mol
EFP	2.78	2.77	-1.2
ROHF	2.93	2.87	-1.1
ZAPT	2.71	2.66	-2.0

The open shell EFP2 method is not limited to the simple types of calculations illustrated in Figures 1 and 2. The method presented here can also be used in combination with the Metropolis-based Monte Carlo (MC)[28] and simulated annealing[29] code within GAMESS. These simulations can be used to search a potential energy surface to find the structures with low-lying energies. The MC code randomly displaces the fragments, while

المنارة للاستشارات

www.manaraa.com

the simulated annealing code starts the simulation at a high temperature and slowly cools it in conjunction with geometry optimizations in order to find low-lying energy minima. To illustrate this for open shell species, simulations of glycyl radical with six water molecules were performed, and the lowest energy structure is shown in Figure 6.3. The water molecules interact with the glycyl radical at various hydrogen bonding sites, and with each other. Five water molecules form a ring of hydrogen bonds with themselves and with the solute in such a way that most of the hydrogens participate in hydrogen bonding as would be expected.

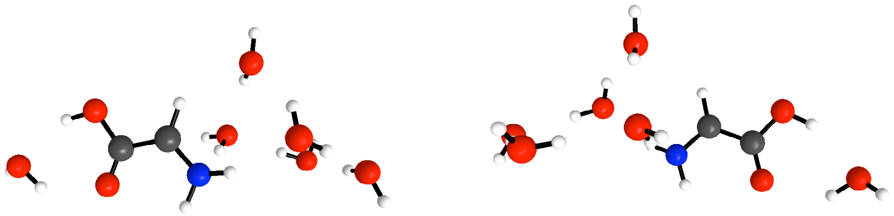

Figure 6.3. The equilibrium geometry of the glycyl radical solvated by six water molecules is provided. The same structure is viewed from two different angles.

Although the method described here allows the user to choose any multiplicity, careful consideration must be given to the system of interest before studying it with the EFP2 method. The EFP2 method is not suitable for studying bond-breaking, bond formation or the sharing of open shell electrons between molecules. Such processes must be studies with quantum mechanics.

المنارة للاستشارات
www.manaraa.com

IV. Conclusions

A new method to describe high spin open shell solvent and solute molecules efficiently has been described in this work. The ROHF-based EFP2 method is suitable for studying intermolecular interactions involving open shell molecules and can be combined with potentials made using the RHF-based EFP2 method.

Acknowledgements

The authors thank Professors Hui Li and Jan Jensen and Dr. Michael Schmidt for helpful discussions regarding the derivations of the exchange repulsion equations and with coding the equations. This work was supported by a grant from the Department of Energy, via the Ames Laboratory at Iowa State University.

References

1. Schmidt, M. W.; Baldridge, K. K.; Boatz, J. A.; Jensen, J. H.; Koseki, S.; Matsunaga, N.; Gordon, M. S.; Ngugen, K. A.; Su, S.; Windus, T. L.; Elbert, S. T.; Montgomery, J.; Dupuis, M. *J. Comput. Chem.* 1993, *14*, 1347.

2. Gordon, M.S.; Schmidt, M.W. “Advances in Electronic Structure Theory: GAMESS a Decade Later”, *Theory and Applications of Computational Chemistry,* Ch.. 41, C. E.

3. Day, P. N.; Jensen, J. H.; Gordon, M. S.; Webb, S. P.; Stevens, W. J.; Krauss, M.; Garmer, D.; Basch, H.; Cohen, D. *J. Chem. Phys.* **1996,** *105*, 1968.

4. Adamovic, I.; Freitag, M. A.; Gordon, M. S. *J. Chem. Phys.*, **2003**, *118*, 6725.

5. Stone, A. J. *Mol. Phys.*, **1985**, *56*, 1065.

6. Stone, A. J. *Mol. Phys.,* **1985**, *56,* 1047.

7. Webb, S.P.; Gordon, M.S. *J. Phys. Chem. A*, **1999**, *103*, 1265.

المنارة للاستشارات

www.manaraa.com

8. Kemp, D. D.; Gordon, M. S. *J. Phys. Chem. A.*, **2008**, *112*, 4885.

9. Merrill, G.N.; Gordon, M.S. *J. Phys. Chem. A*, **1998**, *102*, 2650.

10. Day, P.N.; Pachter, R.; Gordon, M.S.; Merrill, G.N. *J. Chem. Phys.*, **2000**, *112*, 2063.

11. Gordon, M. S.; Freitag, M. A.; Bandyopadhyay, P.; Jensen, J. H.; Kairys, V.; Stevens, W. J. *J. Phys. Chem. A* 2001, *105*, 293.

12. Hui Li, Mark S. Gordon and Jan H. Jensen, Journal of Chemical Physics, 2006, 124, 214108

13. Boys, S. F. "Quantum Science of Atoms, Molecules, and Solids" P.O. Lowdin, Ed, Academic Press, NY, 1966, 253-262.

14. Edmiston, C.; Ruedenberg, K. *Rev. Mod. Phys.*, **1963,** *35,* 457.

15. Adamovic, Ivana; Gordon, M. S. *Mol. Phys.*, **2005**, *103,* 379.

16. Slipchenko, L. V.; Gordon, M. S. *Mol. Phys.*, **2009**, *107*, 999.

17. Binkley, J. S.; Pople, J.A.; Dobosh, P.A. *Mol. Phys.*, **1974**, *28*, 1423.

18. Osamura, Y.; Yamaguchi, Y.; Fox, D.J.; Vincent, M. A.; Schaefer, H. F. *J. Mol. Struct.*, **1983**, *103*, 183.

19. Jensen, J.H.; Gordon, M. S. *Mol. Phys.*, **1996**, *89*, 1313.

20. Li, H.; Gordon, M.S. *Theor. Chem. Accts.*, **2006**, *115*, 385.

21. Jensen, J. H. *J. Chem. Phys.*, **1998**, *108*, 4772.

22. Krishnan, R.; Binkley, J. S.; Seeger, R.; Pople, J. A. *J. Chem. Phys.*, **1980**, *72*, 650.

23. Clark, T.; Chandrasekhar, J.; Spitznagel, G.W.; Schleyer, P.V.R. J. Comp. Chem. **1983,** 4, 294.

24. Kitaura, K.; Morokuma, K. *Intern.J.Quantum Chem.*, **1976,** *10*,325.

25. Stevens, W.J.; Fink, W. H. *Chem. Phys. Lett.*, **1987**, *139*, 15.

المنارة للاستشارات

www.manaraa.com

26. Lee, T.J.; Jayatilaka, D. *Chem. Phys. Lett.*, **1993**, *201*, 1.

27. Lee, T.J.; Rendell, A.P.; Dyall, K.G. *J. Chem. Phys.*, **1994**, *100*, 7400.

28. Metropolis, N.; Rosenbluth, A.; Tellor, A. *J. Chem. Phys.* 1953, *21,* 1089.

29. Kirkpatrick, S.; Gelatt, C. D.; Vecchi, M. P. *Science* 1983, *220*, 671.

المنارة للاستشارات

www.manaraa.com

CHAPTER 7. DISPERSION ENERGY IN THE OPEN SHELL EFFECTIVE FRAGMENT POTENTIAL METHOD

Daniel D. Kemp and Mark S. Gordon

Abstract

An open shell effective fragment potential (EFP) method capable of describing electrostatic, polarization and exchange-repulsion intermolecular energy interactions has been developed previously. This study presents the equations for open-shell dispersion and proposes a means to solve and approximate those equations so that the open-shell dispersion energy may also be included in the EFP method.

I. Introduction

The original implementation of the effective fragment potential (EFP1) was developed to model the water molecule[1]. A more general potential, EFP2, that is free of empirically fitted parameters, was subsequently developed to model any closed shell species[2]. EFP2 initially described intermolecular interactions with electrostatics, static polarization and exchange-repulsion energies. Subsequently, (imaginary) frequency dependent polarization[3] (dispersion) and charge transfer energies[4] were implemented into EFP2.

A basic open shell EFP2 method, including exchange repulsion, polarization, and Coulomb terms, was recently developed to facilitate the generation of potentials for open shell molecules[5]. This method is based upon the spin-restricted open shell Hartree-Fock (ROHF)[6] method and requires that all singly occupied orbitals contain electrons with the same spin.

www.manaraa.com

The present work presents the derivation of open shell dispersion. Following the closed shell procedure[3], the imaginary frequency-dependent polarizabilities are obtained from the ROHF version of the time-dependent Hartree-Fock equations. The equations required for ROHF dispersion and possible implementation procedures in the General Atomic and Molecular Electronic Structure System (GAMESS)[7,8] are discussed.

II. Theory

For the closed shell EFP2 dispersion, Adamovic and Gordon[3] obtain the frequency dependent polarizability tensors by performing a time-dependent Hartree-Fock (TDHF) calculation. These dynamic polarizability tensors are then used to calculate the C_6 dispersion coefficients and the dispersion energy. The procedure followed in ref. 3 is that outlined by Amos and co-workers using TDHF[9]. The latter authors have also derived the analogous equations for time-dependent density functional theory[10] (TDDFT).

One can expand the total dispersion energy as a sum of terms[3]:

$$E_{disp} = \frac{C_6}{R^6} + \frac{C_7}{R^7} + \frac{C_8}{R^8} + \ldots \tag{1}$$

In Eq. (1) the C_i are expansion coefficients that are obtained from the TDHF or TDDFT equations[3,9,10], while R is the distance between interacting centers. The first term in the expansion in Eq. (1) represents the induced dipole-induced dipole contribution to the dispersion energy. Higher order terms in R correspond to higher order multipolar interactions. In the EFP2 method, the dispersion coefficients are expressed in terms of the interactions between specific localized molecular orbitals (LMO), one (*i*) on one fragment (A) and the other (*j*) on another fragment B. This gives rise to Eq. (2), in which R_{ij} is the distance between the centroids of LMOs *i* and *j*.

www.manaraa.com

$$E_{disp} = \sum_{i \in A} \sum_{j \in B} \frac{C_6^{ij}}{R_{ij}^6} \qquad (2)$$

The C_6 coefficient requires the dynamic polarizability tensor, $\alpha(i\nu)$, which depends upon imaginary frequencies. To obtain these values, one must first solve the coupled-perturbed Hartree-Fock (CPHF)[11] equations for the response vector Z:

$$\left(H^{(2)}H^{(1)} - (i\nu)^2\right)Z = -H^{(2)}P \qquad (3)$$

The electronic orbital Hessian matrix is $H^{(1)}$, the magnetic orbital hessian matrix is $H^{(2)}$ and P is the dipole moment matrix. At the TDHF level of theory, $H^{(1)}$, $H^{(2)}$ and P are given by:

$$H_{aibj}^{(1)} = \left(\varepsilon_a - \varepsilon_i\right)\delta_{ab}\delta_{ij} + 4\left(ai \mid bj\right) - \left(ab \mid ij\right) - \left(aj \mid bi\right)$$

$$H_{aibj}^{(2)} = \left(\varepsilon_a - \varepsilon_i\right)\delta_{ab}\delta_{ij} + \left(ab \mid ij\right) - \left(aj \mid bi\right) \qquad (4)$$

$$P_{ai} = \left\langle \phi_a \mid \hat{\mu} \mid \phi_i \right\rangle$$

where *a* and *b* are virtual orbitals, *i* and *j* are occupied orbitals, ε is an orbital energy and $\hat{\mu}$ is the dipole operator. Rearranging equation 3, gives Eq. (5) for Z:

$$Z = -H^{(2)}P\left(H^{(2)}H^{(1)} - (i\nu)^2\right)^{-1} \qquad (5)$$

These values are obtained for isolated monomers when the potential is being formed. Once the response vector Z has been obtained for a given orbital pair, one can form the dynamic polarizability tensor:

$$\alpha_{\alpha\beta}(i\upsilon) = \sum_{ai} 2\left\langle \phi_a \mid \hat{\mu}_\alpha \mid \phi_i \right\rangle Z_{ai}^{(\beta)}(i\upsilon). \qquad (6)$$

The dispersion coefficients are related to the dynamic polarizability tensors by the following expression:

$$C_6^{LMO1-LMO2} = \sum_{i=1}^{12} w_i \frac{2v_0}{(1-t_i)^2} f(v_i) \qquad (7)$$

$$f(v_i) = \bar{\alpha}^{LMO1}(iv) \cdot \bar{\alpha}^{LMO2}(iv) \qquad (8)$$

where w_i is a weighting factor obtained from a 12-point Gauss-Legendre quadrature, ν_0 is the static polarizability at zero frequency, and $\bar{\alpha}$ is 1/3 of the trace of the polarizability tensor matrix[3].

The overall approach to solving for the dispersion energy for an open shell molecule is similar to that for closed shell species, but it is complicated by the fact that the ROHF equations involve multiple Fock operators. In the closed shell case, the orbital Hessian matrices, $H_{aibj}^{(1)}$ and $H_{aibj}^{(2)}$, are obtained by adding a perturbation to the time-dependent Schrödinger equation[12] using the closed shell Fock operator which involves two orbital subspaces- virtual and doubly occupied. This includes perturbing the orbitals and the Fock operator and combining all terms[12]. However, there are three orbital subspaces (virtual, singly occupied and doubly occupied) in the case of restricted open shell Hartree Fock (ROHF). Pople and co-workers[6] devised three Fock operators for ROHF: F_{DS} (doubly occupied-singly occupied Fock operator), F_{DE} (doubly occupied-virtual Fock operator) and F_{SE} (singly occupied-virtual Fock operator). These three operators, which are defined below in terms of molecular orbitals (see Eq. (9)), are used in the time-dependent Schrödinger equation to obtain expressions for the orbital Hessians so that the response vector can be obtained. This was accomplished by adding a perturbation to the orbitals and the Fock operators themselves, as was done in the closed-shell case[3]. Once the response vector is obtained, one can also obtain the polarizability tensors and the dispersion coefficients just as

www.manaraa.com

in the closed shell case. The three Fock operators, each of which couples a pair of subspaces from the set (D, S, E) are[6]

$$F^{DE} = h + \sum_{j}^{D}\left(2J_j - K_j\right) + \sum_{l}^{S}\left(J_l - \frac{1}{2}K_l\right)$$
$$F^{SE} = h + \sum_{j}^{D}\left(2J_j - K_j\right) + \sum_{l}^{S}\left(J_l - K_l\right) \qquad (9)$$
$$F^{DS} = h + \sum_{j}^{D}(2J_j - K_j) + \sum_{l}^{S}\left(J_l\right)$$

In Eq. (9), H is the one-electron operator, and J and K are the Coulomb and exchange operators, respectively. The sums run over the doubly (D) or singly (S) occupied subspaces. These Fock operators are the starting point for deriving the open shell orbital Hessian matrices in much the same way that the RHF operator is used in the time-dependent Schrödinger equation to derive new expressions for the closed shell orbital Hessian matrices.[12] There are six new sets of orbital Hessian matrices, $H^{(1)}$ and $H^{(2)}$, for each Fock operator; each of these will be presented and discussed below.

First, consider the orbital Hessians $H^{(1)}$ for the F_{DE} operator, shown in Eq. (10). There are two expressions for $H^{(1)}$, since the Fock operator for this subspace is composed of the sum of three different components (the Hamiltonian, one set of integrals over the doubly occupied space and one over the singly-occupied space). For the closed shell (RHF) dispersion, a virtual orbital mixes with an occupied molecular orbital in the presence of the perturbing field. For open shell molecules, it has been suggested[13] to mix in virtual, singly occupied and doubly occupied orbitals in the presence of the perturbation. Only two subspaces can be mixed at a time and this increases the number of orbital Hessians for just the first Fock operator to six.

www.manaraa.com

$$
\begin{aligned}
H_{ai,bj}^{(1)-1} &= 4(ai\,|\,bj)-(ab\,|\,ji)-(aj\,|\,bi)+(\varepsilon_a-\varepsilon_i)\delta_{ab}\delta_{ij} \\
H_{ai,bk}^{(1)-2} &= 2(ai\,|\,bk)-\frac{1}{2}(ab\,|\,ki)-\frac{1}{2}(ak\,|\,bi)+(\varepsilon_a-\varepsilon_i)\delta_{ab}\delta_{ik} \\
H_{ai,lj}^{(1)-3} &= 4(ai\,|\,lj)-(al\,|\,ji)-(aj\,|\,li)+(\varepsilon_a-\varepsilon_i)\delta_{al}\delta_{ij} \\
H_{ai,lk}^{(1)-4} &= 2(ai\,|\,lk)-\frac{1}{2}(al\,|\,ik)-\frac{1}{2}(ak\,|\,li)+(\varepsilon_a-\varepsilon_i)\delta_{al}\delta_{ik} \qquad (10) \\
H_{ai,gj}^{(1)-5} &= 4(ai\,|\,gj)-(ag\,|\,ji)-(aj\,|\,gi)+(\varepsilon_a-\varepsilon_i)\delta_{ag}\delta_{ij} \\
H_{ai,gk}^{(1)-6} &= 2(ai\,|\,gk)-\frac{1}{2}(ag\,|\,ki)-\frac{1}{2}(ak\,|\,gi)+(\varepsilon_a-\varepsilon_i)\delta_{ag}\delta_{ik}
\end{aligned}
$$

In Eq. (10), *a* and *b* are virtual orbitals, *i*, *g* and *j* are doubly occupied orbitals and *k* and *l* are singly occupied orbitals. The first two orbital Hessians in Eq. (10) use virtual orbital b to substitute for the perturbed orbital. The next two Hessians use singly occupied orbital *l* and the last two Hessians use doubly occupied orbital *g*.

The expression for the magnetic orbital Hessian matrix $H^{(2)}$ is more complicated than that for the closed shell case and it too contains six different expressions given in Eq. (11).

$$
\begin{aligned}
H_{ai,bj}^{(2)-1} &= (ab\,|\,ij)-(aj\,|\,ib)+(\varepsilon_a-\varepsilon_i)\delta_{ab}\delta_{ij} \\
H_{ai,bk}^{(2)-2} &= \frac{1}{2}(ab\,|\,ik)-\frac{1}{2}(ak\,|\,ib)+(\varepsilon_a-\varepsilon_i)\delta_{ab}\delta_{ik} \\
H_{ai,jl}^{(2)-3} &= (al\,|\,ij)-(aj\,|\,il)+(\varepsilon_a-\varepsilon_i)\delta_{al}\delta_{ij} \\
H_{ai,kl}^{(2)-4} &= \frac{1}{2}(al\,|\,ik)-(ak\,|\,il)+(\varepsilon_a-\varepsilon_i)\delta_{al}\delta_{ik} \qquad (11) \\
H_{ai,gj}^{(2)-5} &= (ag\,|\,ij)-(aj\,|\,ig)+(\varepsilon_a-\varepsilon_i)\delta_{ag}\delta_{ij} \\
H_{ai,gk}^{(2)-6} &= \frac{1}{2}(ag\,|\,ik)-\frac{1}{2}(ak\,|\,ig)+(\varepsilon_a-\varepsilon_i)\delta_{ag}\delta_{ik}
\end{aligned}
$$

المنارة للاستشارات

www.manaraa.com

The same procedure can be used for the F_{SE} operator. The orbital Hessian matrices are given in Eqs. (12), (13) (m is a singly occupied orbital):

$$\begin{aligned}
H_{ak,bj}^{(1)} &= 4(ak \mid bj) - (ab \mid kj) - (aj \mid kb) + (\varepsilon_a - \varepsilon_k)\delta_{ab}\delta_{kj} \\
H_{ak,bl}^{(1)-2} &= 2(ak \mid bl) - (ab \mid kl) - (al \mid kb) + (\varepsilon_a - \varepsilon_k)\delta_{ab}\delta_{kl} \\
H_{ak,gj}^{(1)-3} &= 4(ak \mid gj) - (ag \mid kj) - (aj \mid kg) + (\varepsilon_a - \varepsilon_k)\delta_{ag}\delta_{kj} \\
H_{ak,gl}^{(1)-4} &= 2(ak \mid gl) - (ag \mid kl) - (al \mid kg) + (\varepsilon_a - \varepsilon_k)\delta_{ag}\delta_{kl} \\
H_{ak,mj}^{(1)-5} &= 4(ak \mid mj) - (am \mid kj) - (aj \mid km) + (\varepsilon_a - \varepsilon_k)\delta_{am}\delta_{kj} \\
H_{ak,ml}^{(1)-6} &= 2(ak \mid ml) - (am \mid kl) - (al \mid km) + (\varepsilon_a - \varepsilon_k)\delta_{am}\delta_{kl}
\end{aligned} \tag{12}$$

$$\begin{aligned}
H_{ak,bj}^{(2)} &= (ab \mid kj) - (aj \mid kb) + (\varepsilon_a - \varepsilon_k)\delta_{ab}\delta_{kj} \\
H_{ak,bl}^{(2)-2} &= (ab \mid kl) - (aj \mid km) + (\varepsilon_a - \varepsilon_k)\delta_{ab}\delta_{kl} \\
H_{ak,gj}^{(2)-3} &= (ag \mid kj) - (aj \mid kg) + (\varepsilon_a - \varepsilon_k)\delta_{ag}\delta_{kj} \\
H_{ak,gl}^{(2)-4} &= (ag \mid kl) - (al \mid kg) + (\varepsilon_a - \varepsilon_k)\delta_{ag}\delta_{kl} \\
H_{ak,mj}^{(2)-5} &= (am \mid kj) - (aj \mid km) + (\varepsilon_a - \varepsilon_k)\delta_{am}\delta_{kj} \\
H_{ak,ml}^{(2)-6} &= (am \mid kl) - (al \mid km) + (\varepsilon_a - \varepsilon_k)\delta_{am}\delta_{kl}
\end{aligned} \tag{13}$$

Finally, the F_{DS} operator orbital Hessian matrices are relatively simple because the form of the Fock operator is simpler. Electric and magnetic orbital Hessian matrices are given in Eqs. (14), (15).

www.manaraa.com

$$\begin{aligned}
H_{ki,mj}^{(1)-1} &= 4(ki\,|\,mj)-(km\,|\,ij)-(kj\,|\,im)+(\varepsilon_k-\varepsilon_i)\delta_{km}\delta_{ij} \\
H_{ki,ml}^{(1)-2} &= 2(ki\,|\,lm)+(\varepsilon_k-\varepsilon_i)\delta_{km}\delta_{il} \\
H_{ki,gj}^{(1)-3} &= 4(ki\,|\,gj)-(kg\,|\,ij)-(kj\,|\,ib)+(\varepsilon_k-\varepsilon_i)\delta_{kg}\delta_{ij} \\
H_{ki,gl}^{(1)-4} &= 2(ki\,|\,gm)+(\varepsilon_k-\varepsilon_i)\delta_{kg}\delta_{il} \\
H_{ki,bj}^{(1)-5} &= 4(ki\,|\,bj)-(kb\,|\,ij)-(kj\,|\,ib)+(\varepsilon_k-\varepsilon_i)\delta_{kb}\delta_{ij} \\
H_{ki,bl}^{(1)-6} &= 2(ki\,|\,lb)+(\varepsilon_k-\varepsilon_i)\delta_{kb}\delta_{il}
\end{aligned}\tag{14}$$

$$\begin{aligned}
H_{ki,mj}^{(2)-1} &= (km\,|\,ij)-(kj\,|\,im)+(\varepsilon_k-\varepsilon_i)\delta_{km}\delta_{ij} \\
H_{ki,bj}^{(2)-2} &= (kb\,|\,ij)-(kj\,|\,ib)+(\varepsilon_k-\varepsilon_i)\delta_{kg}\delta_{ij} \\
H_{ki,gj}^{(2)-3} &= (kg\,|\,ij)-(kj\,|\,ig)+(\varepsilon_k-\varepsilon_i)\delta_{kb}\delta_{ij}
\end{aligned}\tag{15}$$

It is convenient to solve these orbital Hessians together. Super-matrices and super-vectors are employed to combine each of these orbital Hessians into one large matrix. This can be illustrated by dividing each Fock operator in Eq. (9) into three pieces: the one electron Hamiltonian and the two sums over orbital subspaces. Starting with Eq. (3), define a super-matrix $H_1^{'}$, the combination of two super-matrices: the first super-matrix, $H_{11}^{'}$, corresponds to the orbital Hessians resulting from the integrals in Eq. (9) which result from the sums over the doubly-occupied space *j* in each Fock operator (F^{DE}, F^{SE} and F^{DS}). The

www.manaraa.com

second super-matrix, $H_{12}^{'}$, corresponds to the terms from each Fock operator that involve the second sum over the singly occupied space *l*. So,

$$H_{1}^{'} = \left(H_{11}^{'} + H_{12}^{'}\right) \qquad (16)$$

where the first '*1*' subscript on *H* denotes that it is the electric field orbital Hessian matrix and the superscript prime distinguishes this matrix as a combination of many matrices, all of which result from the sums over the doubly-occupied space *j* of each Fock operator (F^{DE}, F^{SE} and F^{DS}). For instance, $H_{11}^{'}$ is defined as

$$H_{11}^{'} = \left(H_{FE}^{(1)-1} \quad H_{SE}^{(1)-1} \quad H_{FS}^{(1)-1} \quad H_{FE}^{(1)-3} \quad H_{SE}^{(1)-3} \quad H_{FS}^{(1)-3} \quad H_{FE}^{(1)-5} \quad H_{SE}^{(1)-5} \quad H_{FS}^{(1)-5}\right) \quad (17)$$

Each element within $H_{11}^{'}$ is defined in Eqs. (10), (12) and (14). Note that the subscripts on the orbital Hessians have changed from the orbitals involved, to the Fock operator from which they are derived. Only the odd-numbered terms from Eqs. (10), (12), and (14) are included in $H_{11}^{'}$ because those are the terms that arise from the first sum over the doubly-occupied subspace *j* in each Fock operator. The even numbered terms are included in $H_{12}^{'}$, defined as

$$H_{12}^{'} = \left(H_{FE}^{(1)-2} \quad H_{SE}^{(1)-2} \quad H_{FS}^{(1)-2} \quad H_{FE}^{(1)-4} \quad H_{SE}^{(1)-4} \quad H_{FS}^{(1)-4} \quad H_{FE}^{(1)-6} \quad H_{SE}^{(1)-6} \quad H_{FS}^{(1)-6}\right) \quad (18)$$

$H_{21}^{'}$ and $H_{22}^{'}$ contain all of the magnetic Hessian matrices defined in Eqs. (11), (13) and (15). These two super-matrices are organized in a similar fashion to Eqs. (17) and (18). $H_{21}^{'}$ contains the odd-numbered matrices in Eqs. (11), (13) and (15) (resulting from the sum over *j* from each Fock operator) while $H_{22}^{'}$ contains the even-numbered matrices (resulting from the sum over *l* in each Fock operator).

www.manaraa.com

The H'_{11}, H'_{12}, H'_{21} and H'_{22} super-matrices can then be used to solve for the response vectors Z in a similar manner to that for the closed-shell case. The open-shell CPHF analog of Eq. (3) is:

$$\begin{aligned}&\left(H'_{11}+H'_{12}\right)Y'+\omega Z'=2P\\&\omega Y'+\left(H'_{21}+H'_{22}\right)Z'=0\end{aligned}\tag{19}$$

These equations can be rearranged to solve for Z' by first solving for Y':

$$Y'=-\omega^{-1}\left(H'_{21}+H'_{22}\right)Z'\tag{20}$$

Eq. (20) can now be expressed with Y' eliminated:

$$\left(-\omega^{-1}\left(H'_{21}+H'_{22}\right)\left(H'_{11}+H'_{12}\right)+\omega\right)Z'=2P\tag{21}$$

Solving the previous equation for Z produces the response vectors that can then be used to define the dynamic polarizability tensors and the C_6 dispersion coefficients.

Proposed implementation of the method

It is easy to see that the required number of integrals for the response vector could be very large. If it is not necessary to substitute the perturbation of the molecular orbitals with orbitals from all three MO subsets, one could choose to substitute them with just the virtual orbitals and with the orbitals from only one of the occupied subspaces. For instance, a singly occupied orbital and a virtual orbital could be mixed in to replace a perturbed doubly occupied orbital. Likewise, a perturbed singly occupied orbital would be replaced with orbitals from the doubly occupied and virtual space. This approach would be similar to the closed shell case in which a perturbed doubly occupied orbital is replaced with orbitals from only the virtual space and not other orbitals in the doubly occupied space, because rotations

المنارة للاستشارات

www.manaraa.com

of orbitals within a subspace do not change the energy. This would simplify the equations greatly and reduce the required computational time because the number of integrals would decrease drastically. This simplification would have to be tested to assess how much error it introduces. Using such an approach, the Hessian matrix $H_{11}^{'}$ can be written as

$$H_{11}^{'} = \left(H_{FE}^{(1)-1} H_{SE}^{(1)-1} H_{FS}^{(1)-1} H_{FE}^{(1)-3} H_{SE}^{(1)-3} F_{FS}^{(1)-3} \right) \quad (22)$$

while $Y^{'}$ would be defined as follows:

$$Y^{'} = \begin{pmatrix} Y_{FE} \\ Y_{SE} \\ Y_{FS} \end{pmatrix}. \quad (23)$$

The remaining orbital Hessian matrices have a form that is similar to that of $H_{11}^{'}$ while $Z^{'}$ and $2P^{'}$ have a form that is similar to that of $Y^{'}$. The equation required to solve for Z looks identical to the equation defined above. However, the super-vectors Y', $H_{11}^{'}$, $H_{12}^{'}$ and P are much simpler and smaller in size.

It may be feasible to use an existing solver to obtain the response vectors (with or without approximations). The PGMRES subroutine within GAMESS is a solver used to obtain the closed-shell dynamic polarizability tensors. It was designed to solve for the response vectors when given the orbital Hessian matrices. In addition to being designed for this purpose, it is also able to store strips of data on disk when the available memory is not sufficient. It is likely that disk access will be required for the open shell code.

Acknowledgements

www.manaraa.com

The authors thank Drs. Roger Amos and Ivana Adamovic for valuable discussions. Work at the Ames Laboratory is supported by the Department of Energy-Basic Energy Sciences under Contract No. DE-AC02-07CH11358."

References

1. Day, P. N.; Jensen, J. H.; Gordon, M. S.; Webb, S. P.; Stevens, W. J.; Krauss, M.; Garmer, D.; Basch, H.; Cohen, D. *J. Chem. Phys.* **1996,** *105*, 1968.

2. Gordon, M. S.; Freitag, M. A.; Bandyopadhyay, P.; Jensen, J. H.; Kairys, V.; Stevens, W. J. *J. Phys. Chem. A* 2001, *105*, 293.

3. Adamovic, I.; Gordon, M. S. *Mol. Phys.*, **2005**, *103*, 379.

4. Li, H.; Gordon, M. S.; Jensen, J.H. *J. Chem. Phys.*, **2006**, *124*, 214108.

5. See previous chapter of this thesis.

6. Binkley, J. S.; Pople, J.A.; Dobosh, P.A. *Mol. Phys.*, **1974**, *28*, 1423.

7. Schmidt, M. W.; Baldridge, K. K.; Boatz, J. A.; Jensen, J. H.; Koseki, S.; Matsunaga, N.; Gordon, M. S.; Ngugen, K. A.; Su, S.; Windus, T. L.; Elbert, S. T.; Montgomery, J.; Dupuis, M. *J. Comput. Chem.* 1993, *14*, 1347.

8. Gordon, M.S.; Schmidt, M.W. "Advances in Electronic Structure Theory: GAMESS a Decade Later", *Theory and Applications of Computational Chemistry,* Ch.. 41, C. E.

9. Amos, R. D.; Handy, N.C.; Knowles, P.J.; Rice, J.E.; Stone, A.J. *J. Phys. Chem.*, **1985**, *89*, 2186.

10. Ioannou, A.G.; Colwell, S.M.; Amos, R.D. *Chem. Phys. Lett.,* **1997**, *278*, 278.

11. Osamura, Y.; Yamaguchi, Y.; Fox, D. J.; Vincent, M. A.; Schaefer, H. F. *J. Mol. Structure*, **1983**, *103*, 183.

www.manaraa.com

12. Carole Van Callie, student thesis, University of Cambridge.

13. Roger Amos, personal communication.

www.manaraa.com

CHAPTER 8. IMPLEMENTATION OF EXCHANGE REPULSION ENERGY BETWEEN *AB INITIO* AND EFFECTIVE FRAGMENT POTENTIAL MOLECULES

A paper to be submitted to *Theoretical Chemistry Accounts*

Daniel D. Kemp and Mark S. Gordon

Abstract

The exchange repulsion energy, Fock operator and gradient expressions for systems that contain both effective fragment potentials and *ab initio* molecules have been derived, and the former two have been implemented and tested. Computational timings and the current challenges facing the implementation of the gradient are discussed.

I. Introduction

The effective fragment potential (EFP) method has been used to successfully model a variety of intermolecular interactions, including solvent effects on ions and chemical reaction mechanisms. The original implementation[1], called EFP1, was designed exclusively for the water molecule. It can be used to study a system containing only EFP1 potentials or a system in which EFP1 water potentials solvate an *ab initio* solute within the General Atomic and Molecular Electronic Structure System (GAMESS)[2,3].

The second implementation[4], called EFP2, is a general model potential that can be generated for any molecular species. An EFP2 can interact with other EFP2 molecules via electrostatics, polarization, exchange repulsion, dispersion[5] and charge transfer[6]. Gradients for each interaction type are available allowing the structural geometry to be optimized.

An EFP2 can be used in the presence of an *ab initio* molecule in GAMESS to calculate energies at fixed geometries. Single point energies are described through electrostatics, polarization and exchange repulsion interaction energies. Only single point

www.manaraa.com

energies may be calculated when an *ab initio* molecule is present, because the gradient expression is not available for the exchange repulsion energy, and the currently implemented EFP2-*ab initio* exchange repulsion energy is approximate[7].

This work reviews the rigorous expressions for the exchange repulsion energy[8], and the corresponding Fock matrix[8] and gradient expressions[9] in Section II. Implementations, results and timings are presented in Section III. Successful and unsuccessful approximations are detailed in Section IV. The future of the project and the required derivatives for the gradient are discussed in Section V. Conclusions are drawn in Section V.

II. Theory

The EFP2-EFP2 exchange repulsion energy expression[6] has previously been used to calculate both the inter-fragment exchange repulsion (among EFP2 potentials) and fragment-*ab inito* exchange repulsion energy (between EFP2 potentials and *ab initio* molecules). The expression[6] for the exchange repulsion energy before approximations is

$$
\begin{aligned}
E^{XR} &= -2\sum_{i\in A}\sum_{j\in B}(ij\,|\,ij) - 2\sum_{i\in A}\sum_{j\in B}S_{ij}\left[V_{ij}^{A}+G_{ij}^{A}+V_{ij}^{B}+G_{ij}^{B}\right] \\
&+2\sum_{i\in A}\sum_{j\in B}S_{ij}\left[\sum_{k\in A}S_{kj}\left(V_{ik}^{B}+2J_{ik}^{B}\right)+\sum_{l\in B}S_{il}\left(V_{lj}^{A}+2J_{lj}^{A}\right)-\sum_{k\in A}\sum_{l\in B}S_{kl}\left(ik\,|\,lj\right)\right]
\end{aligned}
\tag{1}
$$

The integrals in Eq. (1) are defined as follows:

$$(ij\,|\,ij)=\iint\phi_i^*(r_1)\phi_j(r_1)\frac{1}{r_{12}}\phi_i^*(r_2)\phi_j(r_2)dr_1dr_2 \tag{2}$$

$$S_{ij}=\left(i\,|\,j\right)=\int\phi_i^*(r_1)\phi_j(r_1)dr_1 \tag{3}$$

$$V_{ij}^{A}=\sum_{I\in A}\left(i\,\Big|\,\frac{Z_I}{R_{1I}}\,\Big|\,j\right)=\sum_{I\in A}\int\phi_i^*(r_1)\frac{Z_I}{R_{1I}}\phi_j(r_1)dr_1 \tag{4}$$

$$G_{ij}^{A}=2J_{ij}^{A}-K_{ij}^{A} \tag{5}$$

المنارة للاستشارات

www.manaraa.com

All orbital indices refer to molecular orbitals. Molecular orbital ϕ_i is always on molecule A (the *ab inito* molecule in the case of EFP2/*ab intio* exchange repulsion) while molecular orbital ϕ_j is always on molecule B (always an EFP2). Electron 1 and electron 2 are represented by r_1 and r_2, respectively. Z_I is the atomic number of the Ith atom and R_{1I} is the distance between electron 1 and the Ith atom. S_{ij} is an intermolecular overlap integral and V_{ij} contains the electron-nuclear attraction terms. J_{ij}^A is commonly referred to as a Coulomb integral and is the electrostatic repulsion between electron 1 and electron 2. K_{ij}^A is commonly referred to as an exchange integral. The exchange integral is a quantum mechanical integral without a simple classical analog. The exchange integral is similar to the Coulomb integral except for the exchange of an electron between the bra and the ket. A hidden sum is located on both integrals in Eq. (5). J_{ij}^A and K_{ij}^A can be defined as follows, where the orbital k always resides on molecule A

$$J_{ij}^A = (ij \mid kk) = \iint \phi_i^*(r_1)\phi_j(r_1)\frac{1}{r_{12}}\phi_k^*(r_2)\phi_k(r_2)dr_1dr_2 \tag{6}$$

$$K_{ij}^A = (ik \mid jk) = \iint \phi_i^*(r_1)\phi_k(r_1)\frac{1}{r_{12}}\phi_j^*(r_2)\phi_k(r_2)dr_1dr_2 \tag{7}$$

Approximations can be made to Eq. (1) to reduce the computational time required to calculate the energy. For example, the spherical Gaussian orbital (SGO) approximation[10] can be applied to the exchange integral to cast it in terms of the intermolecular overlap S_{ij}. Therefore, Eq. (2) can be approximated as

$$(ij \mid ij) \approx 2\sqrt{\frac{-2\ln S_{ij}}{\pi}}\frac{S_{ij}^2}{R_{ij}} \tag{8}$$

www.manaraa.com

Consider the terms in Eq. (2) that depend upon the intermolecular overlap integral to the first power, S_{ij}. These electron-nuclear attraction integrals and two electron integrals, $V_{ij}^{A} + G_{ij}^{A}$ and $V_{ij}^{B} + G_{ij}^{B}$, can be rewritten to avoid the computationally costly two-electron integrals by replacing them with the Fock matrix elements of the monomers and the kinetic energy integrals T_{ij}.

$$\begin{aligned} V_{ij}^{A} + G_{ij}^{A} &= F_{ij}^{A} - T_{ij} = \sum_{k\in A} F_{ik}^{A} S_{kj} - T_{ij} \\ V_{ij}^{B} + G_{ij}^{B} &= F_{ij}^{B} - T_{ij} = \sum_{l\in B} F_{jl}^{B} S_{il} - T_{ij} \end{aligned} \tag{9}$$

The Fock matrix elements of the monomers are obtained by performing a Hartree-Fock calculation. Once the Fock matrix is obtained in the atomic orbital (AO) basis, it is transformed to the molecular orbital basis using the molecular orbital eigenvectors obtained during the Hartree-Fock procedure. This matrix is stored on disk after transformation and is readily available.

By neglecting many of the smaller and off-diagonal integrals which depend upon the overlap to the second power, some simplifications can be made. Specifically, one of the nuclear-electron attraction integrals and a two-electron integrals can be approximated as shown in Eqs. (10) and (11).

$$S_{ij} S_{kj} V_{ik}^{B} \approx S_{ij}^{2} V_{ii}^{B} \delta_{ik} \tag{10}$$

$$S_{ij} S_{kl} \left(ik \mid lj \right) \approx S_{ij}^{2} \left(ii \mid jj \right) \delta_{ik} \delta_{lj} \tag{11}$$

Any integrals that remain are approximated by using classical point-charge models

$$S_{ij}^{2} V_{ij}^{B} => S_{ij}^{2} \left(\sum_{j\in B} -Z_{J} R_{iJ}^{-1} \right) \tag{12}$$

www.manaraa.com

$$S_{ij}^{2}\left(ii \mid jj\right) => S_{ij}^{2} R_{ij}^{-1} \tag{13}$$

The approximate form of the exchange repulsion energy[6] in Eq. (1) can consequently be written as

$$\begin{aligned} E^{XR} \approx & -2\sum_{i\in A}\sum_{j\in B} 2\sqrt{\frac{-2\ln S_{ij}}{\pi}}\,\frac{S_{ij}^{2}}{R_{ij}} - 2\sum_{i\in A}\sum_{j\in B} S_{ij}\left[\sum_{k\in A} F_{ik}^{A} S_{kj} + \sum_{l\in B} F_{jl}^{B} S_{li} - 2T_{ij}\right] \\ & +2\sum_{i\in A}\sum_{j\in B} S_{ij}^{2}\left[-\sum_{J\in B} Z_J R_{iJ}^{-1} + 2\sum_{l\in B} R_{il}^{-1} - \sum_{l\in A} Z_l R_{lj}^{-1} + 2\sum_{k\in A} R_{kj}^{-1} - R_{ij}^{-1}\right] \end{aligned} \tag{14}$$

Eq. (14) has been implemented in GAMESS and is used to calculate the exchange repulsion energy between EFP2 potentials. It has also been implemented to calculate the exchange repulsion energy between an EFP2 and an *ab initio* molecule. When an *ab initio* molecule is present, its orbitals are localized at the end of the self-consistent field (SCF) process, and Eq. (14) is calculated.

However, one of the primary assumptions which Eqs. (1) and (14) are built upon is not rigorously true when an *ab initio* molecule is present. A molecular orbital (ψ_k) on the *ab initio* molecule can be written as linear combination of atomic orbitals (φ_μ), $\psi_k = \sum_{\mu} C_{\mu k}\varphi_\mu$. During the SCF procedure, the *ab initio* Fock operator in the molecular orbital basis operates upon the molecular orbitals to obtain the molecular orbital energy eigenvalues. The Fock operator, F^A, contains both one and two-electron operators. When a molecule is isolated, the use of the Fock operator in Eq. (15) holds true.

$$F^A \psi_i = \sum_{k\in A} F_{ik}^{A} \psi_k \tag{15}$$

However, Eq. (15) is violated during calculations[8] when an EFP2 is present because it does not take the presence of the EFP2 into account. Eq. (15) is the basis for Eq. (1), and

www.manaraa.com

consequently Eq. (14) as well. Therefore, Eq. (14) cannot be used when Eq. (15) does not hold true. An energy expression has been derived for E_{XR} when both EFP2 potentials and *ab initio* molecules are present. This expression[8] is given without approximation in Eq. (16).

$$\begin{aligned} E^{XR} = & -2\sum_{i\in A}\sum_{j\in B}(ij\,|\,ij) - 2\sum_{i\in A}\sum_{j\in B}S_{ij}\left[2\left(V_{ij}^{A}+G_{ij}^{A}\right)+\sum_{l\in B}F_{jl}^{B}S_{li}\right] \\ & +2\sum_{i\in A}\sum_{j\in B}S_{ij}\left[\sum_{k\in A}S_{kj}\left(F_{ik}^{A}+V_{ik}^{B}+J_{ik}^{B}\right)+S_{ij}\left(V_{jj}^{A}+J_{jj}^{A}\right)-\sum_{k\in A}S_{kj}(ik\,|\,jj)\right] \end{aligned} \quad (16)$$

In order to be able to calculate the exchange repulsion energy expression (Eq. 16) efficiently during the Hartree-Fock SCF iterations, approximations must be applied. Because the orbitals on the *ab initio* molecule are canonical (not-localized) molecular orbitals obtained during the SCF iterations, some of the approximations applied to Eq. (1) cannot be used to approximate Eq. (16). The SGO approximation[10] can be applied to the exchange integral in the leading term of Eq. (16), but it must be applied in a different way than done previously. The SGO approximation depends upon localized orbitals, so the molecular orbitals on molecule A are expressed as a linear combination of AOs

$$(ij\,|\,ij)=\sum_{\mu}\sum_{\nu}C_{\mu i}C_{\nu i}(\mu j\,|\,\nu j) \quad (17)$$

where μ and ν are basis functions on the *ab initio* molecule. The atomic orbitals are better suited for the SGO approximation because they are located on the atomic centers.

The SGO approximation defines two localized molecular orbitals as two spherical (s-type) gaussians[10]

$$\Psi_i \approx \left(\frac{2\alpha}{\pi}\right)^{3/4} e^{-\alpha\left|r-R_i\right|^2} \text{ and } \Psi_j \approx \left(\frac{2\alpha}{\pi}\right)^{3/4} e^{-\alpha\left|r-R_j\right|^2} \quad (18)$$

One can then obtain the corresponding exchange integral as[11]

المنارة للاستشارات

www.manaraa.com

$$\left\langle \Psi_i \Psi_j \mid \Psi_i \Psi_j \right\rangle \approx 2\left(\frac{\alpha}{\pi}\right)^{1/2} e^{-\alpha R_{ij}^2} \tag{19}$$

In the SGO approximation[10] α is obtained by equating the Spherical Gaussian overlap with the actual overlap of the appropriate LMOs

$$e^{-\frac{1}{2}\alpha R_{ij}^2} = S_{ij} \tag{20}$$

Taking the log of both sides leads us to Eq. (21)

$$\alpha_{ij} = -\frac{2}{R_{ij}^2} \ln S_{ij} \tag{21}$$

Two-electron integrals over s-type primitives A, B, C, D are obtained as follows[11]

$$\begin{aligned}
&(AB \mid CD) = 2\pi^{5/2} / \left[(\alpha+\beta)(\gamma+\delta)(\alpha+\beta+\gamma+\delta)^{1/2}\right] \\
&*\exp\left[-\alpha\beta/(\alpha+\beta)\left|R_A - R_B\right|^2 - \gamma\delta/(\gamma+\delta)\left|R_C - R_D\right|^2\right] \\
&*F_0\left[(\alpha+\beta)(\gamma+\delta)/(\alpha+\beta+\gamma+\delta)\left|R_p - R_Q\right|^2\right]
\end{aligned} \tag{22}$$

In Eq. (22) γ is the exponent for function C, δ is the exponent for function D, R_p is the center of the product Gaussian resulting from function A and B, R_Q is the center of the product Gaussian resulting from function C and D.

Substituting $\alpha_{\mu j}$ for α and β, $\alpha_{\nu j}$ for γ and δ, and defining R_p and $R_{q,}$ one obtains:

$$\begin{aligned}
&\langle \mu j \mid \nu j \rangle = 2\pi^{5/2} / \left[(2\alpha_{\mu j})(2\alpha_{\nu j})(2\alpha_{\mu j} + 2\alpha_{\nu j})^{1/2}\right] \\
&*\exp\left[-\alpha_{\mu j}^2 / (2\alpha_{\mu j})\left|R_{\mu j}\right|^2 - \alpha_{\nu j}^2 / (2\alpha_{\nu j})\left|R_{\nu j}\right|^2\right] \\
&*F_0\left[(2\alpha_{\mu j})(2\alpha_{\nu j}) / (2\alpha_{uj} + 2\alpha_{\nu j})\left|\left(\frac{R_\mu - R_j}{2}\right) - \left(\frac{R_\nu - R_j}{2}\right)\right|^2\right]
\end{aligned} \tag{23}$$

Eq. (23) can be simplified to

www.manaraa.com

$$\left(\mu j\,|\,\nu j\right)=\frac{2}{\sqrt{\pi}}\sqrt{\frac{2\alpha_{\mu j}\alpha_{\nu j}}{\alpha_{\mu j}+\alpha_{\nu j}}}S_{\mu j}S_{\nu j}F_0\left[\frac{1}{4}\left(\frac{2\alpha_{\mu j}\alpha_{\nu j}}{\alpha_{\mu j}+\alpha_{\nu j}}R_{\mu\nu}^{2}\right)\right] \tag{24}$$

F_0 is the incomplete gamma function $F_0\left[t\right]=\frac{1}{2}\left(\frac{\pi}{t}\right)^{\frac{1}{2}}erf\left(t^{\frac{1}{2}}\right)$. Eq. (24) provides a value for the integral $\left(\mu j\,|\,\nu j\right)$. Transforming this integral to the molecular orbital basis gives Eq. (17)[8].

The one-electron nuclear attraction integral dependent, V_{ij}^{A}, is efficiently calculated without approximation. Approximations based on the SGO approximation have been proposed for the two-electron integrals[8] J_{ij}^{A} and K_{ij}^{A}. Just as for the exchange integral defined in Eq. (17), this approximation must make use of the AOs on the *ab initio* molecule. J_{ij}^{A} can be expressed as

$$J_{ij}^{A}=\left(ij\,|\,kk\right)=\sum_{\mu}\sum_{\lambda}\sum_{\sigma}C_{\mu i}C_{\lambda k}C_{\sigma k}\left(\mu j\,|\,\lambda\sigma\right) \tag{25}$$

Applying the multipole approximation to Eq. (25) gives us

$$\left(\mu j\,|\,\lambda\sigma\right)\approx S_{\lambda\sigma}\left(\mu\left|R_{1Q_{\lambda\sigma}}^{-1}\right|j\right) \tag{26}$$

Next, the SGO approximation is applied to Eq. (26). For s-type primitives, the approximate electron-nuclear attraction integral in Eq.(26) can be written as[11]:

$$(A\,|\left(-Z_I/r_{1I}\right)|\,B)=\frac{-2\pi}{\left(\alpha+\beta\right)}Z_I\exp\left[-\alpha\beta/\left(\alpha+\beta\right)\left|R_A-R_B\right|^2\right]F_0\left[\left(\alpha+\beta\right)\left|R_p-R_I\right|^2\right] \tag{27}$$

المنارة للاستشارات
www.manaraa.com

where Z_I is the atomic number of atom I, α is the orbital exponent of orbital A, β is the orbital exponent on orbital B, R_A is the center of A, R_B is the center of B, R_p is the center of the product Gaussian formed from A and B, and R_I is the position of atom I.

Since α and β are the same, because we are looking at the product spherical Gaussian between the two orbitals A and B, Eq. (27) becomes:

$$(A\,|\left(-Z_I/r_{1I}\right)|\,B)=\frac{-2\pi}{\left(2\alpha_{\mu j}\right)}Z_I\exp\left[-\alpha_{\mu j}^2/\left(2\alpha_{\mu j}\right)\left|R_A-R_B\right|^2\right]F_0\left[\left(2\alpha_{\mu j}\right)\left|R_p-R_I\right|^2\right] \quad (28)$$

Using the $\alpha_{\mu j}$ defined by the SGO approximation in Eq. (21) we obtain Eq. (29):

$$(A\,|\left(-Z_I/r_{1I}\right)|\,B)=\frac{-2\pi}{\left(2\alpha_{\mu j}\right)}Z_I\exp\left[-2/\left(-2*\left|R_A-R_B\right|^2\right)\left|R_A-R_B\right|^2\ln\left|S_{\mu j}\right|\right]F_0\left[\left(2\alpha_{\mu j}\right)\left|R_p-R_I\right|^2\right] \quad (29)$$

Multiplying Eq. (29) by SGO prefactors and simplifying:

$$(A\,|\left(-Z_I/r_{1I}\right)|\,B)=-\left(\frac{8\alpha_{\mu j}}{\pi}\right)^{1/2}Z_I S_{\mu j}F_0\left[\left(2\alpha_{\mu j}\right)\left|R_p-R_I\right|^2\right] \quad (30)$$

Therefore,

$$(\mu j\,|\,\lambda\sigma)\approx-\left(\frac{8\alpha_{\mu j}}{\pi}\right)^{\frac{1}{2}}S_{\mu j}S_{\lambda\sigma}F_0\left[2\alpha_{\mu j}R_{P_{\mu j}Q_{\lambda\sigma}}^2\right] \quad (31)$$

Eq. (30) is the proposed approximation to Eq. (25).

The Fock matrix elements for molecule B in Eq. (16) are supplied in the EFP2 input and are readily available. The overlap integrals are one-electron integrals and are calculated exactly.

www.manaraa.com

Approximations based on multipole expansions can be used to simplify all of the terms which that upon the overlap squared[8]:

$$F_{ik}^{A} + V_{ik}^{B} + J_{ik}^{B} \approx F_{ik}^{A} + V_{ik}^{ES,B} \approx F_{ik}^{A} + V_{ik}^{EFP,B} \tag{32}$$

$$(ik \mid jj) \approx \left(i \middle| \left| r_1 - R_J \right|^{-1} \middle| k \right) = V_{ik}^{j} \tag{33}$$

Because the one-electron nuclear attraction integral involves only one molecular orbital on B with the nuclei on molecule A, it can be replaced[8] with the classical point-charge approximation in Eq. (34).

$$V_{jj}^{A} \approx \sum_{j \in B} \sum_{I \in A} \frac{-Z_I}{R_{jI}} \tag{34}$$

Finally, taking into account all of the foregoing approximations, the exchange repulsion energy becomes[8]

$$\begin{aligned} E^{XR} \approx & -2 \sum_{i \in A} \sum_{j \in B} (ij \mid ij)^{SGO} - 2 \sum_{i \in A} \sum_{j \in B} S_{ij} \left[2 \left(V_{ij}^{A} + G_{ij}^{A,SGO} + \sum_{l \in B} F_{jl}^{B} S_{li} \right) \right] \\ & +2 \sum_{i \in A} \sum_{j \in B} S_{ij} \left[\sum_{k \in A} S_{kj} \left(F_{ik}^{A} + V_{ik}^{EFP,B} \right) + S_{ij} \left(\sum_{I \in A} -Z_I R_{Ij}^{-1} + \sum_{k \in A} V_{kk}^{j} \right) - \sum_{k \in A} S_{kj} V_{ik}^{j} \right] \end{aligned} \tag{35}$$

Before the desired EFP2-*ab initio* gradient can be calculated, an exchange repulsion Fock operator must be added to the one-electron part of the Fock matrix. The EFP2 exchange repulsion contribution to the Fock operator was formed by setting the variational derivative of the exchange repulsion energy equal to zero[8]. By adding this Fock operator to the Fock matrix of the *ab initio* molecule, exchange repulsion effects are incorporated into the Hartree Fock calculation as the *ab initio* orbitals are being optimized during the SCF iterations. The exchange repulsion Fock operator is defined[8] as

www.manaraa.com

$$
\begin{aligned}
V_{mi}^{XR} = &-\sum_{j\in B}(mj|ij)-\frac{1}{2}\sum_{j\in B}S_{mj}\left[2\left(V_{ij}^{A}+G_{ij}^{A}\right)+\sum_{l\in B}F_{jl}^{B}S_{li}\right]\\
&-\frac{1}{2}\sum_{j\in B}S_{ij}\left[2\left(V_{mj}^{A}+G_{mj}^{A}\right)+\sum_{l\in B}F_{jl}^{B}S_{lm}\right]\\
&-\sum_{k\in A}\sum_{j\in B}S_{kj}\left[4(kj|mi)-(km|ji)-(ki|jm)\right]\\
&+\sum_{j\in B}S_{mj}\left[\sum_{k\in A}S_{kj}\left(F_{ik}^{A}+V_{ik}^{B}+J_{ik}^{B}\right)-(ik|jj)+S_{ij}\left(V_{jj}^{A}+J_{jj}^{A}\right)\right]\\
&+\sum_{j\in B}S_{ij}\left[\sum_{k\in A}S_{kj}\left(F_{mk}^{A}+V_{mk}^{B}+J_{mk}^{B}\right)-(mk|jj)\right]\\
&+\frac{1}{2}\sum_{n\in A}\sum_{k\in A}\sum_{j\in B}S_{kj}S_{nj}\left[4(nk|im)-(nm|ik)-(ni|mk)\right]+2\sum_{k\in A}\sum_{j\in B}S_{kj}^{2}(jj|mi)
\end{aligned}
\tag{36}
$$

The expression for V_{mi}^{XR} in Eq. (36) is given without approximation. V_{mi}^{XR} is designed to be calculated for every pair of molecular orbitals m and i (both on the *ab initio* molecule) and added to the one-electron Fock matrix on every SCF iteration. When the approximations detailed in Eqs. (17)-(34) are applied to Eq. (36), one can obtain an approximate expression for V_{mi}^{XR}

$$
\begin{aligned}
V_{mi}^{XR} \approx &-\sum_{j\in B}(mj|ij)^{SGO}-\frac{1}{2}\sum_{j\in B}S_{mj}\left[2\left(V_{ij}^{A}+G_{ij}^{A,SGO}\right)+\sum_{l\in B}F_{jl}^{B}S_{li}\right]\\
&-\frac{1}{2}\sum_{j\in B}S_{ij}\left[2\left(V_{mj}^{A}+G_{mj}^{A,SGO}\right)+\sum_{l\in B}F_{jl}^{B}S_{lm}\right]\\
&-\sum_{k\in A}\sum_{j\in B}S_{kj}\left[4(kj|mi)-(km|ji)-(ki|jm)\right]\\
&+\sum_{j\in B}S_{mj}\left[\sum_{k\in A}S_{kj}\left(F_{ik}^{A}+V_{ik}^{EFP,B}\right)-V_{ik}^{j}+S_{ij}\left(\sum_{I\in A}Z_{I}R_{Ij}^{-1}+V_{kk}^{j}\right)\right]\\
&+\sum_{j\in B}S_{ij}\left[\sum_{k\in A}S_{kj}\left(F_{mk}^{A}+V_{mk}^{EFP,B}\right)-V_{mk}^{j}\right]\\
&+\frac{1}{2}\sum_{n\in A}\sum_{k\in A}\sum_{j\in B}S_{kj}S_{nj}\left[4(nk|im)-(nm|ik)-(ni|mk)\right]+2\sum_{k\in A}\sum_{j\in B}S_{kj}^{2}V_{mi}^{j}
\end{aligned}
\tag{37}
$$

www.manaraa.com

III. Results and implementation

If Eqs. (35) and (37) are implemented as presented here, unpredictable but significant errors are introduced. By comparing each term against the full energy expression (cf., Eq. (16)) and Fock matrix operator (Eq. (36)), it is apparent that the approximated two-electron integrals in Eqs. (25)-(31) are the source of this error. Consider the contribution of the two-electron Coulomb integrals in Eq. (25). The contribution of these integrals to the energy, including the multiplication by the overlap integrals and constants, can be written as

$$-2\sum_{i\in A}\sum_{j\in B}S_{ij}\left(4\sum_{k\in A}(ij\,|\,kk)\right) \tag{38}$$

The sum of all of these contributions for each molecular orbital i, j and k is given for the water, methanol and acetone dimers in Table 8.1. Table 8.1 also provides a comparison of the exact two-electron integrals with the approximated integrals that come from using the approximations in Eqs. (25)-(31). Though the approximated integrals approach the exact value for some of the dimers in the table, other errors are large. The errors do not appear to be predictable.

Table 8.1. The result of summing Eq. (38) over all molecular orbital indices is compared to the approximated values given by Eq. (31). The values of the sums are provided in hartrees and the error between the exact values and the approximated values are provided in kcal/mol.

	Exact Answer (h)	Approximated (h)	Error (kcal/mol)
Water	-0.091867	-0.052722	-24.56
Methanol	-0.121785	-0.123414	1.02
Acetone	-0.082931	-0.078245	-2.94

www.manaraa.com

The errors in Table 8.1 are mainly due to the multipole approximation (Eq. (26)). The multipole approximation is inaccurate when the two electrons are not sufficiently far apart, as occurs if they are both in basis functions on the *ab initio* molecule (μ, λ, σ).

One of the primary goals of the EFP method is to provide reliably accurate results. This cannot be accomplished with the errors that result from using Eq. (26). As an alternative, the exact two-electron integrals are used in place of approximated values. Though more costly, they are exact. That is, the two-electron integrals ($G_{ij}^{A} = 2J_{ij}^{A} - K_{ij}$) in Eq. (16) are calculated exactly while all other integral approximations used in Eq. (35) are retained.

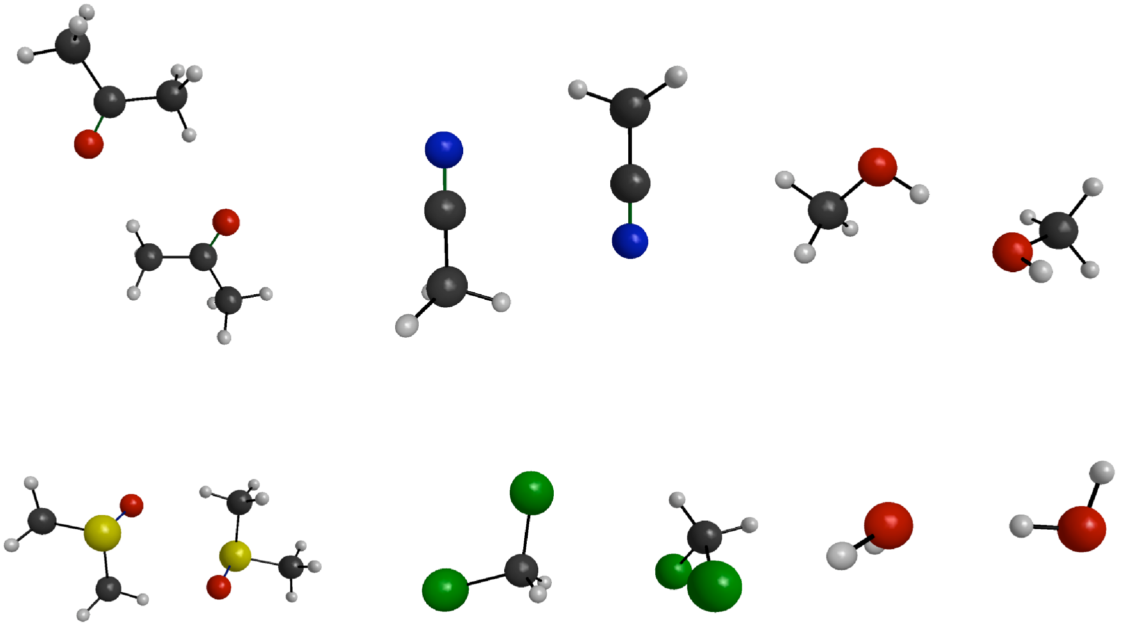

Figure 8.1. The implementation of the EFP2/*ab initio* exchange repulsion energy was tested on six dimers. Starting with the structure in the top left corner and moving to the right, the dimer structures for acetone, acetonitrile, methanol, dimethylsulfoxide, dichloromethane and water provided.

A test set of six dimers was chosen to benchmark the energy and Fock matrix operators for the EFP2/*ab initio* exchange repulsion. The same test set was used to

www.manaraa.com

benchmark the EFP2 exchange repulsion energy and gradient for EFP2-EFP2 interactions[12]. Water, methanol, acetone, acetonitrile, dichloromethane and dimethylsulfoxide (DMSO) dimers were optimized at the HF level of theory. Figure 8.1 illustrates the structures of the six dimer geometries used in this study. At the equilibrium dimer geometries, one monomer (B) was replaced by an EFP2, with the monomer internal geometry.

The series of six dimer calculations was benchmarked against the EFP2 method (both molecule A and B are EFP2s), the previously implemented EFP2/*ab initio* exchange repulsion energy (Eq. (15)), and a Morokuma[13] energy decomposition. The 6-31++G(d,p)[14-16] basis set was used on the *ab initio* molecule; the same basis set was used to generate each EFP2. The results are shown in Table 8.2. The results for the method that is based upon Eq. (38) are also included in Table 8.2. Eq. (39) was added to the Fock matrix of the *ab initio* molecule at each iteration of the HF SCF process.

Table 8.2. Exchange repulsion energy values are given for water, methanol, dichloromethane, acetonitrile, acetone and dimethylsulfoxide (DMSO) dimers. All units are in kcal/mol.

	EFP2/EFP2	Eq. (15)	Morokuma	Eq. (38)
Water	4.35	4.33	4.9	5.26
Methanol	4.34	7.84	5.15	5.25
Dichloromethane	0.27	2.22	0.79	0.58
Acetonitrile	2.05	9145.39	2.21	2.57
Acetone	1.47	1.96	2.27	1.77
DMSO	6.31	Unconverged	6.38	7.53

The Morokuma energy decomposition provides the exact exchange repulsion for a given AO basis set at the Hartree-Fock level of theory. For all six dimers, Eq. (38) qualitatively reproduces the Morokuma exchange repulsion energy. Except for the DMSO

المنارة للاستشارات

www.manaraa.com

dimer, Eq. (39) also quantitatively reproduces the Morokuma exchange repulsion energy. It is clear that Eq. (39) is more accurate than Eq. (15) when an *ab initio* molecule is present.

However, the accuracy of Eqs. (38) and (39) come at the cost of computational expense. Table 8.3 provides the central processor unit (CPU) time required to complete a single point energy calculation at the HF/EFP2 level of theory using Eq. (15), the full HF level of theory for a dimer and a HF/EFP2 calculation using Eqs. (38) and (39). All calculations were performed on a 1200 Mhz IBM Power4+. The cost associated with Eqs. (38) and (39) is more than a full HF dimer calculation.

Table 8.3. The total job CPU time (in seconds) the implementation of Eq. (15), a Hartree-Fock dimer calculation and the implementation of Eqs. (38) and (39).

	Eq. (15)	Hartree-Fock	Eqs. (38), (39)
Water	0.4	1	1.8
Methanol	1.9	12.5	25.7
Dichloromethane	4.2	28.5	69.2
Acetonitrile	3.9	37.3	65.2
Acetone	4.0	136.1	273.5
DMSO	16.7	154.4	375.2

To make the EFP2/*ab initio* exchange repulsion implementation useful, the efficiency must be improved. The first code modification was to calculate the exact two electron integrals in the AO basis and use the integrals in the AO basis to avoid the costly transformation to the MO basis.

The exchange repulsion energy (Eq. 38) is only calculated once during a single point energy calculation once the SCF process has converged. The Fock operator (Eq. (39)) is calculated every SCF iteration. Additionally, more CPU time is spent determining the Fock

المنارة للاستشارات
www.manaraa.com

matrix than the exchange repulsion energy. Fortunately, this cost can be reduced by examining the Fock matrix at various points in the iterative process.

As illustrated in Table 8.4 for water and methanol, the repulsion contribution to the Fock matrix undergoes very small changes from iteration to iteration. The greatest deviation of all of the elements of Eq. (39) was obtained by comparing the results of Eq. (39) at the second SCF iteration to the values of Eq. (39) once the SCF had converged. The absolute value of the greatest deviation between the same element m,i between both iterations is given in Table 8.4 along with the average deviation of all of the elements m,I for water and methanol dimer calculations. The quantitative changes between all of the elements is very small and only 2 of the elements of the Fock matrix experienced a sign change.

Table 8.4. The greatest deviation and the standard deviation of the elements of the Fock matrix V_{mi} are provided (in hartrees) for the water and methanol dimer. The number of elements within the Fock matrix which experienced a sign change is provided as well.

Dimer	Greatest Deviation	Average Deviation	Qualitative Changes
Water	6.20E-06	4.91E-06	2
Methanol	1.05E-03	1.72E-04	0

Because the Fock matrix does not change significantly over ten iterations, it is not useful to spend CPU time re-calculating it every iteration. If the Fock matrix is calculated on the second iteration, and then re-calculated only when the iteration index is divisible by 4 (the 4th, 8th, 12th and so on), one obtains a significant speed. On SCF iterations when the exchange repulsion Fock operator is not re-calculated, the most recently calculated Fock operator is used. Table 8.5 assesses accuracy obtained using this approach. It is clear that there is essentially no accuracy lost by calculating the repulsion contribution to the Fock

www.manaraa.com

matrix only every 4th iteration. The corresponding CPU time comparison is presented in Table 8.6, where it is seen that considerable reduction in CPU time is achieved with virtually no loss of accuracy.

Table 8.5. The resulting exchange repulsion energies (in kcal/mol) when Eq. (39) is recalculated every SCF iteration is compared against the use of an approximate Eq. (39).

	Eqs. (38), (39)	Approx. V
Water	5.26	5.26
Methanol	5.25	5.24
Dichloromethane	0.58	0.58
Acetonitrile	2.57	2.56
Acetone	1.77	1.77
DMSO	7.53	7.54

Table 8.6. CPU time (in seconds) required to use Eq. (15) for a Hartree-Fock/EFP2 calculation, a full Hartree-Fock dimer calculation and a Hartree-Fock/EFP2 calculation which recalculates Eq. (39) on the 2nd, 4th and every other iteration number divisible by four.

	Eq. (15)	Hartree-Fock	Approx. V
Water	0.4	1	0.7
Methanol	1.9	12.5	5.9
Dichloromethane	4.2	28.5	14.6
Acetonitrile	3.9	37.3	11.7
Acetone	4	136.1	50.3
DMSO	16.7	154.4	63.2

IV. Other Approximations

For the DMSO dimer the cost of forming the exact two-electron integrals needed to calculate $G_{ij}^{A} = 2J_{ij}^{A} - K_{ij}$ without approximation is 23.6 seconds, roughly 1/3 of the time spent in the entire calculation (see last column in Table 8.6). If the number of two-electron integrals to calculate could be reduced, it would help reduce the largest bottleneck of the calculation.

www.manaraa.com

The Schwarz inequality can be a useful tool for avoiding the calculation of many integrals that are negligibly small (or zero). For example, if $(ij \mid kl)$ is less than $\sqrt{(ij \mid ij) * (kl \mid kl)}$, then a block of integrals can be skipped. The Schwartz inequality is commonly used in electronic structure programs to avoid calculating integrals that are too small to make significant contributions to the energy. Currently, the EFP2/*ab initio* algorithm for the exact two-electron integrals $G_{ij}^{A} = 2J_{ij}^{A} - K_{ij}$ does not use the Schwarz inequality. Some small modifications will be needed to implement a Schwarz inequality code for this purpose, because not all of the required integrals are currently available. At present, only integrals of the form $(\xi\mu \mid \lambda\sigma)$ are calculated (where ξ is the only index on molecule B). In order to calculate the Schwarz inequality, one also needs the integrals $(\xi\mu \mid \xi\mu)$ and $(\lambda\sigma \mid \lambda\sigma)$. A future study will make use of the Schwarz inequality by using the SGO-approximated $(ij \mid ij)$ integrals.

Semi-empirical methods have a long and successful history of ignoring many two-electron integrals while retaining qualitative accuracy. So, preliminary tests have been conducted to assess the possibility of employing semi-empirical approximations to avoid the calculation of many two-electron integrals. Traditionally, the complete neglect of differential overlap (CNDO)[17] simplifies the two-electron integral to $(\xi\xi \mid \lambda\lambda)\delta_{\xi\mu}\delta_{\lambda\sigma}$. For the EFP2/*ab initio* integrals of interest here, the first index ξ resides on the EFP2 and must be considered as an entirely different basis set from μ. So, the zero differential overlap approximation can only be applied to the right hand (ket) side of the $(\xi\mu \mid \lambda\sigma)$ integral. This leads to $(\xi\mu \mid \lambda\lambda)\delta_{\lambda\sigma}$ as a CNDO-like approximation for these two electron integrals.

www.manaraa.com

Neglect of diatomic differential overlap (NDDO)[17] is a less drastic approximation than CNDO. If basis functions λ and σ are on the same atom center (but not necessarily the same basis function), then the integral $(\xi\mu | \lambda\sigma)$ is not ignored. As noted above for CNDO, the NDDO approximation can only be applied to the ket side of the integral.

A third approximation, similar to NDDO, has also been considered, that excludes all four-center two-electron integrals. Unlike CNDO this third approach does not neglect any three-center integrals. Therefore, if ξ, μ, λ and σ all reside on different atom centers, the $(\xi\mu | \lambda\sigma)$ integral is not calculated. However, if a common atom center is shared between any two of the three *ab initio* basis functions (μ, λ and σ) then the integral is calculated. This approximation is referred to as the three-center method.

Table 8.7. Exchange repulsion energies (in kcal/mol) for the three-center, NDDO and INDO methods compared to the predicted exchange repulsion energy from a Morokuma energy decomposition.

	three-center	NDDO	CNDO	Morokuma
Water	6.1	11.7	25.4	4.9
Methanol	6.2	18.8	39.6	5.15
Dichloromethane	0.85	2.4	6.1	0.79
Acetonitrile	5.3	14.1	25.3	2.21
Acetone	4.2	12.9	27.9	2.27
DMSO	11.4	33.0	80.5	6.38

The results obtained using the CNDO-like, NDDO-like and three-center methods are summarized in Table 8.7. The CNDO-like method is based on the most radical approximation of three methods so it is no surprise that it suffers from the largest errors. The NDDO-like approximations are less radical, and the results are improved relative to those of CNDO, but the errors are still unacceptably large. Of the three methods, the three-center

المنارة للاستشارات
www.manaraa.com

method provides the most accurate predicted exchange repulsion energies. In fact, for water, methanol and dichloromethane dimers, the predicted energies are within 1.5 kcal/mol. However, the errors grow to unacceptable levels for acetonitrile, acetone and DMSO dimers.

Despite the fact that the three-center method does modestly well for three of the six dimers, it does not reduce the computational time requirement significantly. Of the 63.2 seconds required for the DMSO dimer calculation in the last column of Table 8.6, approximately 23.6 seconds are spent calculating the two-electron integrals. When the three-center method is used, the total time of the run is reduced to 104 seconds. Even though this saves roughly 17% of the time required to calculate the two electron integrals, the accuracy suffers too much for it to be a useful approximation.

One consideration to keep in mind is that semi-empirical methods include approximations for the one-electron integrals as well as the two-electron integrals, and methods like CNDO and NDDO, these approximations are related to each other. To be consistent, one should introduce both the one-electron and two-electron approximations. None of the one-electron integral approximations were included in this present study. It is possible that the errors experienced in the two-electron integrals could be canceled or offset by errors associated with the one-electron integrals. In order to fairly assess the use of semi-empirical methods, the approximations to the one-electron integrals should be included as well. This will be the basis for a future study.

The Mulliken approximation[18,19] approximates the $(\xi\mu \mid \lambda\sigma)$ two-electron integrals by replacing them with $\frac{1}{2}(\xi\mu \mid \lambda\lambda)S_{\sigma\lambda} + \frac{1}{2}(\xi\mu \mid \sigma\sigma)S_{\sigma\lambda}$. The Mulliken approximation has been tested for the water dimer, and it provides inconsistent results. Though many integrals are

www.manaraa.com

approximated very closely, some individual integrals can experience unacceptable errors (as much as 1 kcal/mol for just one individual integral).

V. Gradient Considerations

The gradient (first derivative of the energy with respect to the nuclear coordinates) of the exchange repulsion energy was derived by Rintelman[9]. This is done in two steps, giving rise to two equations. The first equation provides the derivative of the exchange repulsion energy with respect to the *ab initio* coordinates (x_a)

$$
\begin{aligned}
\frac{\partial E^{XR}}{\partial x_a} = & -2\sum_{i\in A}\sum_{j\in B}(ij\,|\,ij)^a - 2\sum_{i\in A}\sum_{j\in B}S_{ij}^a\left[2\left(V_{ij}^A + G_{ij}^A\right) + \sum_{l\in B}F_{jl}^B S_{li}\right] \\
& -2\sum_{i\in A}\sum_{j\in B}S_{ij}\left[2\left(V_{ij}^{A^a} + G_{ij}^{A^a}\right) + \sum_{l\in B}F_{jl}^B S_{li}^a\right] \\
& +2\sum_{i\in A}\sum_{j\in B}S_{ij}^a\left[\sum_{k\in A}S_{kj}\left(F_{ik}^A + V_{ik}^B + 2J_{ik}^B\right) + S_{ij}\left(V_{jj}^A + 2J_{jj}^A\right) - \sum_{k\in A}S_{kj}(ik\,|\,jj)\right] \\
& +2\sum_{i\in A}\sum_{j\in B}S_{ij}\left[\begin{aligned}&\sum_{k\in A}\left(S_{kj}^a\left(F_{ik}^A + V_{ik}^B + 2J_{ik}^B\right) + S_{kj}\left(F_{ik}^{A^a} + V_{ik}^{B^a} + 2J_{ik}^{B^a}\right)\right) + S_{ij}^a\left(V_{jj}^A + 2J_{jj}^A\right) \\ &+S_{ij}\left(V_{jj}^{A^a} + 2J_{jj}^{A^a}\right) - \sum_{k\in A}\left[S_{kj}^a(ik\,|\,jj) + S_{kj}(ik\,|\,jj)^a\right]\end{aligned}\right] \qquad (38) \\
& +\sum_{m\in A}\sum_{i\in A}\sum_{j\in B}S_{mi}^a\left[\begin{aligned}&2(mj\,|\,ij) + S_{mj}\left(2\left(V_{ij}^A + G_{ij}^A\right) + \sum_{l\in B}F_{jl}^B S_{li}\right) \\ &+S_{ij}\left(2\left(V_{mj}^A + G_{mj}^A\right) + \sum_{l\in B}F_{jl}^B S_{lm}\right) \\ &-S_{mj}\left(\sum_{k\in A}S_{kj}\left(F_{ik}^A + V_{ik}^B + 2J_{ik}^B\right) + S_{ij}\left(V_{jj}^A + 2J_{jj}^A\right) - \sum_{k\in A}S_{kj}(ik\,|\,jj)\right) \\ &-S_{ij}\left(\sum_{k\in A}S_{kj}\left(F_{mk}^A + V_{mk}^B + 2J_{mk}^B\right) + S_{mj}\left(V_{jj}^A + 2J_{jj}^A\right) - \sum_{k\in A}S_{kj}(mk\,|\,jj)\right)\end{aligned}\right] \\
& +\sum_{m\in A}\sum_{i\in A}\sum_{n\in A}\sum_{j\in B}S_{mn}^a S_{ij}\left[\begin{aligned}&2\left[4(ij\,|\,mn) - (im\,|\,jn) - (in\,|\,jn)\right] \\ &-\sum_{k\in A}S_{kj}\left[4(ik\,|\,mn) - (im\,|\,kn) - (in\,|\,km)\right]\end{aligned}\right] \\
& -\sum_{m\in A}\sum_{i\in A}\sum_{k\in A}\sum_{j\in B}S_{mk}^a S_{ij}\left[\begin{aligned}&S_{mj}\left(F_{ik}^A + V_{ik}^B + 2J_{ik}^B\right) + S_{kj}\left(F_{im}^A + V_{im}^B + 2J_{im}^B\right) + 4S_{ij}(jj\,|\,mk) \\ &-S_{mj}(ik\,|\,jj) - S_{kj}(im\,|\,jj)\end{aligned}\right]
\end{aligned}
$$

المنارة للاستشارات
www.manaraa.com

The second gradient expression is the first derivative of the energy with respect to the coordinates of the EFP (x_b):

$$\begin{aligned}\frac{\partial E^{XR}}{\partial x_b} &= -4\sum_{i\in A}\sum_{j\in B}\left(ij^b \mid ij\right) - 2\sum_{i\in A}\sum_{j\in B} S_{ij}^b\left[2\left(V_{ij}^A + G_{ij}^A\right) + \sum_{l\in B} F_{jl}^B S_{li}\right] \\ &-2\sum_{i\in A}\sum_{j\in B} S_{ij}\left[2\left(\left(i \mid V^A \mid j^b\right) + G_{ij}^{A^b}\right) + \sum_{l\in B}\left(F_{jl}^{B^b} S_{li} + F_{jl}^B S_{li}^b\right)\right] \\ &+2\sum_{i\in A}\sum_{j\in B} S_{ij}\left[\begin{array}{l}\sum_{k\in A} S_{kj}^b\left(F_{ik}^A + V_{ik}^A + 2J_{ik}^A\right) + S_{kj}\left(\begin{array}{l}\left(i \mid \sum_{J\in B}\frac{Z_J\left(x_1 - x_J\right)}{r_{1J}^3} \mid k\right) \\ +2\sum_{l\in B}\left(ik \mid l^b l\right)\end{array}\right) \\ +S_{ij}^b\left(V_{jj}^A + 2J_{jj}^A\right) + S_{ij}V_{jj}^{A^b} + 2S_{ij}J_{jj}^{A^b} - \sum_{k\in A} S_{kj}^b\left(ik \mid jj\right) - \sum_{k\in A} S_{kj}\left(ik \mid jj\right)^b\end{array}\right]\end{aligned} \tag{39}$$

Because of the use of the product rule and the chain rule, many of the terms in Eqs. (38) and (39) do not contain a derivative. These terms will be easy to implement because they can be obtained in the same manner as the energy. Many of the terms do involve the first derivative with respect to the nuclear coordinates. However, GAMESS already includes algorithms to obtain many of these derivatives. For instance, the derivative of the overlap integrals with respect to the nuclear coordinates, S_{ij}^a, can be obtained in the AO basis through the subroutine DSTINT and then transformed to the MO basis. Derivatives of the classical point-charge approximations used in Eq. (34) can be handled in the same manner as they are in the EFP2-EFP2 (fragment-fragment) gradient because they are used in the EFP2-EFP2 energy and gradient expression. These examples can be found in the GAMESS subroutine GEXREP.

Some new subroutines will need to be created for certain derivatives, but they can be obtained in a relatively easy fashion by slightly modifying existing subroutines. The derivative of the one-electron nuclear-attraction integral $V_{ij}^{A^a}$ can be obtained by making a

www.manaraa.com

modified version of STVDER, just as a modified version of STVINT was created to obtain the V_{ij}^{A} integrals. The derivative of the electrostatic integrals, $V_{ik}^{EFP,B}$, can be formed by modifying DEFCEF just as EFCEF was modified to form the integrals. GAMESS contains subroutines to calculate the derivatives of two-electron integrals. However, all of these routines, starting with the driver JKDER will have to be copied and modified. All of the information about the j shell in the $(ji|kl)$ integral will have to be modified in every routine called by JKDER so that the code is using the EFP basis set information rather than the *ab initio* basis set. A similar procedure had to be done to the GAMESS subroutine TWOEI to obtain the $(ji|kl)$ integrals. This new driver, called EFP2EI, can be used as a model to learn how these changes must be made correctly to the JKDER driver and the subroutines it calls. Lastly, derivatives of Fock matrix elements must be obtained. GAMESS already has the ability to calculate these for molecule A, so some small changes must be made to handle them for molecule B as well.

VI. Conclusions

The implementation of the proper *ab initio*/EFP2 exchange repulsion energy into the GAMESS program is complete. The corresponding exchange repulsion Fock operator has also been coded. Both expressions have been tested upon six dimers and provide promising results. The accuracy of both expressions is good when the real two-electron integrals are used in those instances in which current approximations fail. The code has been made more efficient by avoiding the re-calculation of the Fock operator during every SCF iteration and by computing the integrals directly in the AO basis. Though computationally slower than the energy expression it replaces, the implemented energy is physically correct. The current

www.manaraa.com

computational bottleneck lies in the calculation of the two-electron integrals and it is likely that a future implementation of the Schwarz inequality will reduce this bottleneck. As it is currently implemented, the method is faster than a Hartree-Fock dimer calculation yet it provides results that approach perturbation theory in accuracy. With this in mind, the method is obtains very good results with modest efficiency.

Geometry optimizations cannot be calculated because the gradient is not implemented. However, the first derivative of the energy was considered and the means to obtain each derivative type was discussed. A future implementation of the gradient can reuse many subroutines of the energy and several existing subroutines will need modification for the gradient.

Acknowledgements

This work was supported by a grant from the Chemistry Division, Basic Energy Sciences, Department of Energy, administered by the Ames Laboratory. Special thanks is given to Professors Jan Jensen and Hui Li for numerous and insightful discussions. The authors also thank Dr. Michael Schmidt and Professor Timothy Dudley for helping with various details of the implementation into GAMESS.

References

1. Day, P. N.; Jensen, J. H,; Gordon, M. S.; Webb, S. P.; Stevens, W. J.; Krauss, M.; Garmer, D.; Basch, H.; Cohen, D. *J. Chem. Phys*., **1996**, *105*, 1968.

2. Schmidt, M. W.; Baldridge, K. K.; Boatz, J. A.; Jensen, J. H.; Koseki, S.; Matsunaga, N.; Gordon, M. S.; Ngugen, K. A.; Su, S.; Windus, T. L.; Elbert, S. T.; Montgomery, J.; Dupuis, M., *J. Comput. Chem*. **1993**, *14*, 1347.

www.manaraa.com

3. Schmidt, Michael W., Gordon, Mark S. Theory and Applications of Computational Chemistry: The First Fourty Years. Elsevier, 2005, 1167-1189.

4. Gordon, M. S.; Freitag, M. A.; Bandyopadhyay, P.; Jensen, J. H.; Kairys, V.; Stevens, W. J. *J. Phys. Chem. A*, **2001**, *105*, 293.

5. Adamovic, Ivana; Gordon, M. S. *Mol. Phys.*, **2005**, *103,* 379.

6. Li, H.; Gordon, M. S.; Jensen, J. H. *Journal of Chemical Physics*, **2006**, *124*, 214108

7. Jensen, J. H.; Gordon, M. S. *Mol. Phys.*, **1996**, *89*, 1313.

8. Jensen, J. H. *J. Chem. Phys.*, **2001**, *114*, 8775.

9. Rintleman, J. M. Quantum Chemistry, an eclectic mix: from silicon carbide to size consistency. Ph.D. Thesis, Iowa State University, Ames IA, 2004.

10. Jensen, J. H., *J. Chem. Phys.*, **1996**, *104*, 7795.

11. Szabo, A.; Ostlund, N. S., *Modern Quantum Chemistry*; Dover Publications: Mineola NY, 1996, 410-416.

12. Jensen, J. H.; Gordon, M. S. *J. Chem. Phys.*, **1998**, *108*, 4772.

13. Kitaura, K.; Morokuma, K. *Intern.J.Quantum Chem.*, **1976,** *10*,325.

14. Ditchfield, R.; Hehre, W. J.; Pople, J. A. *J. Chem. Phys.*, **1971**, *54*, 724.

15. Hehre, W. J.; Ditchfield, R.; Pople, J. A. *J. Chem. Phys.*, **1972**, *56*, 2257.

16. Francl, M. M.; Pietro, W. J.; Hehre, W. J.; Binkley, J. S.; Gordon, M. S.; DeFrees, D. J.; Pople, J. A. *J. Chem. Phys.*, **1982**, *77*, 3654.

17. Pople, J.A.; Santry, D. P.; Segal, G. A. *J. Chem. Phys.*, **1965**, *43*, 129.

18. Mulliken, R. S. *J. Chim. Phys.*, **1949**, *46*, 500 and 521.

19. Ruedenberg, K. *J. Chem. Phys.*, **1951**, *19*, 1459.

المنارة للاستشارات

www.manaraa.com

CHAPTER 9: CONCLUSIONS

The solvation of fluorine and chlorine anions was detailed in chapter 2. The goal of the study was to find how large an aqueous solvent cluster must be in order to achieve complete solvation. Fluorine anions preferred to reside on the surface of the solvent cluster until fifteen or more water molecules are present and the chlorine anion required eighteen water molecules before the completely solvated structure was favored. Though the water molecules were expressed as Effective Fragment Potentials, fully *ab initio* single point energies qualitatively confirmed the results. The binding energies and differential binding energies predicted by the calculation qualitatively agree with those obtained from *ab intio* calculations and experimental data from the literature. The internal geometries of the water molecules were held frozen by the potential but the fully *ab initio* optimizations showed that this was not an unreasonable approximation to make.

The dipole moment of the water molecule, and how it changes as that water molecule is surrounded with other water molecules, is presented in chapter 3. The goal of this project was to see how many water molecules must be present for the dipole to be enhanced from the monomer value (1.85 Debye) to the bulk value (approximately 2.9 Debye). The smallest cluster size examined contained a total of six water molecules and the dipole moment was closer to the bulk value than to the monomer value. As more solvent molecules were added, it was found that the dipole moment had matched the bulk value (2.9 Debye) with only twenty total molecules even though the structures for n=20 did not resemble bulk water. A dipole that agreed well with the bulk dipole was obtained for n=32,41 and 50 water molecules and all of these structures preferred to have a bulk-like arrangement of the solvent molecules. Of most interest to this project though is learning why the dipole moment

المنارة للاستشارات

www.manaraa.com

changes when in solution. Use of localized molecule orbitals and localized charge distributions show that the dipoles of each individual orbital do not change drastically but the orientation of those vectors does. The dipole vectors along the lone pair orbitals come closer together (ie, the angle between them decreases). This leads to less vector cancellation of these dipole vectors and to a greater enhancement of the molecular dipole. The bonding orbitals did not contribute significantly to the molecular dipole, nor do they change significantly when placed in the presence of a water solvent.

The structure of bihalide anions solvated by water was studied with *ab initio* MP2 and CCSD(T) calculations and is detailed in chapter 4. This study was inspired by previous research done by Newmark and co-workers who solvated bihalide anions with one solvent molecule and used many different solvents. Newmark and co-workers were able to determine which solvated species was observed experimentally by the results of their theory. However, a similar theoretical investigation needed to be done for when more solvent molecules are present. Though up to four water molecules donate all of their hydrogen atoms to solute for hydrogen bonding, these species are higher in energy when three or four water molecules are present. This was found to be true of both anions. As the number of water molecules increases, the negative Mulliken charges on the halide atoms and the positive charge on the hydrogen atom are reduced. Besides basic steric hindrance, this may help provide some insight into why the water molecules prefer interaction with each other over exclusive interaction with the bihalide anion.

The aqueous solvation of the nitrate anion was presented in chapter 5. Only clusters containing n=15,32 water clusters were considered. The goal of this study was to determine if the Effective Fragment Potential method would predict whether the anion resided on the

المنارة للاستشارات

www.manaraa.com

surface or inside the cluster. Comparisons were made to previous literature studies which were based upon molecular mechanics. The literature tends to be conflicted about the nature of these anions and many results seem to depend upon the type of molecular mechanics potential used in the simulation. In order to put these issues to rest, MP2 single point energies were used to compare with the EFP results. Full MP2 optimizations were performed so that the true nature of the lowest energy anions could be discovered.

المنارة للاستشارات
www.manaraa.com

ACKNOWLEDGMENTS

I would like to thank my family and friends for the love and support that they have shown to me over the last six years. I would specifically like to thank my parents, John and Joyce Kemp, as well as my brother, Steven Kemp. Their encouragement to remain diligent has been instrumental in my success.

I would like to thank my advisor, Dr. Mark Gordon, for the instruction that has has provided to me. His leadership and advice have made the last six years an enjoyable learning process. I will value what I have learned for years to come.

I would also like to thank my committee membersfor insightful questions, comments and suggestions about my research. I would also like to thank my committee members for their willingness to attend annual meetings even when it was least convenient for themselves.

www.manaraa.com